Pontificia Universidad Católica de Chile
Facultad de Medicina
Programa de Doctorado en Neurociencias

TESIS DOCTORAL:

"RELATIONSHIP BETWEEN THE AFFERENT INNERVATION PATTERN AND THE SPONTANEOUS AND AVERSIVE STIMULUS DRIVEN ACTIVITY OF INDIVIDUAL VTA DOPAMINERGIC NEURONS"

Por

TRINIDAD MONTERO OSSANDÓN

Diciembre 2019

Pontificia Universidad Católica de Chile
Facultad de Medicina
Programa de Doctorado en Neurociencias

"RELATIONSHIP BETWEEN THE AFFERENT INNERVATION PATTERN AND THE SPONTANEOUS AND AVERSIVE STIMULUS DRIVEN ACTIVITY OF INDIVIDUAL VTA DOPAMINERGIC NEURONS"

Tesis entregada a la Pontificia Universidad Católica de Chile en cumplimiento parcial de los requisitos para optar al Grado de Doctor en Neurociencias

Por

TRINIDAD MONTERO OSSANDON

Director de Tesis: Dr. Pablo Henny V.

Comisión de Tesis: Dra. María Estela Andres C.
Dra. Margarita Calvo B.
Dr. Jorge Campusano A.
Dr. Gonzalo Marín G.

Acknowledgments

Al Dr. Pablo Henny por el tiempo y dedicación para formarme en la rigurosidad y perfeccionismo de nuestro trabajo. También al Dr. Cristián González, que me enseñó todas las técnicas utilizadas en esta tesis y me ayudo a salir adelante cuando los experimentos no resultaban. A Paulina Merino, Alejandro Oñate, Dr. Rodrigo Meza, Andrea Riveros, Rafael Gatica, Simón Salgado, Nicole del Solar y a todos los miembros del laboratorio de la Dra. Marcia Gaete por estar en el día a día compartiendo en el laboratorio y también en la discusión de los resultados.

Gracias a los profesores del Rayo, Juan Carlos Letelier, Gonzalo Marín y Jorge Mpodozis, y a sus estudiantes por acogerme en su laboratorio cuando no tenía donde trabajar ni hacer experimentos.

Gracias a mis amigos, Andrea, Consuelo, Claudia, Deny, Joaquín, Nicole, Roddy y Stephanie por estar ahí para conversar de nuestros problemas y alegrías, de política, educación, farándula y, en resumen, de cualquier cosa menos de ciencia.

Muchas gracias a mis padres y hermanos que siempre me han apoyado en este proyecto y aunque nunca les pude explicar bien lo que estaba haciendo, siempre se han alegrado con mis avances y se han preocupado con mis tropiezos.

Por sobre todo, gracias a Enrique, mi marido, que ha estado conmigo estos cinco años, acompañándome, soportándome y levantándome del piso en los malos momentos y alegrándose, incluso mas que yo, con mis éxitos. Finalmente, gracias a nuestra hija, Adriana, por alegrarme los días y las noches con su sonrisa y entusiasmo.

Funding

Project FONDECYT N° 1141170 (P.H.V)

Project FONDECYT N° 1191147 (P.H.V)

Project Anillo ACT 1109 (P.H.V)

Scholarship CONICYT-PCHA Doctorado Nacional 2015-21150324 (T.M.O)

Personal contributions

I recorded and labeled 12 VTA single neurons, with occasional help from Cristian Gonzalez. I processed, and performed immunohistochemistry and imaging for tyrosine hydroxylase, three-dimensional reconstruction and detection of inhibitory and excitatory postsynaptic density markers of the 12 VTA neurons. I three-dimensionally reconstructed from high resolution images the 12 VTA neurons and stereologically counted and estimated the inhibitory and excitatory putative postsynaptic puncta on all of them. I performed the distribution analysis and correlations with electrophysiological activity.

The 12 SNc and 1 VTA neuron in section 8.1.3. were labeled and reconstructed by Rodrigo Meza. Pablo Henny and Rafael Gatica have participated in the production of the figures of the manuscript in preparation of section 8.1. Pablo Henny has also importantly participated in the production of the manuscript.

The 9 VTA dopaminergic neurons electrophysiologically recorded and labeled, but not reconstructed were recorded by Cristian Gonzalez

Table of Contents

List of Figures

List of tables

Abbreviations

AIS	Axon Initial Segment
AP	Action Potential
Cli	Caudal Linear nucleus
CNS	Central Nervous System
CV2	Coefficient of Variation 2
DA	Dopamine
ECoG	Electrocorticogram
EM	Electronic Microscopy
FSCV	Fast-Scan Cyclic-Voltammetry
GABA	Gamma-Aminobutyric Acid
Geph	Gephyrin
Hom	Homer
IF	Interfascicular
ISI	Interspike Interval
LH	Lateral Hypothalamus
LHb	Lateral Habenula
mPFC	medial Prefrontal Cortex
NA	Numerical Aperture
NAc	Nucleus Accumbens
Nb	Neurobiotin
NHS	Normal Horse Serum
NMDA	n-methyl-d-aspartate

PBP	Parabrachial Pigmented nucleus
PBS	Phosphate Buffered Saline
PFA	Paraformaldehyde
PN	Paranigral nucleus
PSD	Postsynaptic Density
PSP	Putative Postsynaptic Puncta
RLi	Rostral Linear nucleus
RMTg	Rostromedial Tegmentum
SFR	Spike Firing Rate
SN	Substantia Nigra
SNc	Substantia Nigra compacta
SNr	Substantia Nigra reticulata
SWB	Spikes Within Bursts
TH	Tyrosine Hydroxylase
VGAT	Vesicular GABA Transporter
VGluT	Vesicular Glutamate Transporter
VIAAT	Vesicular Inhibitory Aminoacid Transporter
VTA	Ventral Tegmental Area

1. Abstract.

Ventral tegmental area (VTA) dopaminergic (DA) neurons have been implicated in several brain functions such as attention, memory, behavioral reinforcement and motivation. Dysfunction of these neurons has been associated with depression, schizophrenia, attention deficit hyperactivity disorder and addictive behaviors among others. Anatomically, VTA DA neurons have been shown to send projections mainly to telencephalic and diencephalic areas of the brain, with little or no collateralization and to receive its most abundant input from ventral basal ganglia structures.

Because of the above-mentioned multiplicity of normal and also disease states, understanding the biological bases that determine VTA DA neurons firing behavior is fundamental. Among several other underlying factors controlling their activity, we are interested in studying the organization of their dendritic tree and the inputs it receives, how many there are and how they are distributed onto the different compartments of the somatodendritic tree.

To accomplish the study, we recorded and labelled single VTA neurons *in vivo* in anesthetized mice and subsequently immunohistochemically identified their neurochemical phenotype by tyrosine hydroxylase. Next, we labeled inhibitory and excitatory postsynaptic puncta to identify putative synaptic contacts on individual neurons, which were three dimensionally reconstructed. Then, postsynaptic profiles were counted and located on the different neuronal compartments. Next, we studied the morphological and geometrical properties of the reconstructed neurons and compared them with three-dimensionally reconstructed substantia nigra compacta (SNc) DA neurons. Finally, we correlated spontaneous and aversive stimulus response electrophysiological recordings with morphological and synaptic contacts distribution data.

From morphological analyses we found that when considering the entire dendritic domain, the dendrites of ventral VTA neurons are smaller and simpler than dorsal VTA neurons and, independently of their location, both groups exhibited a dorso-medial and ventro-lateral preferential location of their dendrites which is significantly different from SNc DA neurons. Furthermore, we describe that they have large dendritic trees, encompassing a large proportion of the VTA are and they overlap significantly more than adjacent substantia nigra DA neurons. These last two properties partly explain why only overlapping input topologies have been described in the VTA; if the neuronal trees are so big and overlapping, incoming inputs, even if they were very well localized in the VTA could stablish contact with neuronal cell bodies that might be actually far away.

Concerning input number and distribution, we found that VTA DA neurons received an average of 1001 putative postsynaptic puncta (PSP) of which 55.6% were glutamatergic and 44.4% GABAergic and regarding their distribution we found significantly more excitatory than inhibitory PSP in distal dendrites and in higher order dendrites.

Electrophysiologically we found a wide range of values in spontaneous activity (firing rate, spike train irregularity, bursting activity and spike duration were analyzed) which is in agreement with what has been described in the literature for VTA DA neurons. We found that none of these variables related to the overall PSP number, density or distribution. After analyzing aversive stimulus-driven responses in our sample of 21 VTA DA neurons, we found 15 neurons inhibited by the aversive stimulus, 4 neurons were activated and 2 neurons were unresponsive. Activated neurons were significantly more medially located than inhibited neurons. In 12 reconstructed and further analyzed neurons there was, also, no significant difference in the total number, density or distribution of excitatory or inhibitory PSP between these groups. However, when considering

only the inhibited neurons we found a correlation, that neurons with a higher density of inhibitory PSP also had a greater inhibition in response to the aversive stimulus. This result is consistent with what has been described for substantia nigra compacta DA neurons where the extent of inhibition was related to the amount of GABA inputs. These results support the notion that different responses might be related to differences in organization of synaptic inputs onto individual neurons.

In summary, in this thesis we identify two morphologically different groups of VTA DA neurons, describe the location and overlapping of their dendritic trees that is significantly different from SNc DA neurons. We also find that they receive more excitatory synaptic contacts on their distal dendrites and last but not least, describe a correlation between the degree of inhibition by an aversive stimulus and the density of inhibitory synaptic contacts. These results not only help us discover the morphological features of VTA DA neurons and improve our knowledge of a system that has been implicated in a great number of normal and disease states, but also contribute to decoding learning of avoidance behaviors by describing how, in VTA DA neurons, aversive stimulus inhibition relates to the amount of inhibitory inputs.

Resumen.

Las neuronas dopaminérgicas (DA) del Área Tegmental Ventral (VTA) han sido implicadas en diversas funciones cerebrales tales como atención, memoria, refuerzo conductual y motivación. Por otra parte, la disfunción de estas neuronas se ha asociado con depresión, esquizofrenia, síndrome de déficit atencional e hiperactividad y conductas adictivas entre otros. Anatómicamente se sabe que las neuronas DA del VTA envían, con poco o nada de colateralización de sus axones, proyecciones principalmente a áreas telencefálicas del cerebro y reciben sus inputs más abundantes de las estructuras ventrales de los ganglios basales.

A causa de la multiplicidad de estados normales y enfermedades asociados, es fundamental entender las bases biológicas que determinan la actividad de disparo de las neuronas DA del VTA. Entre los diversos factores que subyacen el control de la actividad de estas neuronas, nosotros estamos interesados en estudiar la organización de su árbol dendrítico y de los inputs que éste recibe, cuántos son los inputs que recibe y como están distribuidos en los diferentes compartimentos del árbol somatodendrítico.

Para lograr este estudio, registramos y marcamos neuronas individuales del VTA *in vivo* en ratones anestesiados y luego identificamos el fenotipo neuroquímico de las neuronas marcadas por medio de inmunohistoquímica contra tirosina hidroxilasa. A continuación, marcamos las punctas postsinápticas inhibitorias y excitatorias para identificar contactos sinápticos putativos en neuronas individuales que habían sido previamente tridimensionalmente reconstruidas. Luego, contamos los perfiles postsinápticos y los ubicamos en los distintos compartimentos neuronales. También, estudiamos las propiedades morfológicas y geométricas de las neuronas reconstruidas, las comparamos con neuronas DA de la sustancia negra compacta (SNc) y luego, correlacionamos

la actividad electrofisiológica espontánea y en respuesta a un estímulo aversivo con los datos morfológicos y de distribución de contactos sinápticos.

En cuanto a los análisis morfológicos encontramos que cuando consideramos el dominio dendrítico en su totalidad, las dendritas de las neuronas DA del VTA más ventral son más pequeñas y simples que las dendritas de las neuronas del VTA más dorsal y que independientemente de su ubicación en el VTA, ambos grupos exhibían una distribución de sus dendritas preferentemente en ubicación dorso-medial y ventro-lateral respecto al soma, la cual es significativamente diferente de la distribución de dendritas que encontramos en las neuronas DA de la SNc. Adicionalmente, describimos que estas neuronas tienen árboles dendríticos grandes, abarcando una gran proporción del VTA y que estos se solapan significativamente más que en las neuronas DA de la adyacente substantia nigra. Estas dos últimas características explican parcialmente porque, para el caso de los inputs, solo se han descrito topografías solapadas; si los árboles neuronales son tan grandes y se solapan, los inputs que llegan al área podrían establecer contacto con cuerpos neuronales que podrían estar lejos unos de otro en virtud de que sus dendritas podrían estar cerca.

Respecto al número y distribución de los inputs, encontramos que las neuronas DA del VTA reciben, en promedio, 1001 punctas postsinápticas putativas (PSP) de las cuales 55,6% son glutamatérgicas y 44,4% GABAérgicas. Al estudiar la distribución, encontramos que había significativamente más PSP excitatorios que inhibitorios en dendritas distales y también en dendritas de ordenes dendríticos mayores.

Electrofisiológicamente, encontramos un amplio rango de valores en parámetros de actividad espontánea (frecuencia de disparo, irregularidad de disparo, actividad en bursts y duración de la espiga), los cuales son consistentes con lo que ha sido descrito en la literatura para las neuronas DA del VTA. Vemos, por otra parte, que ninguna de estas variables

electrofisiológicas que correlaciona con número, densidad o distribución de PSP. Al analizar las respuestas al estímulo aversivo encontramos que de nuestra muestra de 21 neuronas DA del VTA 15 neuronas son inhibidas por el estimulo aversivo, 4 son activadas y 2 no responden. Las neuronas activadas se encuentran significativamente mas medialmente localizadas en el VTA que las neuronas inhibidas. En las 12 neuronas reconstruidas y analizadas, respecto a la distribución de PSP vemos que, en cuanto al número total, densidad o distribución de PSPs no hay diferencias entre inhibidas y activadas. Sin embargo, al considerar únicamente las neuronas inhibidas, encontramos una correlación, donde a mayor densidad de PSP inhibitorios mayor es la inhibición en respuesta al estímulo aversivo. Los resultados mencionados apoyan la noción de que distintas respuestas neuronales a un mismo estímulo podrían estar relacionados con diferencias en la organización de los inputs sinápticos sobre neuronas individuales.

En resumen, los resultados principales de esta tesis son: se identifican dos grupos de neuronas DA del VTA morfológicamente distintos, se describe la orientación y solapamiento de sus árboles dendríticos los cuales son significativamente distintos respecto a las neuronas DA de la SNc. También vemos que las dendritas distales de estas neuronas reciben más contactos sinápticos excitatorios que inhibitorios y finalmente vemos que hay una correlación entre el grado de inhibición y la densidad de contactos sinápticos inhibitorios. Estos resultados no solo nos ayudan a descubrir las características morfológicas de las neuronas DA del VTA y a mejorar nuestro conocimiento sobre un sistema que ha sido implicado en un gran número de estados normales y alterados, sino que también contribuyen al entendimiento de las conductas de evasión describiendo como, en las neuronas DA del VTA, la inhibición por un estímulo aversivo se relaciona con la cantidad de inputs inhibitorios.

2. Introduction.

The ventral tegmental area (VTA) constitutes one of the three midbrain dopaminergic groups along with the substantia nigra compacta (SNc) and the retrorubral field. Approximately 65% of VTA neurons are dopaminergic, but there also GABAergic and glutamatergic neurons, which in the rat represent 30% and 2-3% of VTA neurons respectively (Nair-Roberts et al., 2008). More recently, combinatorial neurons that co-release dopamine and glutamate, dopamine and GABA, or glutamate and GABA have been described (Kim et al., 2015; Root et al., 2014; Tritsch et al., 2014; Yamaguchi et al., 2011; Zhang et al., 2015).

VTA dopaminergic neurons have been implicated in several brain functions such as attention, memory, behavioral reinforcement and motivation (G. V. Carr et al., 2017; Chudasama and Robbins, 2004; Pekcec et al., 2018; Tsai et al., 2009; Wise, 2004). Moreover, dysfunction of VTA dopamine (DA) neurons has been implicated in depression, schizophrenia, attention deficit hyperactivity disorder and addictive behaviors among others (Chaudhury et al., 2013; Flores, 2011; Mulinari, 2012; Nieoullon, 2002; Wise, 2009).

VTA DA neurons have been shown to send projections mainly to telencephalic areas of the brain, with little or no collateralization (Fallon, 1981; Swanson, 1982). Some of the most studied target areas include nucleus accumbens (NAc), medial prefrontal cortex (mPFC), central and basolateral amygdala, ventral pallidum and lateral habenula (LHb) (Breton et al., 2019; Loughlin and Fallon, 1984; Menegas et al., 2015; Swanson, 1982). Furthermore, VTA neurons receive its most abundant input from basal ganglia nuclei; NAc core and shell, dorsal striatum, olfactory tubercle, ventral pallidum and globus pallidus (Geisler and Zahm, 2005; Watabe-Uchida et al., 2012), among others. Nevertheless, they also receive important inputs from lateral and medial

hypothalamus, preoptic area and some midbrain and hindbrain areas such as the dorsal raphe, parabrachial nucleus, pedunculopontine nucleus and the laterodorsal tegmentum (Geisler and Zahm, 2005; Mena-Segovia et al., 2008; Watabe-Uchida et al., 2012).

Understanding the biological bases of VTA DA neurons activity is fundamental, due to the above-mentioned plethora of normal and disease states that have been associated with. Among several others, some of the underlying factors affecting this activity are: the organization of these neurons in nuclei and their projections (under the assumption that different populations are segregated in space and receive different inputs), related to the previous but much less studied is the localization and organization of the somatodendritic tree and receptive field and the inputs to single VTA DA neurons and how they are distributed onto the soma and dendrites.

In the following part of the introduction, we will provide a background summary of the current literature regarding: (a) the electrophysiological activity of VTA DA neurons, (b) VTA cytoarchitectonic descriptions and the morphology of VTA DA neurons, (c) mapping of their afferent and efferent connections and (e) whether they target specific subpopulations of neurons and (d) what has been published regarding input distribution of single VTA DA neurons.

2.1. Electrophysiological Behavior of VTA DA Neurons.

The release of dopamine in the ventral striatum and other target regions is essential to VTA DA neuron function. DA release is largely controlled by the DA neuron's firing (Gonon, 1988; Heien and Wightman, 2006) which is characterized by two distinct activity patterns:

- An irregular firing rate, or tonic activity, with a frequency range of 0.5 to 10 Hz, and an average of 4 - 5 Hz. (Grace and Bunney, 1984a). DA tonic neurotransmission in

targeted areas is mediated by the irregular firing rate, and is thought to play a facilitating role (Berke and Hyman, 2000), but see (Owesson-White et al., 2012))

- Burst firing, which consists of clusters of approximately 2 to 5 spikes discharged at high frequencies (10 – 20 Hz). The burst firing mediates phasic DA neurotransmission and induces large transient increases of dopamine in target areas (Grace and Bunney, 1984b).

In vivo electrophysiological recordings have shown that VTA DA neurons respond with an increase in bursting to several behavioral conditions such as unexpected rewards, reward predictive cues, novel stimuli, feeding and paradoxical sleep (Dahan et al., 2007; Dommett et al., 2005; Hyland et al., 2002; Schultz, 2007). In addition, phasic increases in DA neuron discharge are generally associated with behavioral reinforcement (Chaudhury et al., 2013; Tsai et al., 2009), hyperactivity (Costa et al., 2006) and synaptic plasticity within the striatal microcircuit (Tritsch et al., 2012; Tritsch and Sabatini, 2012). On the other hand, decrease or complete stop of DA neuron activity is associated with punishment, reward omission and aversive or noxious stimuli (Matsumoto and Hikosaka, 2009; Schultz, 2007; Ungless et al., 2004).

Interestingly, the population response of VTA DA neuron is not homogeneous for some types of stimuli. Such is the case of aversive stimuli; noxious airpuffs in awake monkeys (Matsumoto and Hikosaka, 2009), footshocks (Brischoux et al., 2009), footpinchs (Maeda and Mogenson, 1982) and tailpinchs (Eddine et al., 2015) in anesthetized rodents all may elicit either increases or decreases in the activity of different VTA DA cells.

2.1.1. Spontaneous Activity.

In the absence of external stimuli (e.g. under anesthesia) DA neurons may be spontaneously active and exhibit both, tonic and bursting firing (Grace and Bunney, 1984b; 1984a). Tonic activity pattern arises from an intrinsic membrane pacemaking mechanism (Khaliq and Bean, 2010) yet is also modulated by afferent inputs (Kitai et al., 1999). Moreover, bursting activity is highly dependent on afferent inputs, and largely absent in *in vitro* preparations where the afferent input is severed.

The above-mentioned pacemaking activity of VTA DA neurons is a homogeneous discharge pattern, normally seen in slices or preparations of acutely isolated neurons were the neuron is deafferented. Pure pacemaking is not commonly recorded spontaneously in either anesthetized or awake animals (Grace and Onn, 1989; Kita et al., 1986; Shepard and Bunney, 1988). However, the irregular firing pattern is thought to arise both from the pacemaker activity and the influence of afferent inputs. Thus, glutamate and gamma-aminobutyric acid (GABA) the two main neurotransmitters that innervate VTA dopaminergic neurons affect the irregular firing rate.

Glutamate increases VTA DA cells firing rate (Mercuri et al., 1992) and GABA, as expected, decreases the firing rate (Grace and Bunney, 1985). Conversely, inhibition of either GABA receptors (Paladini and Tepper, 1999) or GABAergic cells may disinhibit dopaminergic cells and increase their firing rate (Bocklisch et al., 2013; Tan et al., 2012).

Midbrain DA neurons also show a particular firing pattern that has been called burst activity, that is characterized by a large increase in the firing frequency for a short period of time. The frequency and characteristics of burst activity may be modified (Anstrom et al., 2009; Dahan et al., 2007; Marinelli et al., 2003) and also, cells in, what authors described as a ‘non-bursting

mode' may shift their firing pattern to a 'bursting mode' (Bioulac et al., 1997; Drion et al., 2010; Lalive et al., 2014). Moreover, even in the absence of external stimuli, if we look at the population of VTA DA neurons the amount of bursting may be described as a continuum where there will be neurons with no bursting activity, others with an intermediate level of bursting and yet other neurons presenting very high bursting levels with up to 90% of their spikes being emitted in bursts, with an overall population average of 30% (Grace and Bunney, 1984b).

From early studies on DA cell activity it was noticed that activation of glutamatergic afferents or microiontophoretic application of glutamate induced an increase in burst firing in midbrain dopaminergic neurons *in vivo* (Chergui et al., 1993; Grace and Bunney, 1985; 1984b; Mercuri et al., 1992; Overton and Clark, 1992) and direct application of N-methyl-d-aspartate (NMDA) receptor antagonists blocks spontaneous burst firing (Chergui et al., 1993; Overton and Clark, 1992). Nonetheless glutamate alone is not sufficient to induce burst firing. In midbrain slices, in which the afferent input is severed, addition of glutamate agonists by itself it is not enough to induce burst firing of DA neurons (Grace and Onn, 1989; Mercuri et al., 1992; Seutin et al., 1990). However, more recently, burst firing may be induced *in vitro* preparations. Bath application of NMDA induced burst firing in DA neurons, (Johnson and Wu, 2004). Furthermore, phasic iontophoretic application of glutamate agonists or electrical stimulation of excitatory afferents may produce bursts identical than those seen *in vivo* (Morikawa et al., 2003)

Mechanisms mediated by GABA have also been implicated in burst firing activity of DA neurons. Particularly, blockage of $GABA_A$ receptors by local pressure administration of antagonists increased the number of bursts and of spikes within bursts (SWB) in SNc DA neurons (Paladini and Tepper, 1999) Similarly, Erhardt and collaborators reported an increase in the percentage of spikes in bursts in VTA DA neurons after systemic administrations of $GABA_B$

antagonist CGP35348 (Erhardt et al., 2002b).

Notwithstanding all the work regarding either tonic or bursting activity modulation by either, glutamatergic or GABAergic synaptic inputs there are few investigations addressing innervation at the single cell level, although it is at this level that synaptic input integration occurs, and remains a fundamental area of investigation (Henny et al., 2012; Klausberger and Somogyi, 2008; Kole and Stuart, 2012). Because inputs are differentially distributed throughout the neuronal somatodendritic domain, establishing the weight of a specific type of input requires a detailed description of input location and somatodendritic architecture (Henny et al., 2012; 2014; Katz et al., 2009; Megías et al., 2001). In this thesis we evaluate the innervation pattern of glutamatergic and GABAergic inputs on individual VTA DA neurons and correlate it with the spontaneous (both irregular and bursting activity), activity pattern.

2.1.2. Driven Activity: Nociceptive Somatosensory Stimulation.

Classical studies have shown that mesolimbic VTA DA neurons signal errors in reward prediction; they increase their activity when a rewards is greater than expected and decrease their activity when the reward is smaller than expected (Schultz et al., 1997). Related to this, it has been shown that they also increase their firing rate in response to cues predicting rewards and are inhibited by aversive stimuli or reward omission (Fiorillo, 2013; Schultz et al., 1997; Watabe-Uchida et al., 2017). However, several lines of evidence indicate that VTA neurons are also activated by aversive stimuli. Specifically, experiments measuring DA extracellular levels in target nuclei, mainly NAc, by fast-scan cyclic-voltammetry (FSCV) and microdialysis, were among the first to report an increase in DA release in response to aversive stimuli (Abercrombie et al., 1989; Badrinarayan et al., 2012; Budygin et al., 2012; Young, 2004). More recently, a report measuring

calcium transients by fiber photometry in VTA DA neurons in awake mice, shows increased activity in response to aversive stimuli (Moriya et al., 2018). One hypothesis sustains that this increase in response to aversive stimuli is due to bidirectional and temporal differences of a single population of VTA neurons, and not a different group of neurons signaling aversion. However, a growing body of evidence supports the idea that instead of one population of neurons signaling both reward and aversion, there are two populations: one signaling reward and the other aversion. Electrophysiological studies either with identified DA neurons in rodents or putative DA neurons in primates were the first to identify a separated population of DA neurons that were activated by aversive stimuli (Brischoux et al., 2009; Matsumoto and Hikosaka, 2009). These results led to the argument that reward-excited VTA neurons signaled the motivational value of stimuli and aversive-excited VTA neurons were signaling motivational salience. Thus these aversive stimulus activated neurons are responding to attention-drawing stimuli (salient) that may actually be or rewarding (Bromberg-Martin et al., 2010).

Several VTA DA circuits involved in aversive processing have been identified. For instance, a study identified a specific circuit of LHb inputs that arrive to medial VTA neurons that project to mPFC. They showed that optogenetic stimulation of LHb terminals in the VTA induced conditioned place aversion, a known paradigm measuring aversive-related conducts (Lammel et al., 2012). Another report from the same group, this year, identified another aversion-related circuit (de Jong et al., 2019). They found, using rabies virus retrograde tracing and fiber photometry, a population of medial VTA DA neurons that project specifically to the NAc ventral medial shell (vNAcMed) and is excited by aversive stimuli in awake, behaving mice. Moreover these medial VTA vNAcMed-projecting neurons are innervated by lateral hypothalamus excitatory neurons that are driving the excitatory response to aversive stimulus (de Jong et al., 2019).

However, it is unknown whether the response to aversive stimuli and synaptic innervation of individual VTA dopaminergic cells are related. In mouse SNc dopaminergic cells, Henny and colleagues evaluated the distribution of glutamatergic and GABAergic synaptic inputs. They identified the neurochemistry of synaptic terminals by labeling either the vesicular glutamate transporter (VGluT) or the vesicular GABA transporter (VGAT or VIAAT, vesicular inhibitory aminoacid transporter) and performed electronic microscopy (EM) to detect synaptic contacts among axon terminals and previously labeled DA neurons by the juxtacelular technique. Upon analysis of the distribution of synaptic contacts they found that GABA synapses were preferentially located on dendrites that extended into to the SN reticulata (SNr) (Henny et al., 2012a). Furthermore, when neurons inhibited by an aversive stimulus and non-responsive neurons were compared, they found that responsive cells had a higher proportion of dendrites extending into the SNr and a higher number of GABA synapses. Additionally the proportion of dendrites extending into SNr was correlated with the inhibitory response to the aversive stimulus (Henny et al., 2012a). However, although the VTA has subnuclei, the distinctive anatomical, hodological and cytoarchitectonic differences such as what is seen in substantia nigra (SN), with a SNc and a SNr well separated from each other, are not seen in the VTA (Nair-Roberts et al., 2008; Phillipson, 1979a) Moreover, as already mentioned, in the VTA there are not only inhibitory responses to aversive stimuli, but also excitatory responses. Hence, in this thesis we evaluate the distribution of synaptic inputs into individual VTA DA neurons and correlate it to different responses to an aversive stimulus.

2.2. Ventral Tegmental Area Morphological and Cytoarchitectonic Descriptions.

For the reasons discussed in previous sections, important efforts have been made to improve our understanding of the VTA dopaminergic system from its electrophysiological behavior to the anatomical data. Anatomical studies have looked into VTA´s cell morphology (Fu et al., 2012; Halliday and Törk, 1986; Ikemoto, 2007; Phillipson, 1979a; 1979b; Sizemore et al., 2016). Early studies described VTA neuron morphology mostly with histochemical stains such as Golgi or cresyl violet, and two-dimensional approaches. These initial studies gave us the first ideas about VTA DA neurons morphology; mostly small to medium cell bodies with 2 – 5 primary dendrites and noticeably, they identified in some of them, that the axon did not begin from the cell body but rather from a dendrite (Ikemoto, 2007; Phillipson, 1979b; 1979a). Additionally, most studies reported the orientation of the neurons based on the single tissue section where the cell body was placed and although the studies did not always agree on the finer points it was commonly reported that lateral VTA neurons had a mediolateral orientation (Halliday and Törk, 1986; Ikemoto, 2007; Phillipson, 1979b; 1979a). A single study looked at the dendritic fields, and even though it was qualitative and in 2D the author still reported a high degree of overlap between the dendritic fields (Phillipson, 1979a).

However, and despite the thousands of publications that can be found on the VTA, looking at its role in drug addiction, mood disorders, circadian rhythms and also mapping its afferent and efferent connections with ever more detail, no high-resolution reconstructions using modern techniques has been done in these neurons. We still know very little about their dendritic arbor, e.g. we do not know how much dendritic surface these neurons have, how far their dendrites may reach, or whether their dendrites stay within the VTA or they may extend processes into adjacent nuclei. Furthermore, we have no knowledge of three-dimensional organization of their dendrites,

or how big their dendritic field is. These are some of the morphological questions we seek to answer in this thesis.

2.3. Mapping VTA Connections: The Specificity Issue.

Likewise, a sizeable amount of literature has been devoted into describing the cytoarchitecture and mapping of VTA connections. Several subnuclei or cell clusters have been identified over the years and, although, there is still no absolute consensus on how many conform the VTA, most histological studies nowadays recognize at least 5; the parabrachial pigmented (PBP), the paranigral (PN), which are more lateral and the largest, and the three midline nuclei, rostral linear (RLi), caudal linear (CLi) and interfascicular (IF) nuclei (Aransay et al., 2015; Ferreira et al., 2008; Fu et al., 2012; Ikemoto, 2007; Mongia et al., 2019; Nair-Roberts et al., 2008; Trutti et al., 2019). On the logic that discernable cellular groups within the VTA may have specific connections, tracing studies mapping afferents or efferents from the VTA have been performed. However, no clear, well defined association between a projection or an input and a VTA subnucleus has been found. What researchers have discovered are preferential distributions rather than specific associations (Geisler and Zahm, 2005; Ikemoto, 2007; Lammel et al., 2012). For example, using fluorogold retrograde tracing in rats, Ikemoto described a topographical arrangement of VTA-ventral striatum projection, such that ventromedial structures of the striatum receive more DA inputs from the posteromedial VTA and ventrolateral striatum structures receive more DA projections from the more lateral VTA (Ikemoto, 2007). In a recent study, ten VTA projection sites were injected with a retrograde tracer and the distribution of either DA or GABA cell bodies in the VTA was described (Breton et al., 2019). Broadly they found that even though there were discernable differences in the distribution pattern of the cell bodies according to their

projection site, also each projection site received inputs from neurons in every one of their ipsilateral sampling areas, indicating that VTA neurons that are close together may project to different striatal or other brain areas, and conversely, that VTA neurons that may be separated might project to the same target area (Breton et al., 2019). Others, due to the absence of a relationship between connections and a specific, clearly delimited anatomical location, have looked for specific input/output relationships (Beier et al., 2015; Menegas et al., 2015). Menegas and collaborators succeeded to separately label the inputs to dDA neurons of the VTA or SNc that projected to 8 selected nuclei. Firstly, and as previously described, DA cell bodies with different projection sites are found in different but overlapping areas. Secondly, they found that the inputs distribution for each differently projecting group of neurons is very similar with the exception of those that project to the posterior striatum (Menegas et al., 2015). Previously, in order to anatomically explain the above-mentioned lack of specificity in input and output relationships, Geisler and Zahm, injected an anterograde tracer into 14 areas that were known to target the VTA and looked at their axons and how they were distributed in the VTA. Although they only did a qualitative assessment it is interesting that, with the exception of nucleus accumbens (NAc) shell inputs, independently of where the axons came from, they all had a similar distribution throughout the VTA (Geisler and Zahm, 2005), suggesting that the lack of input topography may arise from the pattern of axonal terminals in the VTA. From the results of this thesis we will add another factor that might be contributing to this phenomenon which is the overall size and orientation of the VTA DA neurons dendritic tree within their nucleus.

2.4 Inputs Distribution onto the Somatodendritic Domain.

In the 1950's first appeared evidence that action potentials (AP) were initiated near the soma, in the axon initial segment (AIS). It was later confirmed using direct recordings in the axon (Palmer and Stuart, 2006; Schmidt-Hieber et al., 2008), indicating that not only the intrinsic features of an input (i.e. neurochemistry) are important in the production of the AP, but also, where in the dendritic tree that input is placed, because its location may affect its capacity to influence the membrane potential at the location the AP is being produced. Because, in midbrain DA neurons the AIS, although usually born from a dendrite and not from the cell body, is relatively close to the soma (~32 μm (Meza et al., 2018)) it is still reasonable to perform location analyses centered on the cell body, which is significantly more easy to identify.

It has been well stablished that VTA neurons receive glutamatergic inputs from cortical, but mainly from subcortical regions (D. B. Carr and Sesack, 2000; Geisler et al., 2007; Omelchenko and Sesack, 2007; Sesack and Grace, 2010). Cortical inputs derive mainly from the medial and lateral prefrontal cortex (Geisler et al., 2007) and subcortical excitatory afferents come from the lateral hypothalamus, lateral preoptic area, lateral habenula, pedunculo pontine nucleus and laterodorsal tegmental nucleus among others (Geisler et al., 2007) (Sesack and Grace, 2010). GABAergic innervation comes, mostly, from NAc, ventral pallidum, rostro-medial tegmentum (RMTg) and GABA neurons within the VTA (Jhou et al., 2009; Kalivas et al., 1993; Omelchenko and Sesack, 2009; Usuda et al., 1998; Watabe-Uchida et al., 2012) but also likely from lateral hypothalamus, lateral septum, periaqueductal grey, pedunculopontine nucleus, latero-dorsal tegmentum, among others (Geisler and Zahm, 2005)

Furthermore, several studies have shown that both glutamatergic and GABAergic inputs into VTA dopaminergic cell play a major role in modulating its activity (Chergui et al., 1993; Erhardt et al.,

2002a; Mercuri et al., 1992; Waroux et al., 2005). However, few have looked at how these inputs might be distributed onto VTA DA neurons, as such if there is, for example, a preference of inhibitory innervation at the cell body or if some dendrites receive more excitatory synapses. Regarding this subject, a study by Smith and collaborators, using EM and immunohistochemistry in squirrel monkey brain preparations, noted that VTA DA neurons dendrites received consistently more glutamatergic enriched terminals with more than 70% in distal dendrites versus 30-40% in distal dendrites of SNc DA neurons (Smith et al., 1996). Moreover, a more recent study in the rat, also quantified the synapses in the cell bodies and proximal dendrites of VTA DA neurons using electronic microscopy (Sizemore et al., 2016). They found that there were, 63% and 79% of symmetric synapses in cell bodies and proximal dendrites respectively (Sizemore et al., 2016).

In summary, we completed a thesis that studies factors that underlie the firing behavior of VTA DA neurons, specifically, on one hand the morphology and geometry of these neurons dendritic trees and on the other, how the innervation pattern onto the somatodendritic domain of glutamatergic and GABAergic inputs may explain the spontaneous and driven activity to an aversive stimulus. To accomplish the study, we recorded and labelled VTA DA neurons *in vivo* and immunohistochemically marked PSP on individual neurons. Labeled neurons were three dimensionally reconstructed and PSPs were counted and located on the different neuronal compartments. Finally, we correlated the baseline and aversive stimulus response electrophysiological recordings with morphological and synaptic contacts distribution data.

3. Hypothesis.

There is a relationship between the afferent innervation pattern and the spontaneous and aversive stimulus driven activity of VTA DA neurons.

4. General Aim.

Describe the dendritic tree and determine the relationship between the innervation pattern, the spontaneous activity and the response to an aversive stimulus in VTA DA neurons.

5. Specific Aims.

1. Anatomically describe the dendritic tree organization of single VTA dopaminergic neurons.

2. Estimate the number and describe the localization onto the somatodendritic tree of putative glutamatergic and GABAergic synaptic contacts that individually labeled VTA DA neurons receive.

3. Analyze the spontaneous and driven electrophysiological activity of VTA DA neurons.

4. Correlate the innervation pattern with spontaneous activity and with the response to an aversive stimulus.

The material and methods sections of this thesis are included within the Results sections 6.1.2 and 6.2.1. as if they were both parts of two different manuscripts.

6. Results.

6.1. Anatomical Description of Single VTA and SNc DA Neurons Dendritic Tree Organization.

This section contains a manuscript in preparation

6.1.1. Introduction.

Dopaminergic neurons of the substantia nigra pars compacta (SNc) and ventral tegmental area (VTA) are involved in important brain functions, including motor control, behavioral reinforcement and learning (Fahn, 2008; Gantz et al., 2018; Wise, 2004) SNc and VTA dopaminergic neurons differ in various aspects, including not only the efferent and afferent connections they establish with forebrain and hindbrain regions (Beier et al., 2015; Sanchez-Catalan et al., 2014; Watabe-Uchida et al., 2012; Yetnikoff et al., 2014), but also the specific cellular mechanisms responsible for spontaneous firing pattern (Gantz et al., 2018; Roeper, 2013), their differential susceptibility to neurodegeneration (Brichta and Greengard, 2014) and, when considering dopamine release onto respective major striatal outputs, differential involvement in limbic and sensorimotor aspects of addictive processes (Willuhn et al., 2012). These differences have led to the notion concept of a “motor” SNc vs a more “limbic” VTA (discussed in (Wise, 2009)).

In most central neurons, the vast majority of afferent inputs reach the dendritic domain (Gulyás et al., 1999; Häusser et al., 2000; Henny et al., 2012) and, along with its structural organization, the dendritic domain is essential to the electrical, integrative and computational capabilities of neurons (Häusser et al., 2000; Spruston, 2008; Vetter et al., 2001). In dopaminergic

neurons, dendrites have been shown to play a role in synaptic integration and activity profile (Hajós and Greenfield, 1994; Häusser et al., 1995; Henny et al., 2012; J. Jang et al., 2014; M. Jang et al., 2011; López-Jury et al., 2018; Meza et al., 2018; Moubarak et al., 2019; Vetter et al., 2001).

Based on this evidence, we carried out a descriptive and comparative analysis on various morphological characteristic of the dendritic domain of individual SNc and VTA of the mouse, with the hypothesis that differences in dendritic organization between (or among) these two populations, may underlie or relate to differences in function between these two populations.

An important number of studies have looked already into individual SNc neurons morphology (Grace and Bunney, 1983; Henny et al., 2012; Juraska et al., 1977; Tepper et al., 1987; Yelnik et al., 1987), to name a few), and described the basic features of their dendritic tree, including number of primary dendrites and arborization, main orientation axis and the presence of specialized dendritic projections onto the underlying SNr. Yet apart from quantitative studies carried out in primates (François et al., 1987; Yelnik et al., 1987) and rats (Henny et al., 2012; Moubarak et al., 2019), reports have been usually qualitative and for the most part two-dimensional descriptions. Also, apart from recent studies (Meza et al., 2018) none has looked the organization of the dendritic tree in the mouse.

In the case of VTA the number of studies is much scantier. Early studies reported VTA neurons dendritic organization in the rat using the Golgi method and 2D projections, so were highly dependent on the orientation of tissue processing (Kline and Felten, 1985; Phillipson, 1979a). Critically, several of these studies looking at the morphology of individual VTA neurons did not distinguish between the different neurochemical phenotypes that we now know are present in this region (Morales and Margolis, 2017)

Using in vivo juxtacellular labeling, high-resolution confocal microscopy acquisition and vector-based reconstruction (Ascoli, 2006) of the complete somatodendritic domain (SD) of 12 SNc and 13 VTA dopaminergic neurons of the adult mouse, we characterized and compared the size, complexity and organization of the dendritic domain of SNc and VTA individual neurons in the adult mouse, including its physical extension, orientation and, by analyzing the neurons convex hull volume, receptive domains. We further examined the size of neurons in relation to the entire SNc or VTA, and carried out a comparative analysis on the degree to which SNc or VTA neuron overlap with neighboring neurons.

6.1.2. Material and Methods

6.1.2.1. Animals. Experimental procedures were performed on adult male mice C57BL/6 strain obtained from the animal house at the Faculty of Biological Sciences, Pontificia Universidad Católica de Chile, and were approved by the Ethics Committees of the School of Medicine of the Pontificia Universidad Católica de Chile and of the Comisión Nacional de Investigación Científica y Tecnológica (CONICYT), both of which conform to the guidelines of the U.S. National Institutes of Health (NIH).

6.1.2.2. Recording and labeling of single midbrain neurons. Ten SNc neuronal reconstructions come from a pool of neurons which had their electrophysiology, general dendritic arrangement and axon initial segment described (Meza et al., 2018), and were deemed suitable for further anatomical analysis. Two recently labelled and reconstructed SNc were added to the group. For VTA, experiments were performed in 30 mice (23–30 g) of which we obtained 23 neurons and of which 12 were finally reconstructed. Anesthesia was initially induced with isoflurane (Isoflurano USP, Baxter Healthcare), and maintained with urethane (1.5 g per kg, i.p., ethyl carbamate, Sigma). Animals were placed in a rat stereotaxic frame adapted to mouse using a MA-6N head-holding adaptor (Narishige). Body temperature was maintained at 37°C using a homeothermic heating device (ATC 1000, World Precision Instruments). Anesthesia levels were assessed by examination of the electrocorticogram (ECoG) and by testing reflexes to a cutaneous pinch or gentle corneal stimulation. Topical benzocaine (20%, Mayon) and PBS solution, pH 7.4, were applied to all surgical incisions to prevent pain and dehydration, respectively. Extracellular recordings of single-unit activity were made using borosilicate glass electrodes (1 – 1.5 μm

diameter, tip resistance 10–15 M or <1 μm diameter and tip resistance 35 - 45 MΩ depending on the labeling method used [see below]; World Precision Instruments), obtained using a vertical puller (Narishige Scientific Instrument Laboratory PC-10 model). Pipettes were filled with a solution consisting of 0.5 M NaCl or 0.25 M K^+-gluconate and 1.7% neurobiotin (w/v; Vector Laboratories). A single-axis in vivo micromanipulator (IVM-1000; Scientifica) connected to an ultralow noise IU controller rack was used to descend electrodes in the z-axis into the brain. Stereotaxic coordinates for ventral tegmental area single-unit recording were derived from Franklin and Paxinos (2007) (AP: -3.1 mm, ML: 0.4 mm, see Meza et al. 2018 for description of experiments for SNc neurons labeling). After the neuronal activity was stable, spontaneous firing was recorded for at least 3 min. Following the recordings, neurons were labeled by the juxtacellular method (Pinault, 1996) or intracellular methods. Briefly, in the first method, the electrode was advanced slowly toward the neuron while a microiontophoretic square current was applied (2–10 nA positive current, 200 ms duration, 50% duty cycle). The optimal position of the electrode was identified when the firing of the neuron was robustly modulated by the positive current injection. Modulation was performed for at least 5 min to obtain reliable labeling. An almost identical protocol was used for SNc neurons recording and labeling (see (Meza et al., 2018) for further details). In the second protocol, after the extracellular recordings were made, using a 35-50 ΩM electrode, AC pulses were given in order to gain intracellular access. The amount of current in each AC pulse was progressively increased and the electrode moved closer in 2 μm steps, until the intracellular medium was accessed (evidenced by spike waveform change from biphasic to monophasic and a small negative shift in potential measured by the electrode; 5 to 25 mV). Then, if necessary, the electrode was moved up to 2 μm closer to the cell and the recording stabilized by negative current. for labeling, a micro square current was applied (0.4 – 1 nA positive current,

200 ms duration, 50 % duty cycle) for 10 – 20 minutes. In both protocols, after current injection, the neurobiotin was left to transport along neuronal processes for at least 2 h. After the labeling sessions, the animals were perfuse-fixed with 25 ml of PBS, pH 7.4, followed by 50 ml 4% paraformaldehyde (w/v) in phosphate buffer, pH 7.4. Finally, the brains were postfixed in 4% paraformaldehyde in PBS overnight, maintained in 30% sucrose in distilled water for 48 h, and sectioned.

6.1.2.3. Neuronal identification. The brains were cut in the coronal plane on a freezing-stage microtome (Reichert–Jung Hn-40) at 25 or 40 μm. All VTA containing sections were incubated with Cy3-conjugated streptavidin (1:1,000, Jackson ImmunoResearch) for 2 - 3 h to reveal the neurobiotin. After mounting, the sections were examined with an epifluorescent microscope (Nikon Eclipse Ci) to confirm that neurons were completely filled with tracer. One or two sections were selected, blocked with 3% normal horse serum (NHS) in PBS (v/v; Jackson ImmunoResearch), and incubated with guinea-pig anti tyrosine hydroxylase (TH) antibody (1:10,00; Synaptic Systems) in PBS 3% NHS, and 0.3% Trinton-X overnight at room temperature. They were then incubated in Alexa Fluor 488 or Dylight 405-conjugated donkey anti-guinea pig antibody (1:1,000; Jackson ImmunoResearch). Three to four 8 min washes were performed in between and after incubation in streptavidin or antibodies. Labeling for neurobiotin and colocalization of neurobiotin-labeled processes with TH was assessed. Only those neurons that were neurochemically identified as VTA DA neurons by immunoreactivity for TH were further analyzed. An almost identical protocol was used for SNc neurons identification (see Meza et al., 2018 for further details).

6.1.2.4. Microscopy and imaging. Fluorescence imaging for all neurobiotin-labeled profiles across sections was performed with either one of the three following laser-scanning confocal microscopes: Nikon Eclipse C2, using NIS-Elements C program (Nikon software) to acquire and export images (3 neurons), a Zeiss LSM 700, using ZEN2012 program (Zeiss software) (2 neurons) and Olympus FV1000 using Fluoview program (Olympus software) (7 neurons). Low-magnification images were acquired with appropriate 10x and 20x objectives. High-magnification and z-stack images were acquired with a 60 oil or water-immersion objective (1.3 - 1.4 numerical aperture). Images taken for 3D neuronal reconstruction were 512x512 pixels in size with resolution of 0.19 or 0.41 μm/pixel and taken in z-stacks of 0.5 μm steps between images. To ensure the best signal-to-noise ratio in all stack images, maximum and minimum intensity pixels were established independently in each channel and for each z-stack acquired during the acquisition sessions using the appropriate software. An almost identical protocol was used for SNc neurons microscopy and imaging (see Meza et al., 2018 for further details).

6.1.2.5. Neuronal reconstructions. All neurons that were selected for digital reconstruction were completely filled and all of the dendrites extended to natural tapering ends. Axons were usually traced for longer distances on their way to the forebrain. Neurons were reconstructed in three dimensions from all z-stack images taken with the confocal microscope using Neurolucida (MicroBrightField). Neuronal fragments from every section were traced onto a corresponding digital section using the Serial Section Manager in Neurolucida (Henny et al., 2012; 2014; Meza et al., 2018). For the entire somatodendritic domain, a correction factor in the z-axis was applied to account for the shrinkage that follows dehydration and histological processing, which in our

hands is 50%. Quantitative data for anatomical parameters were obtained using the Neurolucida Explorer software.

6.1.2.6. Morphological Analyses. To determine the location of each reconstructed SNc and VTA neuron, double immunostaining for TH and neurobiotin was performed in the section containing the soma or the adjacent section if the cell body was missing. Images were acquired in a Nikon Eclipse C2 laser-scanning microscope or an Olympus FV1000 Confocal System. The SNc and VTA were delimited in the TH-stained cell body section and compared to the sections provided by Fu et al. (2012) and Franklin and Paxinos (2007). Then, a three-dimensional rendering of the substantia nigra (SN, including pars compacta (SNc), pars lateralis (SNl), and pars reticulata (SNr)), all VTA sub-regions (including rostral VTA (VTAR), parabrachial pigmented (PBP), paraintrafascicular (PIF), paranigral (PN), infrascicular (IF), and caudal (CLi) and rostral (RLi) linearis), and relevant landmark tracts or nuclei, was created in Neurolucida from the data published in Fu et al. (2012). Individual neuronal reconstructions were placed in the 3D rendering according to the medio-lateral (ML), dorso-ventral (DV) and antero-posterior (AP), location of the cell body, obtained from the TH immunostaining and further tilted-corrected by matching the position of the furthest dendritic tips to anatomical landmarks. Reconstructions of neurons labeled in the left hemisphere were vertically flipped and projected onto the right hemisphere.

To evaluate the orientation of the dendritic trees a 3D wedge analysis from Neurolucida Explorer software was performed. Briefly, the analysis shows the distribution of the processes as they extend from the centroid of the cell body in every direction. To achieve this the neuron is placed in the center of a cylinder, which was divided in 4 angular wedges, and in 4 parallel planes perpendicular to the direction of the cylinder, each plane 25% of the maximum extent of each

neuron in that direction. For instance, if the cylinder is placed parallel to the antero-posterior axis, the four angular wedges report the location of the processes in the dorso-medial, ventro-medial, ventro-lateral and dorso-lateral quadrants, at each of the four planes defined in the AP axis (see Fig 5A).

6.1.2.7. Convex hull volumes, maximal extensions, filling factor and overlap analysis. Convex hull volumes, and maximal ML, DV and AP dendritic extensions of individual neurons were calculated directly in the Neurolucida Explorer software. 3D filling factor was derived from its 2D equivalent "coverage factor" used in sensory receptive fields studies (Farajian et al., 2004; Lefebvre et al., 2015). In our study, it was calculated by multiplying the average convex hull volume by the estimated number of neurons in the region, divided by that region volume (Table 2).

For convex hull intersection analysis, a custom Matlab code was used. Reconstructed neurons and their exact coordinates on SNc and VTA were used (see above). Segment points-dendrites data files from each reconstructed neuron were obtained from Neurolucida Explorer and used to obtain the 3D convex hull volume from each neuron and confirmed with those obtained directly from Neurolucida Explorer. Then, the inside of a neuron convex hull was filled with points using Matlab 'ndgrid' function. This allows to have an exact point-grid representation of a neuron 3D convex hull. Using the point-grid representation of each neuron 3D convex hull, the intersection between neuron-pairs point-grid convex hull's within SNc and VTA was performed using Matlab 'intersect' function. Finally, the convex hull from the intersected point-grid was calculated (Intersected volume). The intersected ratio between a pair of neurons convex hull's was calculated as follows:

$$\text{Intersected ratio} = \frac{\text{Int}}{\text{CVH1} + \text{CVH2} - \text{Int}}$$

with Int being the intersected volume, CVH1 the convex hull from the first neuron of the pair and CVH2 the convex hull from the second neuron of the pair. The Euclidian distance between pairs of neurons cell bodies centroids was determined, using the Matlab 'norm' function.

6.1.2.8. Statistical Analysis. To assess whether data sets were normally distributed, we performed single sample Kolmogorov-Smirnov test or, if the n was too small, Shapiro-Wilk normality test using GraphPad Prism 7 in all data sets. In normally distributed datasets one-way or two-way ANOVA with Tukey's post hoc testing were performed using GraphPad Prism 7. Nonparametric tests were used in non-normally distributed data; Kruskal-Wallis with Dunn's post hoc testing and two-tailed Mann-Whitney U test were performed using GraphPad Prism 7. Significance for all statistical tests was set at $p < 0.05$. Boxplots are explained in figure 6 legend.

6.1.2.9. Code Accessibility. All custom Matlab codes will be available upon request.

6.1.3. Results

We were able to study the entire somatodendritic domain of midbrain dopaminergic neurons by using juxtacellular labeling of single neurons with neurobiotin (Nb); one neuron per hemisphere either in the SNc (Meza et al., 2018) or the VTA. A requirement for reconstruction was that neurons had to have complete labeling of their cell body, the dendritic tree, and at least part of axon as it heads up towards the forebrain. Nb labeled neurons were identified as dopaminergic by the expression of the catecholamine synthetic enzyme tyrosine hydroxylase (TH) (Fig. 1A). We determined the ML, DV and AP location of the reconstructed neurons' cell bodies in relation to the standard map of Fu et al. 2012 (Fig. 1B) and complemented with the atlas of Franklin and Paxinos (2007) when necessary (Fu et al., 2012; Paxinos and Franklin, 2007).

The cell bodies of the sampled labeled SNc neurons located centrally (ML), although with a tendency towards posterior (AP) levels (see dorsal view, Fig. 1C). Cell bodies of VTA neurons were mostly located medial to the medial lemniscus (ml), in the PBP, and at various DV depths (Fig. 1B). One neuron located in the PBP lateral to the ml (dorsal to the SNc), another in the PN and another in the limit between rVTA and PBP (Fig 1C-D).

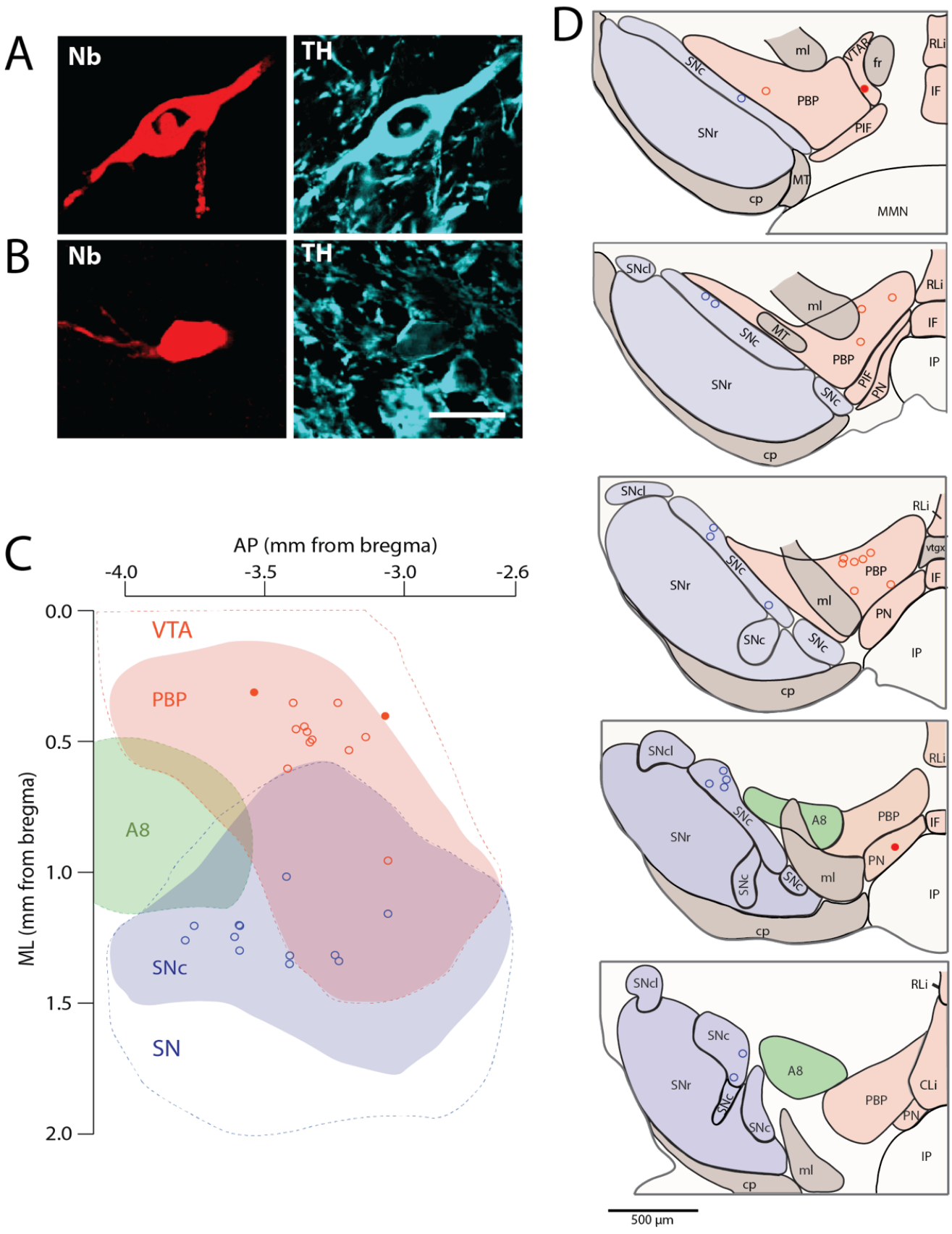
A
Nb
TH
B
Nb
TH
C
AP (mm from bregma)
-4.0
-3.5
-3.0
-2.6
ML (mm from bregma)
0.0
0.5
1.0
1.5
2.0
VTA
PBP
A8
SNc
SN
D
SNc
SNr
ml
VTAR
fr
RLi
IF
PBP
PIF
MT
cp
MMN
SNcl
IP
PN
vtgx
CLi
500 µm

Figure 1: Localization and identification of SNc and VTA dopaminergic neurons. (A-B) SNc **(A)** and VTA **(B)** neurons were labeled with neurobiotin (red, left) and expressed tyrosine hydroxylase immunoreactivity (cyan, right). **(C-D)** Location of cell bodies of the twelve SNc and thirteen VTA dopaminergic neurons used in this study in one dorsal view **(C)** and 5 frontal views **(D)**. Scales bars represent 25 µm **(A-B)** and 500 µm **(D)**. AP, anteroposterior; ML, mediolateral; CLi, caudal Linear nucleus; cp, cerebellar peduncle; fr, fasciculus retroflexus; IF, interfascicular nucleus; IP, interpeduncular nucleus; ml, medial lemniscus; MMN, medial mammillary nuclei; MT, medial terminal nucleus; PBP, parabrachial pigmentosus nucleus; PIF, parainterfascicular nucleus; PN, paranigral nucleus; RLi, rostral linear nucleus; SNc, substantia nigra compacta; SNcl, substantia nigra compacta, lateral; SNr, substantia nigra reticulata

6.1.3.1 Ventral VTA neurons are smaller and less complex than dorsal VTA neurons

The dendritic tree of labeled SNc and VTA dopaminergic neurons was observed and analyzed in their physical (length, surface area, volume) and topological (number of primary trees, segments, branch order) characteristics (Fig. 2 and Table 1). As also evident from examining the reconstructions (Fig. 2), quantitative data (Table 1) showed SNc and VTA neurons were diverse, with differences of up to 3-fold or 4-fold in physical and topological parameters. Although we did not notice any obvious difference between SNc and VTA neurons in these aspects, we did notice that more ventrally located VTA (vVTA) neurons appeared smaller than more dorsally (dVTA) located neurons (Table 1, Fig 2 B2). We compared the three groups and found that vVTA neurons had reduced dendritic length (One-way ANOVA $F_{(2,22)} = 4.517$, $p = 0.023$, Tukey's *post hoc* dVTA vs vVTA, $p = 0.032$) and dendritic surface area (One-way ANOVA $F_{(2,22)} = 5.5$, $p = 0.01$, Tukey's *post hoc* dVTA vs vVTA, $p = 0.035$) as well as maximum dendritic order (Kruskal-Wallis $p = 0.01$, Dunn's *post hoc* dVTA vs vVTA $p = 0.009$) and number of segments (Kruskal-Wallis $p = 0.03$, Dunn's *post hoc* dVTA vs vVTA $p = 0.046$) than dVTA neurons. When comparing either dVTA or vVTA neurons with SNc neurons, however, we found no significant differences, with the exception of the dendritic surface, which overall appeared larger in dVTA vs SNc neurons (one-way ANOVA, $F_{(2,22)} = 5.5$, $p = 0.01$, Tukey's *post hoc* dVTA vs SNc $p = 0.0167$; Table 1). Even though SNc neurons were diverse (Fig. 2), we did not observe any obvious relation between localization of these neurons and physical or topological characteristics. In summary, while SNc and dVTA neurons do not appear different from each other, dVTA neurons are larger and topologically more complex than vVTA neurons.

Additionally, we noticed it was fairly common, for both SNc and VTA neurons, that second or even first order dendrites had small diameters (> 2 μm, not shown), indicating that the assumption a thin/distal vs thick/proximal dichotomy for SNc and VTA neurons dendrites should not be considered a rule. Moreover, we would occasionally detect spine-like appendices, which were very few in number and usually presented an amorphous and elongated morphology,

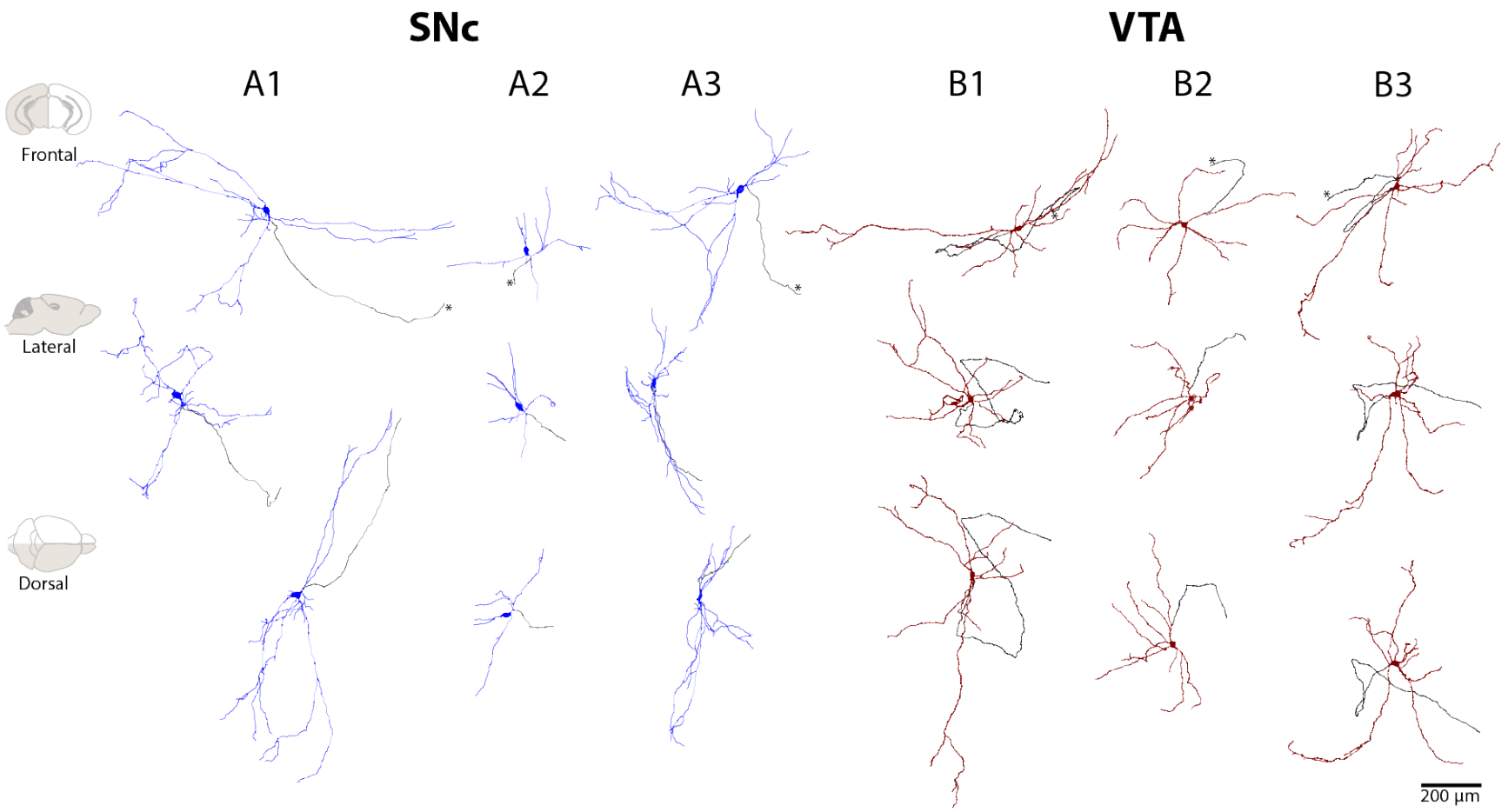
SNc
VTA
A1
A2
A3
B1
B2
B3
Frontal
Lateral
Dorsal
200 µm

Figure 2: Identified SNc and VTA dopaminergic neurons three-dimensional reconstructions. Three SNc (A1-A3) and three VTA (B1-B3) dopaminergic neurons seen from the frontal (top), lateral (middle) and dorsal view (bottom). A1 and B1 are representative neurons and A2-3 and B2-3 are neurons with a different (not representative) size and/or orientation of the dendritic tree. Axons are shown in black and pinpointed with an * in the frontal view. Scale bar represents 200 μm.

Table 1: Cell body and dendritic arbor size and complexity measures in VTA and SNc reconstructed neurons

Table 1: Cell body and dendritic arbor size and complexity measures in VTA and SNc reconstructed neurons

Parameter	SNc			VTA dorsal			VTA ventral			VTA total	
	Average	S.e.m.	Range	Average	S.e.m.	Range	Average	S.e.m.	Range	Average	S.e.m.
Dendritic Length (µm)	4,380	463	1,618 - 6,339	5,938 [1]	359	4,424 - 8,094	3,750 [1]	309	2,508 - 5,406	5,096	458
Dendritic Surface (µm²)	9,253 [2]	1,035	3,445 - 16,100	14,192 [1,2]	967	10,656 - 20,429	8,711 [1]	1,145	3,481 - 12,283	12,084	1,274
Convex Hull volume (mm³)	0.0398	0.0083	0.0038 - 0.0841	0.0595	0.0074	0.0135 - 0.1019	0.0315	0.0057	0.0097- 0.0551	0.0436	0.0073
Soma Surface Area (µm²)	1,769	245	765 - 3,168	1,584	202	817 - 2,927	1,050	104	670 - 1,575	1,378	183
Soma Volume (µm³)	5,523	861	2,427 - 11,236	4,798	722	2,017 - 9,348	2,792	416	1,450 - 4,928	4,026	669
Dendritic Trees N°	5.4	0.48	2 - 8	5.1	0.45	2 - 7	5.2	0.13	5 - 6	5.15	0.35
Max. Dendritic order	6.5	0.75	3 - 13	7.3 [1]	0.48	5 - 9	4.2 [1]	0.24	3-5	6.08	0.59
Number of segments	42.9	6.04	18 - 94	45.1 [1]	5.14	27 -74	23.2 [1]	2.05	15 - 32	36.69	5.2

1 Depending on the distribution of the data-sets a One-Way ANOVA or Kruskal-Wallis test with a Tukey's or Dunn's post-hoc test respectively, showed a significant difference between VTA dorsal and VTA ventral neurons in dendritic length (P = 0.032), dendritic surface (P = 0.035), number of segments (P = 0.0468) and Max. dendritic order (P = 0.0086) 2 One-Way ANOVA with a Tukey's post-hoc test showed a significant difference between VTA dorsal and SNc neurons in dendritic surface (P = 0.0167).

6.1.3.2. Differences in preferential distribution of dendrites between SNc and VTA neurons

In order to get an overall appreciation of the dendrites distribution in individual cells, we obtained the total dendritic length in each of four quadrants centered in the cell body as seen from frontal, lateral and dorsal views. To compare the distribution across neurons, we normalize by each neuron's total dendritic length. Because our interest was defining the total length of dendrites in each quadrant and not the orientation of each dendritic segment *per se*, we did not perform the traditional polar histogram provided in the Neurolucida Explorer software (as used for instance in Tahvildari and Alonso, 2005) but instead a *dendritic distribution polar histogram* to determine the total dendritic length in each region.

As shown in Fig. 3, it was observed that SNc neurons have a higher proportion of their dendrites located in the dorso-lateral quadrant, followed by the ventro-lateral, ventro-medial and lowest in in dorso-medial quadrants when analyzed from a frontal view (Fig. 3, top left). Both dVTA and vVTA individual neurons, instead, exhibit a high percentage of their dendritic tree located in dorso-medial and ventro-lateral quadrants, as seen from a frontal view (Fig. 3, top right). When analyzed from a lateral view, SNc neurons dendrites located for dorso-posterior and ventro-anterior quadrants (Fig. 3, middle, left) and both VTA neuron dendrites for posterior quadrants overall (Fig. 3, middle right). Finally, when observed from a dorsal view, SNc neurons dendrites are seen more laterally (Fig. 3, bottom left) and VTA neurons dendrites more posteriorly (Fig. 3, bottom right).

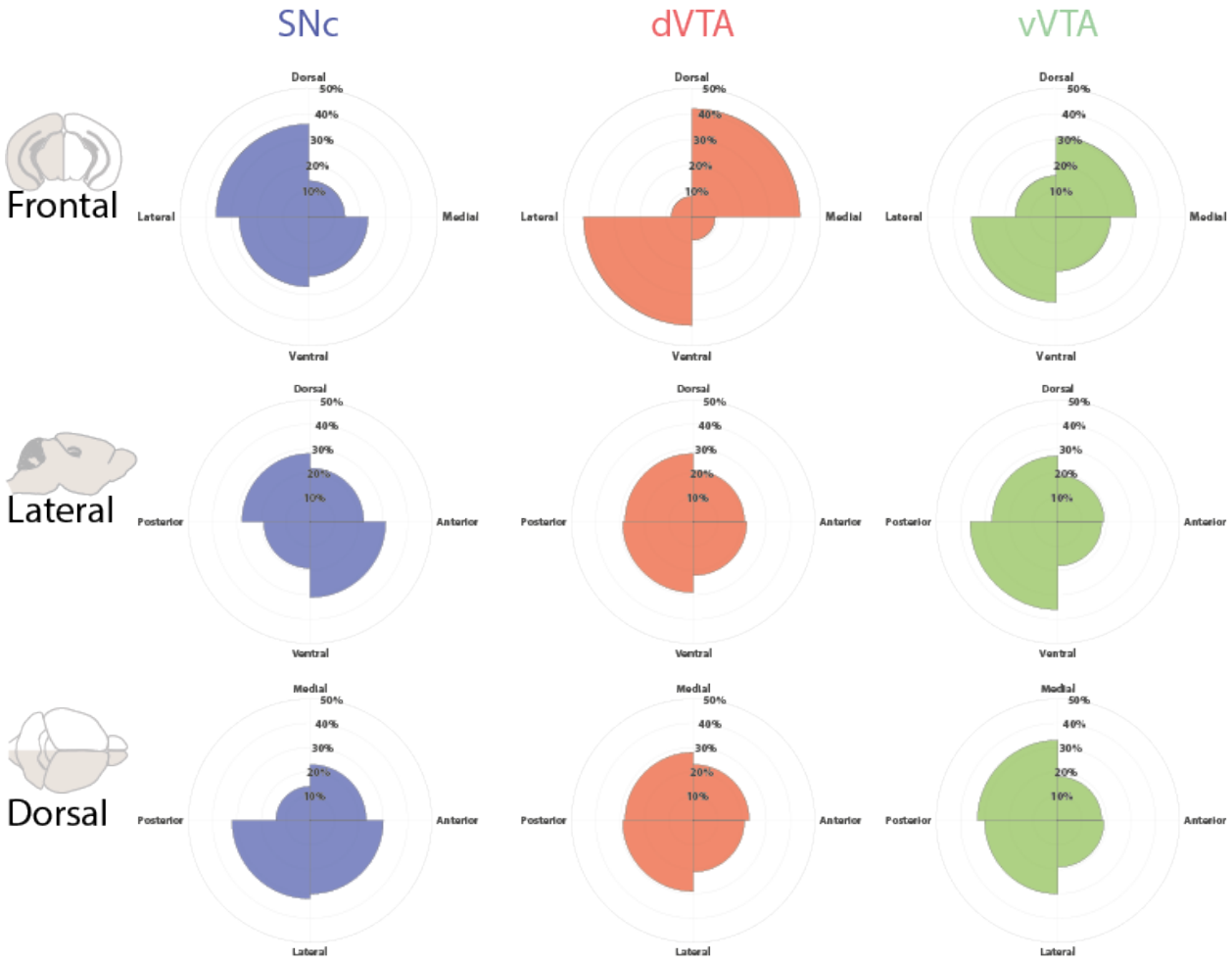

Figure 3: Orientation analysis of SNc and VTA DA neurons. Dendritic localization polar histograms from dendritic trees of SNc (left), dVTA (center) and vVTA (right) neurons show the orientation of their processes when the neurons are analyzed from the frontal (top), lateral (middle) or dorsal view (bottom). The length in each bin in the histogram is the sum of lengths that fall within that bin, expressed as percentage of the total dendritic length

To provide statistical support for these observations, as well as taking into account the natural 3D configuration of neurons, we performed a 3D wedge analysis (Fig. 4). In this analysis the neuron is placed in the center of a cylinder that runs parallel to a given axis and is divided into four angular quadrants and several planes that run perpendicular to the orientation of the cylinder, which defines the wedges. Then the total and percentage of dendritic length is calculated for each "wedge" (Fig 4A). We started by placing the cylinder parallel to the antero-posterior axis and defined four AP planes, each one extending 25% of the maximal dendritic length observed in the antero-posterior axis. We then calculated percentage of dendritic length in each of these 16 "wedges". We run a two-way ANOVA to compare proportion of dendritic length as function of wedge and region. Because dVTA and vVTA did not show obvious differences in dendritic distribution in any of the views analyzed, we pooled them together. As seen in Fig. 4B, differences concentrated in the two planes closer to the cell body: posterior plane 1 (two-way ANOVA, main effect of interaction $F_{(3,69)} = 10.72$, $p < 0.0001$; main effect of orientation $F_{(3,39)} = 4.58$, $p = 0.0055$) and anterior plane 1 (two-way ANOVA, main effect of interaction $F_{(3,39)} = 6.28$, $p = 0.0008$). Regarding SNc neurons dendritic trees, there were significantly more dendrites in the dorso-lateral position than in the dorso-medial and ventro-medial position of posterior plane 1 (D-M vs D-L, $p = 0.0073$; D-M vs V-M, $p = 0.0039$). In anterior plane 1 dorso-laterally located dendrites were significantly more than ventro-medial dendrites (D-M vs V-M, $p = 0.033$). For VTA neurons dendritic trees, posterior plane 1 had significantly more dorso-medially and ventro-laterally located dendrites than in the other orientations (D-M vs D-L, $p = 0.0007$; D-M vs V-M, $p = 0.0017$; V-L vs D-L, $p = 0.0008$; V-L vs V-M, $p = 0.002$). Similarly, in the anterior plane 1 there were more dendrites located in the dorso-medial and ventro-lateral position (D-M vs D-L, $p = 0.047$; D-M vs V-M, $p = 0.044$; V-L vs D-L, $p = 0.038$; V-L vs V-M, $p = 0.036$). In correspondence to

what was appreciated in Fig. 3, VTA neurons have a dorso-medial to ventro-lateral orientation which is more clearly seen in the dendritic distribution posterior to the cell body. It can be appreciated that compared to VTA neurons, SNc neurons have a higher percentage of their dendritic tree located dorso-laterally, either in the posterior plane 1 ($p < 0.0001$) or in the anterior plane 1 ($p = 0.0103$). On the other hand, VTA neurons had more dendrites than SNc neurons, located dorso-medially in the posterior plane 1 ($p = 0.0015$) and anterior plane 1 ($p = 0.032$). We ran further wedge analyses changing the main cylinder axis direction and found essentially similar results as those described above (data not shown). Wedge analysis results (Fig. 4) are consistent with the qualitative appreciation presented in Fig. 3 and indicate, in general, that the location of dendrites in SNc differ from VTA neurons, with the former presenting a bias towards dorso-lateral locations and the latter towards dorso-medial and ventro-lateral locations.

.

.

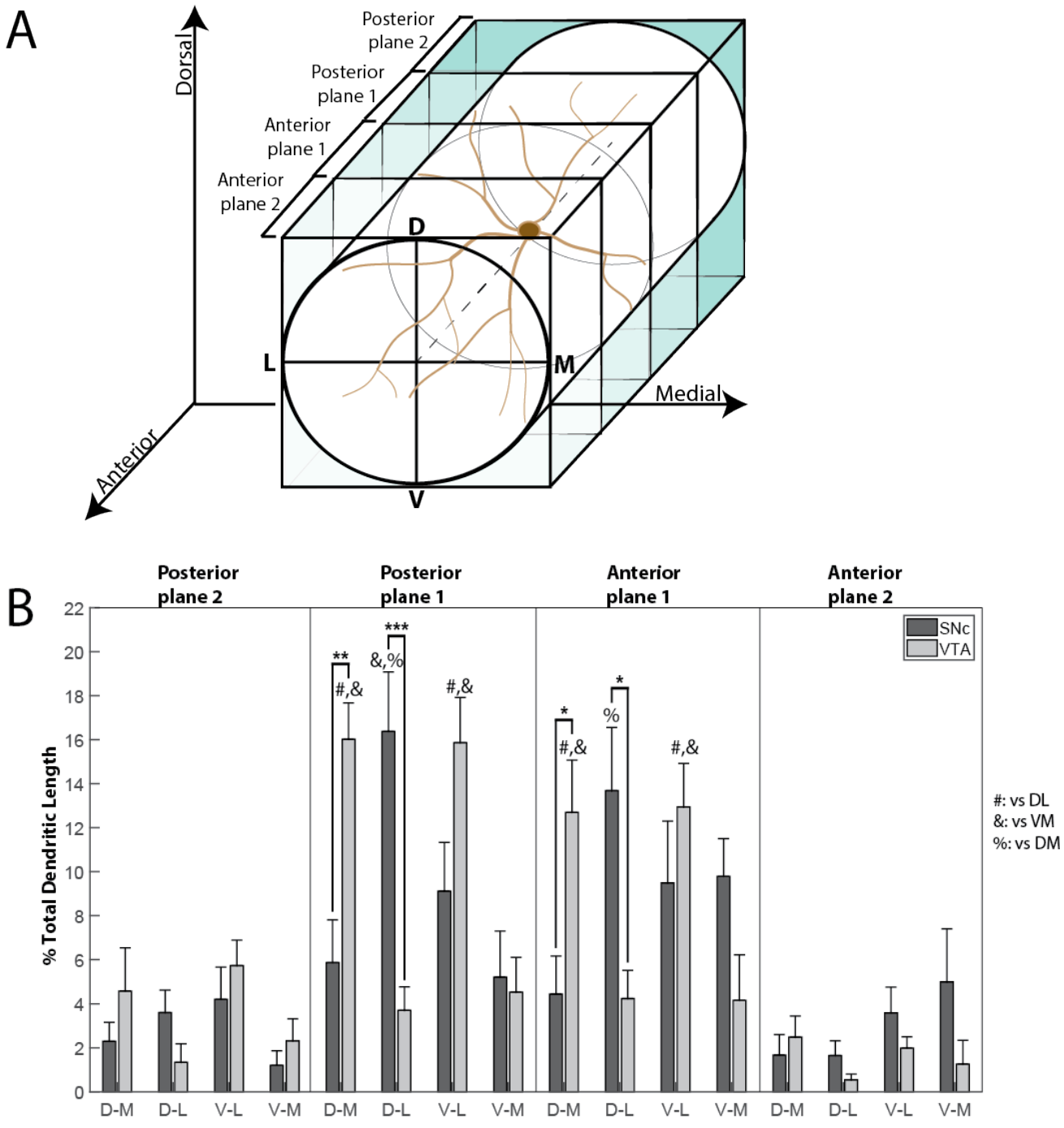

Figure 4: Three-Dimensional orientation analysis of SNc and VTA dopaminergic neurons. **(A)** Schematic illustrating the 3D wedge analysis, where the cell body centroid is placed in the center of a cylinder, which is divided in 4 angular wedges (D-M, D-L, V-L and V-M) and 4 planes (anterior 1, anterior 2, posterior 1 and posterior 2). The planes run perpendicular to the direction of the cylinder, each plane 25% of the maximum extent of each neuron in the anteroposterior axis.

(B) Orientation 3D wedge analysis of VTA and SNc dendritic trees show significant differences between areas at the posterior plane 1 (repeated measures two-way ANOVA, main effect of interaction $F_{(3,69)} = 10.72$, $p < 0.0001$; main effect of orientation $F_{(3,39)} = 4.58$, $p = 0.0055$, followed by Tukey's *post hoc* testing: $SNc_{D\text{-}M}$ vs $VTA_{D\text{-}M}$, $p = 0.0015$; $SNc_{V\text{-}L}$ vs $VTA_{V\text{-}L}$, $p < 0.0001$) and anterior plane 1 (repeated measures two-way ANOVA, main effect of interaction $F_{(3,39)} = 6.28$, $p = 0.0008$, followed by Tukey's *post hoc* testing: $SNc_{D\text{-}M}$ vs $VTA_{D\text{-}M}$, $p = 0.0322$; $SNc_{V\text{-}L}$ vs $VTA_{V\text{-}L}$, $p = 0.0103$). In SNc neurons there were also intragroup significant differences, between D-M vs D-L (%, $p = 0.0073$) and D-M vs V-M (&, $p = 0.0039$) orientations at posterior plane 1 and also, between D-M vs V-M (%, $p = 0.033$) at anterior plane 1. VTA neurons showed significant differences at posterior plane 1, between D-M vs D-L (#, $p = 0.0007$), D-M vs V-M (&, $p = 0.0017$), V-L vs D-L (#, $p = 0.0008$) and V-L vs V-M (&, $p = 0.002$) and at anterior plane 1, between D-M vs D-L (#, $p = 0.047$), D-M vs V-M (&, $p = 0.044$), V-L vs D-L (#, $p = 0.038$) and V-L vs V-M (&, $p = 0.036$). Error bars indicate S.e.m.

6.1.3.3. Mice midbrain dopaminergic neurons extend and occupy a large proportion of their respective nuclei regions.

To examine the organization of the dendritic domain as part of the region in which they locate, we created a common 3D map of SN and VTA and placed the reconstructions inside according to the location of their cell bodies (Fig. 5). An obvious first impression was the large size of the dendritic domain of individual neurons in relation to the size of the nuclei of origin, as it can be appreciated in the examples of individual neuronal reconstructions (Fig. 5). In fact, and as shown in detail in Table 2, the average relative maximal extensions of dendrites in SNc was of 51%, 42%, and 26% that of the ML, DV and AP extensions of SN Statistical comparison showed that relative AP extension in SNc neurons was significantly smaller from that of ML and DV (Kruskal-Wallis $p = 0.0013$ with Dunn's post hoc testing SNc AP vs SNc ML $p = 0.0023$ and SNc AP vs SNc DV $p = 0.0167$).). Average relative maximal extensions of dendrites in the VTA were 49%, 42% and 37% that of the ML, DV and AP extensions of the VTA. In this case, however, we did not find evidence for differences between them (Kruskal-Wallis $p = 0.156$). Also, we found that relative AP extension was smaller in SNc neurons than in VTA (Mann-Whitney test, $U = 34.5$, $p = 0.0164$, two tailed).

We used the convex hull volumes of SNc and VTA neurons (Fig 5A) to estimate their size in relation to the volume of the respective nuclei. Because an important proportion of dendrites of SNc neurons extended into the underlying SNr (see below), and occasional the SNl, we used the volume of the entire SN as the reference volume for SNc neurons. For VTA neurons, the reference volume was the added volume of all VTA nuclei according to Fu et al., 2012 (see Methods). The SN and the VTA had an estimated volume of 0.71 mm^3 and 0.43 mm^3, respectively. As shown in Table 2, the average relative volume of SNc and VTA neurons was 5.6% and 11% of their

respective region, a difference that was statistically significant (Students t-test, $p = 0.012$, two-tailed).

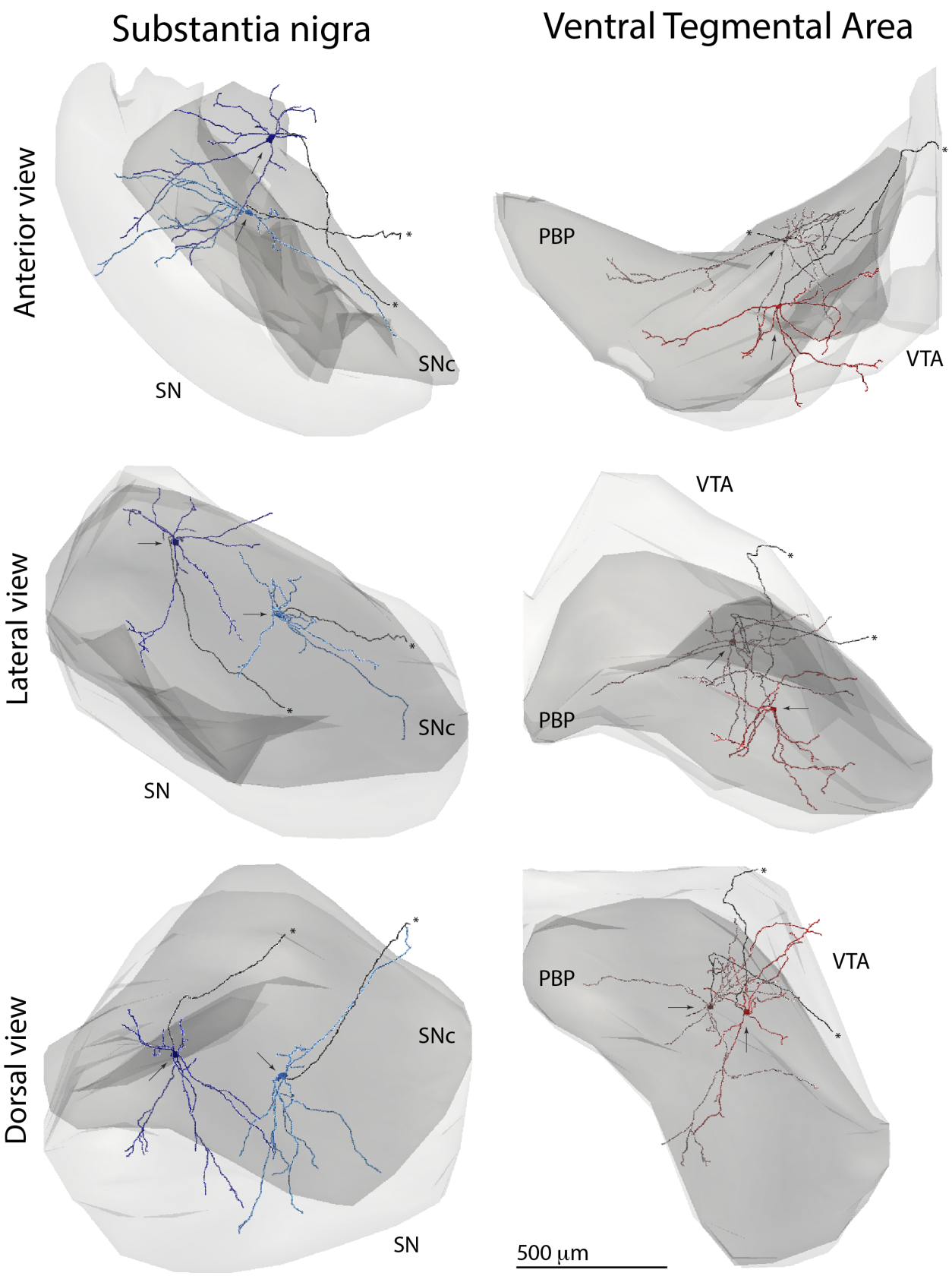
Substantia nigra
Ventral Tegmental Area
Anterior view
Lateral view
Dorsal view
SNc
SN
PBP
VTA
500 µm

Figure 5: Relative size of SNc and VTA dopaminergic neurons with respect to their nucleus in the mouse. Two reconstructed SNc (left) and two reconstructed VTA (right) neurons are shown inside their nucleus in an anterior (top), lateral (middle) and dorsal view (bottom) to illustrate how much big they are respective to their nucleus. * indicates de axon and arrows indicate location of the cell bodies. Scale bar = 500 μm.

Table 2: Relative dimensions and filling factor of SNc and VTA neurons in relation to region

Item	SNc			VTA		
	Average	S.e.m.	Range	Average	S.e.m.	Range
Max. ML extension	738.3	91.2	233.5 - 1269.9	770.4	53	523.4 - 1092.2
% max. ML extension	51.2	6.3	16.2 - 88.1	49.2	3.4	33.4 - 69.7
Maximal DV extension	591.7	36.8	381.2 - 827.9	576.5	39.2	308.1 - 783.5
% max. DV extension	41.8	2.6	26.9 - 58.4	41	2.8	21.9 - 55.8
Maximal AP extension	366.4	45.4	185.0 - 607.4	549.4	48.2	225.2 - 937.2
% max. AP extension	25.6	3.2	12.9 - 42.4	39.6	3.5	16.2 - 67.6
Relative volume to region*	5.6	1.2	5.4 - 11.9	11.5	1.8	2.3 - 23.9
Filling factor**	350.8	73.4	33.6 - 740.6	1000.2	152.8	199.8 - 2095.2

*Relative volume to region is the neurons' CHV (see Table 1) relative to region volume (see Results). **Filling factor is relative volume times the number of TH+ cells in SNc and VTA, as taken from the literature. Cell counts were taken from McCormack et al 2007 (~6250 for SNc and ~8750 for VTA per hemisphere, which are approximate values taken from bilateral counts provided in bar charts). See Results.

Another aspect of dendritic organization we considered was the degree to which dendrites of a given region or nucleus cross-over to adjacent ones (Fig. 6). Considering the entire sampled population, while dendrites of SNc neurons tended to stay in the SN (above 75% of total dendritic length, with over 40% of dendritic length in SNc and over 30% in SNr), a proportion of dendrites cross-over to innervate the medially located PBP (~10%) or the dorsal tegmentum located above the SN (~10%). In the case of VTA neurons, around 90% of dendritic length stayed within the boundaries of the VTA, with some neurons sending dendrites into the adjacent SN (~5% of all estimated dendritic length, Fig. 5A) or towards adjacent mesencephalic or p1 reticular formation (not shown, also ~5%). Finally, most dendrites within the sampled VTA neurons stayed in the PBP (above 70%), and around 10% extended into PN, PIF, or midline VTA nuclei, not shown). Because the extent to which each neuron crosses-over to adjacent regions heavily depends on its location near or far from the limit of the region or nucleus, further systematic studies may be necessary to quantify in greater detail crossing-over phenomena in this population.

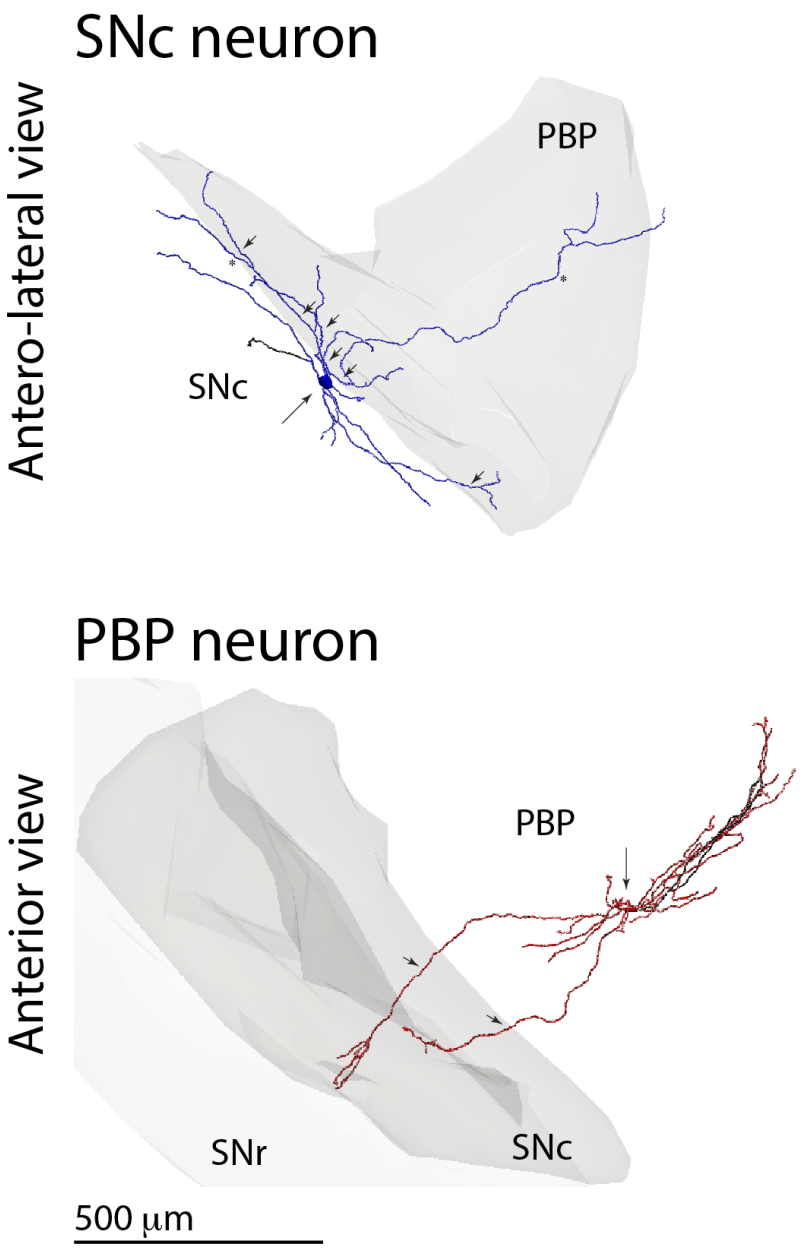

Figure 6: Crossing over of SNc and VTA dopaminergic neurons dendritic processes. Top, an example of a SNc neuron that sends dendrites outside the SNc into the VTA subnucleus, PBP. Bottom, a VTA neurons that sends dendritic processes outside the VTA, into the SNc. Large arrows indicate position of the cell body. Small arrows are indicating dendritic processes outside their nucleus. Scale bar = 500 µm.

6.1.3.4. Receptive Space and Overlap Among Midbrain Dopaminergic Neurons

Given the large size of individual neurons in relation to their region of origin, we wondered how much overlap there exist between neighboring SNc or VTA neurons. For that, we calculated a "filling factor" for SNc and VTA neurons, which is the 3D equivalent to the 2D "coverage factor" used for sensory receptive fields and that is defined as the "average number of cells that cover a single point in space with their dendrites" (Farajian et al., 2004; Lefebvre et al., 2015). Using published stereological estimates of TH+ cells from McCormack and collaborators report (McCormack et al., 2006) the filling factor for the SNc is ~350 and ~1001 for the VTA neurons (VTA to SNc ratio of 2.86), a difference that was statistically significant (Table 2). Filling factors calculated using other stereological TH+ cell estimates for SNc and VTA, as provided in Coban and Filipov and Prasad and Richfield reports (Coban and Filipov, 2007; Prasad and Richfield, 2008), although different due to differences in absolute cell numbers (not shown), resulted nonetheless in similar VTA to SNc "fillingness" ratios of 3.40 and 2.37, respectively. These data indicate that VTA neurons tend to "fill" the VTA more than SNc neurons the SN.

Although overall conclusive, results from the filling factor analysis have some caveats, because it depends 1) on accurate estimates of cell numbers in the SNc and VTA, and 2) the assumption that dendrites stay within the limits of their respective regions, something true for the majority of, but not all, dendrites (see above). Additionally, the provided filling factor analysis does not consider either the convex hull (geometry that could affect the degree of overlap between neurons (e.g. "rounder" neuron vs. "flatter" neuron). Because of that, we took a more direct approach and asked how much of the convex hull volume could be overlapping between pairs of neighboring neurons without dismissing shape, orientation or distance between neurons and without assumptions on the size, organization or cell density of the respective regions. To do that,

we took the convex hull of each neuron's dendritic domain (Fig 7A-B) and then evaluated, according to the position and orientation experimentally determined for each neuron inside their region (Fig. 1), how much of its convex hull volume overlapped with the convex hull of every other neuron in pairs. Because the convex hull volume of dVTA and vVTA neurons was not statistically different (Table 1) and the dendrites distribution was also similar (Fig. 3) we pooled them back together as VTA neurons. We checked that the average convex hulls of SNc and VTA groups did not statistically differ (Table 1). We also controlled for the distance between pairs of our sampled neurons cell bodies and found that the difference was not statistically significant (Mann-Whitney, U= 2147, $p = 0.087$, two tailed; Fig. 7C). We then calculated an intersected ratio between two neurons as the ratio of the intersected volume divided by the added non-intersected volume of the pair (ie: the added convex hull of the two neurons less the intersected volume), and whose minimal and maximal values were: 0 (0%) for cells which did not overlap and 1 (100%) for perfectly overlapped cells. We calculated the percentage of pairs as a function of intersection ratios and found that the number of SNc neuronal pairs were always less than VTA pairs, for every ratio analyzed (Fig. 7D). For instance, only 18.2% of all SNc pairs exhibited a ratio of 5% or more, whereas almost 50% of VTA pairs did so. We then, analyzed the intersection ratio between SNc and VTA neurons according to the Euclidean distance between pair of neurons (cell body to cell body) and observed that VTA neurons presented a statistically significant higher ratio (Fig. 7F) than SNc neurons when >100 and ≤ 200 µm and >300 µm and ≤ 400 µm away. Overall VTA neurons had more overlapping that SNc neurons as can be seen in figure 7E (Mann-Whitney, U = 770, $p = 0.0025$, two tailed; Fig. 7E)To examine the organization of the dendritic domain as part of the region in which they locate, we created a common 3D map of SN and VTA and placed the reconstructions inside according to the location of their cell bodies (Fig. 5). Overall, while

dendrites of neurons whose cell bodies located in the SNc tended to stay in the SNc and underlying SNr, as lengthily reported in the literature, they could also cross barriers and innervate the medial VTA and dorsal tegmentum located above the SN (see below). Also, dendrites of neurons whose cell bodies located in the VTA, as a norm stayed in the VTA although could also send dendrites into the SN or dorsal tegmentum (see below).

.

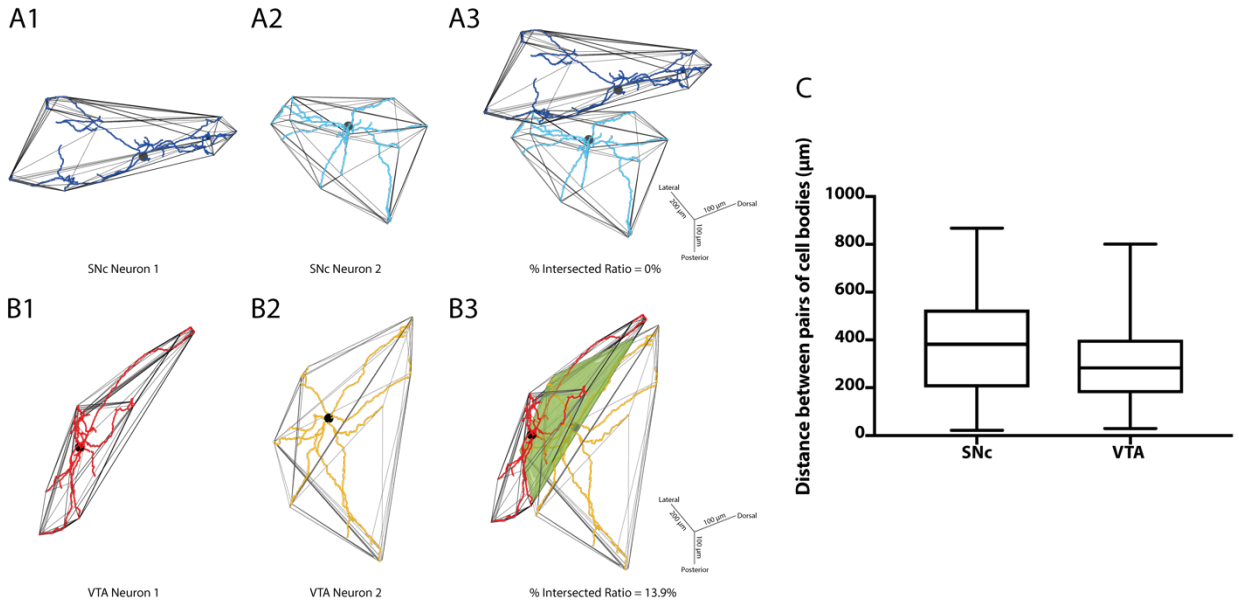
A1
A2
A3
SNc Neuron 1
SNc Neuron 2
% Intersected Ratio = 0%
B1
B2
B3
VTA Neuron 1
VTA Neuron 2
% Intersected Ratio = 13.9%
Lateral
Dorsal
Posterior
100 µm
C
Distance between pairs of cell bodies (µm)
1000
800
600
400
200
0
SNc
VTA

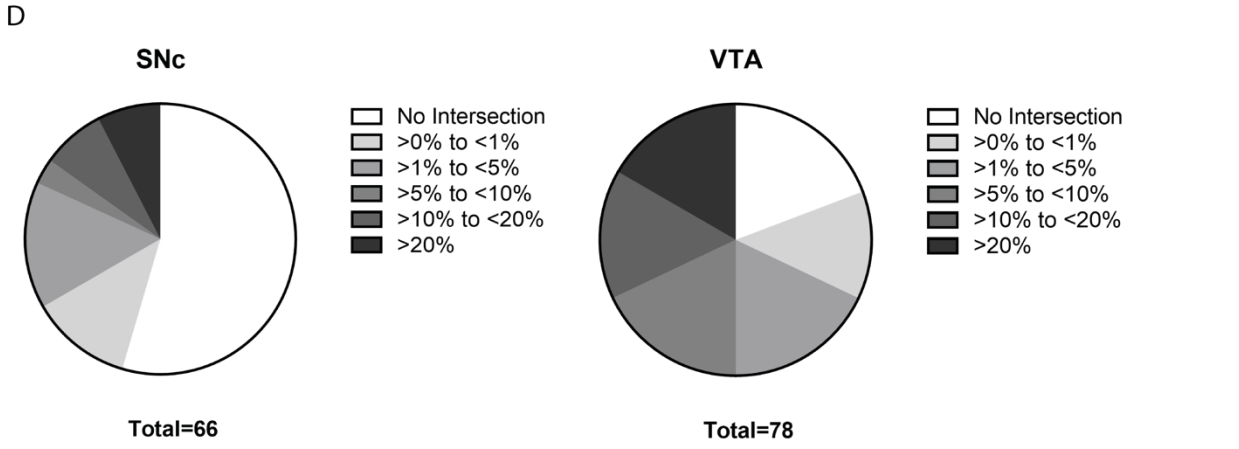
D
SNc
VTA
No Intersection
>0% to <1%
>1% to <5%
>5% to <10%
>10% to <20%
>20%
Total=66
Total=78

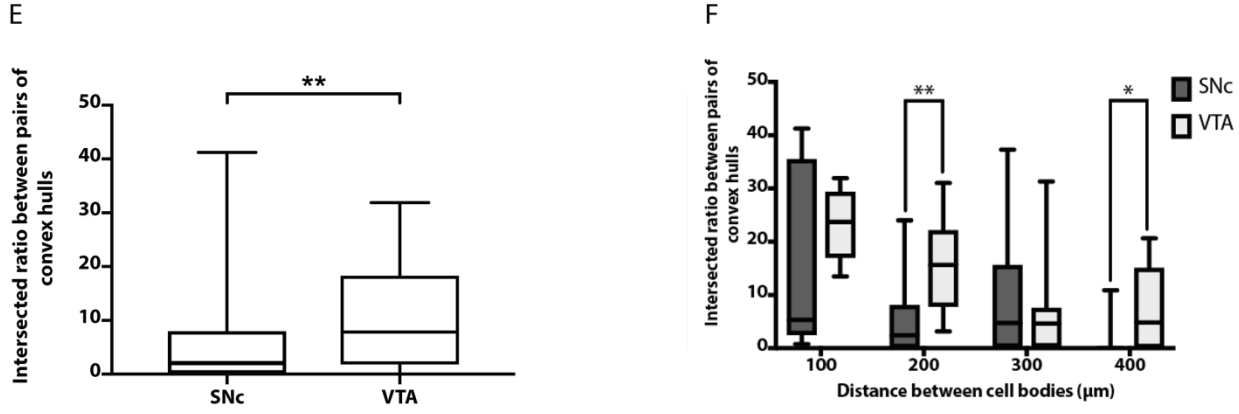
E
Intersected ratio between pairs of convex hulls
**
50
40
30
20
10
0
SNc
VTA
F
Intersected ratio between pairs of convex hulls
**
*
SNc
VTA
100
200
300
400
Distance between cell bodies (µm)

Figure 7: Dendritic trees field overlap significantly more in VTA dopaminergic neurons than in SNc neurons. (A-B) Convex Hulls Overlap Analysis Diagram. (A1-2) Two SNc and (B1-2) two VTA reconstructed neurons examples are drawn inside their respective convex hulls. (A3) In this example the two SNc neurons when placed in their respective anatomical locations do not overlap, whilst (B3) VTA example neurons have overlap of their convex hulls (green area). (C) The distance between pairs of cell bodies was not significantly different between SNc and VTA in our sample. (D) Pie chart showing the percentage of neuronal pairs showing various intersection ratios, from which it can be appreciated that SNc neurons exhibited lesser number of neuronal pairs for any given intersection ratio. (E) Overall, VTA neurons had higher intersection ratio than SNc neurons (Mann-Whitney, U = 770, nSNc = 41, nVTA = 58, p = 0.0025, two tailed) (F) Intersection ratio was significantly different between SNc and VTA dopaminergic neurons when their cell bodies were between > 100 and ≤ 200 μm of distance (Mann-Whitney, U = 29, nSNc = 10, nVTA = 18, p = 0.0025, two tailed) or >300 and ≤ 400 μm of distance (Mann-Whitney, U = 41.5, nSNc = 12, nVTA = 13, p = 0.028, two tailed). Graphs are shown with box and whiskers plots where whiskers are min-max interval, the hinges are the 25th and 75th percentile and the line inside the box is the median

6.1.4. Discussion.

Four main findings are reported in this study. First, we show that while SNc and dVTA neurons appear not to differ in size or overall complexity, vVTA neurons present a smaller and simpler dendritic domain. Second, there is a bias for a dorso-lateral location of SNc neurons' dendrites, which contrasts with the dorso-medial and ventro-lateral bias that VTA dendrites exhibit. Third, emerging from both population and neuronal pair-to-pair analyses, overlap between individual neurons dendritic space was consistently higher for VTA than SNc neurons. Finally, mice dopaminergic neurons appear noticeably large in relation to the size of their region, with average maximal dendritic extensions covering up to 50% of the region's extent.

6.1.4.1. Size, complexity and orientation

We report that, from a morphological point of view, there are two neuronal groups in the VTA: larger and more complex dorsal neurons and smaller and simpler ventral VTA neurons. We are not aware of any study that has reported differences in dendritic organization between identified VTA dopaminergic neurons, mostly because studies usually focus on gross cytoarchitectural features such as cell body size and main axis orientation (Fu et al., 2012; Phillipson, 1979b). Using Golgi staining, a previous study in the rat reported that ventrally located neurons in the PN nucleus were smaller and with less obvious dendritic orientation (Phillipson, 1979a) than dorsal VTA neurons of the PBP, which is in line with our results as long as it relates to the dopaminergic population and to a possible dorso-ventral difference in size and complexity of neurons within the VTA. Interestingly, studies focusing on functional differences between individual identified dopaminergic VTA neurons in the rat, found that more ventrally located

neurons exhibited different responses to phasic, noxious stimuli than the most typical and more commonly studied dorsal VTA neurons (Brischoux et al., 2009).

From our sample, we could not find that mouse SNc DA neurons were different in physical and topological characteristics to both VTA neuronal populations, with the exception of dendritic surface. Regarding the orientation of SNc DA neuron dendritic domain, our results (Fig. 2, 3 and 5) are consistent with the literature on SNc dopaminergic neurons reporting orientation of dendrites parallel to the orientation of the SNc (in coronal planes presenting a dorsolateral to ventromedial orientation) (Henny et al., 2012; Juraska et al., 1977; Tepper et al., 1987). And, from morphological analysis based on 3D reconstructions, an additional tendency for dendrites to locate lateral and posterior in primates (François et al., 1987), something also observed occasionally in rats (Tepper et al., 1987) (see Figs. 3, 5). We also consistently observed the presence of dendrites descending towards the SNr, as extensively reported in mice (Fu et al., 2012b), rats (Bolam and Smith, 1990; Hajós and Greenfield, 1994; Henny et al., 2012; Juraska et al., 1977; Tepper et al., 1987) (Fig. 3, Fig. 5) and primates (François et al., 1987). The contribution of dendrites into the SNr in our neurons was not, however, sufficient to show any statistically significant presence of those dendrites in the ventrolateral quadrant, where we would have expected the most (Fig. 3). This may be due to the fact that not all dopaminergic neurons send extensive dendrites down to SNc, as also previously noted (Henny et al., 2012b) and reviewed in (Gantz et al., 2018; Sanchez-Catalan et al., 2014; Yetnikoff et al., 2014). Regarding VTA, our results are consistent with what previously described in coronal views of Golgi-stained individual VTA neurons in the rat (Phillipson, 1979a), and with what suggested by assessing the orientation of cell body and main trunk dendrites using TH staining in the mouse (Fu et al., 2012). We further found that, when

considering lateral or dorsal views, it was not obvious that the dendritic tree oriented in any particular direction, apart from presenting a tendency to locate posterior to the cell body (Fig. 3).

Orientation of the dendritic tree in both the SNc and VTA populations seems to reflect the overall orientation of the nuclei which they belong to: dorsolateral-to-ventromedial in the case of the SNc, and dorsomedial-to-ventrolateral for most of the VTA (leaving aside the PBP portion lateral to the medial lemniscus described in the mouse, Fu et al., 2012) (compare Fig. 2, 3 and 5, for neurons, with Fig. 5, for regions). The orientation and shape of the SNc and VTA regions seem to derive from the developmental processes that shape the dopaminergic ventral midbrain (Bodea et al., 2014; Brignani and Pasterkamp, 2017; Kawano et al., 1995) in that precursors of SNc dopaminergic neurons in the ventricular zone first move ventrally as part of initial radial migration, and then turn laterally and dorsally, as part of a subsequent tangential migration. In contrast, precursors of VTA dopaminergic neurons start their migration later and exhibit mainly radial and less so tangential migration (see Fig. 3 in Brignani and Pasterkamp 2017). Considering that neurites of migrating SNc and VTA dopaminergic neurons make use of, and orient themselves in relation to, radial glia-like cell and axonal processes (Bodea et al., 2014; Kawano et al., 1995), it seems then that the distribution of the adult dendritic trees in individual neuron (this study) may reflect the orientation of neurites during migration. This phenomenon, at a population level, would result in the adult shape of SNc and VTA. These results disregard our initial hypothesis that the dendritic tree, at least for VTA neurons, would organize perpendicularly to the main descending (from ventral striatum, ventral pallidum and hypothalamic areas) and some important ascending (from parabrachial nucleus, retrorubral field, mesopontine tegmentum and reticular formation) paths (Geisler and Zahm, 2005; Watabe-Uchida et al., 2012), in a fashion akin to that proposed for

reticular neurons (Jones, 1995; Ramón-Moliner and Nauta, 1966) although see (Mitani et al., 1988)).

6.1.4.2. Relative size

Analysis of maximal dendritic extension showed that individual SNc and VTA dopaminergic neurons span a large portion of their respective nuclei (Table 2). If most synaptic inputs in dopaminergic neurons, as in all neurons, reaches the dendritic domain (Bayer and Pickel, 1991; Bolam and Smith, 1990; Henny et al., 2012; Omelchenko and Sesack, 2007) then a single locus of afferent input onto the SNc or VTA could influence neurons that locate distantly. Conversely, a single individual SNc or VTA neurons could be potentially influenced by afferences reaching distant regions of the SN or VTA. This phenomenon, which for the most part may be explained by the relative small size of a brain such as the mouse's highlights the integrative capacity of dopaminergic neurons but also brings into question the extent to which fine point to point afferent topography in afferent projections exists in small brain animals.

6.1.4.3. Receptive domain and overlap

We used the convex hull to evaluate the degree of overlap between SNc and VTA dopaminergic neurons. Although the convex hull volume has been usually utilized as an simple indicator of the 3D shape and size of neurons (Gertler et al., 2008; Malmierca et al., 1995; Vrieler et al., 2019) we instead used it here as basic, though useful, indicator of a neuron's "receptive domain", in the sense of a space, with well-defined limits, within which interaction between an afferent system and a neuron occurs (and also one outside which interaction cannot occur). We firstly used the convex hull volume to study overlap, carrying out a population-based approach.

We calculated a "filling factor", which is a 3D analogous to the 2D coverage factor typically used in study of receptive field morphology for somatosensory or visual systems neurons (Farajian et al., 2004; Lefebvre et al., 2015). Based on reported estimations of SNc and VTA neurons (McCormack et al., 2006) we calculated that, on average, any single locus of the SN will be occupied by the receptive domain (convex hull volume) of 351 neurons and any locus of the VTA by 1002. To see these numbers in perspective, they can be compared with those reported in sensory systems; for instance, *Drosophila* body wall dendritic arborization neurons tile the surface with coverage factors of ~1 (Y.-N. Jan and L. Y. Jan, 2010); retinal ganglion cells exhibit coverage factors between 1 and 3 (Bae et al., 2018; Farajian et al., 2004), and some highly overlapping amacrine cells of the mouse retina reach values of ~33 (Farajian et al., 2004; Lefebvre et al., 2015). Although we did not find a similar analysis for central, 3D-structured neurons to compare the filling factor of dopaminergic neurons, it is fair to conclude that dopaminergic neurons present a high overlap in their receptive domains, and that overlap between VTA neurons is higher than SNc neurons. As discussed in the Results section, because filling factor values, of course, depend directly on the number of neurons that SNc or VTA contain, we also estimated filling factors based on other estimations (see Result section) and found that, irrespective of estimations VTA receptive domains fill the VTA space ~3 times more than SNc neurons the SN. A likely factor contributing to this difference may be the dissociation that exists in SNc neurons between cell body location (most in SNc) and the location of an important proportion of dendrites (SNr), which, among other things, necessarily drops down the overall density of SNc neurons, in turn impacting filling factor values. This dissociation is not apparent in VTA dopaminergic neurons, where for the most part, cell body and dendrite location is the same.

In parallel, we carried out a more direct approach which took into account individual neurons' shape and location, and avoided assumptions of cell number, density, volume or organization of the regions which they belong to. We estimated convex hull volume (CHV) overlap between every single pairs of those SNc and VTA sampled neurons. Again, we found that VTA neurons shared more of their receptive domain with each other, than did SNc neurons. This was not due to substantial differences in average CHV (they did not differ significantly), neither an artifact of the sampling because 1) the average Euclidean distance between pairs of cell bodies did not differ between SNc and VTA pairs and 2) when normalized by distance, the degree to which VTA neurons overlap was still higher than for SNc neurons (i.e. for a same distance, a pair of VTA neurons has a higher probability of sharing space with each other, than a pair of SNc neurons). The reasons for this difference in overlap are not clear. Neither size or complexity (Table 1), nor dendritic distribution (Fig. 3, 4) showed any substantial difference in overall shape that could clearly account for differences in overlap. Although highly speculative, a plausible hypothesis is that the observed differences in total or relative maximal extension of dendrites in the AP axis (Table 2), which were consistently smaller in SNc than in VTA neurons, could imply a higher degree of anisotropy in otherwise more "flattened" SNc neurons versus more "rounded" VTA CHVs, which in turn may result in differences in overlap.

The characteristics just described of VTA neurons seem to confirm early (Phillipson, 1979a; Ramón-Moliner and Nauta, 1966) and more recent (Geisler and Zahm, 2005) propositions, in VTA neurons conforming to the "isodendritic" cell type (Ramón-Moliner and Nauta, 1966), similar to other neurons belonging to the reticular core. Although quantitative dendritic distribution analysis did not reveal a pure isodendritic arrangement (Fig. 3, 4), relatively few and straight

dendrites and highly overlapping dendritic fields seem to support it. Such characteristics could help to explain, for instance, the fact that intersecting topographies have been usually described for the distribution of inputs into the VTA both in primates (Haber et al., 2000; Lynd-Balta and Haber, 1994) rats (Geisler and Zahm, 2005) and mice (Beier et al., 2015), These results, in general, contrasts those observed for SNc neurons where there is a segregated arrangement of inputs reaching either dendritic domain of SNc neurons which is present in both SNc and SNr, two regions that differ not only functionally, but also hodologically (Gerfen et al., 1985; Hajós and Greenfield, 1994; Henny et al., 2012) in that inputs to the SNc regions (Comoli et al., 2003; Jhou et al., 2009; Lavoie and Parent, 1994) differ considerable of those reaching the SNr (Smith et al., 1998; 1990) Furthermore, it is well documented that the striatal projection to the SNr is topographic and organized in "laminas" or layers within the SNr (Maurin et al., 1999), something so far not described for any projection to VTA nuclei in relation to accumbens or other VTA projecting regions.

Although in several respects SNc and VTA neurons play similar or complementary roles in behavior (Wise, 2009) and that, at the same time, there exist consensus in that both population are rather heterogeneous in molecular, firing mechanisms, function and hodology (Roeper, 2013), long standing evidence from neurodegenerative and region-specific lesion (reviewed in (Bolam and Pissadaki, 2012)), neuropharmacological studies (Willuhn et al., 2012) as well as more recent studies based on novel recording and experimental techniques (da Silva et al., 2018; Dodson et al., 2016; Howe and Dombeck, 2016), support the idea that the SNc is, at least, more involved in motor aspects of behavior than VTA neurons. Our results provide some support to these contentions in the sense that components of a motor system would be expected to present a higher degree of specificity and afferent topographical organization in their connections in contrast to VTA neurons

which, with their more overlapping dendritic receptive domains would indicate a more "integrative" role, better suited for limbic functions involving global motivational and global states modulation (Geisler and Zahm, 2005).

6.2. Electrophysiological Analysis and Estimation and Distribution Analysis of Inhibitory and Excitatory Putative Postsynaptic Puncta (PSP).

This section contains what would become the second manuscript associated with this thesis, although it is still not written as a paper we have separated it in order to avoid redundancy with the first manuscript of the materials and methods section.

6.2.1. Materials and Methods

For **Animals** description see section 6.1.2.1.

For **Recording and Labeling** of VTA single neurons see section 6.1.2.2.

For **Neuronal Identification** see section 6.1.2.3.

For **Neuronal Reconstruction** see section 6.1.2.5

6.2.1.1 Inhibitory and Excitatory PSP detection.

Neurobiotin (Nb) labeled profiles were additionally labeled for gephyrin, an inhibitory postsynaptic density (PSD) marker or homer, an excitatory PSD marker. Gephyrin has been shown to be present in most inhibitory PSD of several CNS synapses, such as cerebellar cortex, retina, spinal cord and hippocampal cultures (Essrich et al., 1998; Geiman et al., 2002; Sassoè-Pognetto et al., 1995; 2000) making in it a suitable GABAergic PSD marker (Belmer et al., 2017; Bragina and Conti, 2018; Henny and Jones, 2008; 2006). Additionally, several studies have also shown

that homer is present at dorsal horn, cerebellar, retinal and cortical excitatory PSD, (Brandstätter et al., 2004; Gutierrez-Mecinas et al., 2016; Shiraishi et al., 2004; Tao-Cheng et al., 2014). Homer is present in three isoforms and two of them, Homer 1 and Homer 2 and present in the VTA, thus we used a pan homer antibody, Homer 1/2/3. We labeled each neuron for both proteins, but in alternate sections: half of the sections from each neuron were labeled with gephyrin whilst the remaining half was labeled with homer antibody. All sections containing Nb-labeled fragments were included in an antigen retrieval protocol. They were incubated for 30 min at 80ºC in a 10 mM sodium citrate solution diluted in distillated water (Morgan et al., 1994; Kanai et al., 1998), followed by 3 x 10 min washes in PBS. After, sections being stained with anti-Geph antibody sections were blocked with 3 % NHS (v/v, Jackson Immuno Research Laboratories Inc.) in PBS and 0.3 % Triton-X. The sections were subsequently incubated overnight with mouse anti-Geph antibody (1:30,000, Synaptic System) in PBS, 3 % NHS and 0.3 % Triton-X. In the case of Homer staining, sections were blocked with 10% NHS in PBS and 0.3% Triton-X and incubated for 48 - 72 h at 4ºC with rabbit anti-Homer 1/2/3 antibody (1:5,000, Synaptic Systems) in PBS, 5% NHS and 0.3% Triton-X. Afterwards, in both cases, sections were then washed 3 x 8 in PBS, incubated for 2 – 3 h in either Alexa488-conjugated donkey-anti-mouse or Alexa488-conjugated donkey-anti-rabbit (1:1,000, Jackson Immuno Research Laboratories Inc.) secondary antibody. Next, they were washed 5 x 8 min in PBS, mounted onto glass slides, allowed to dry and covered with mounting medium (Vectashield, Vector Laboratories).

Finally, in order to anatomically locate the cell body after image acquisition, sections containing the soma were recovered and washed in PBS for 3 - 5 days at 4ºC and incubated with either rabbit or mouse anti-TH antibody (1:5,000, Santa Cruz Biotechnology) in PBS, 3% NHS and 0.3% Triton-X overnight at room temperature. They were then incubated for 2 - 3 h in

Alexa488-conjugated donkey-anti-mouse or anti-rabbit (1:1,000, Jackson Immuno Research Laboratories Inc.) secondary antibody, mounted onto glass slides, allowed to dry and covered with mounting medium (Vectashield, Vector Laboratories)

6.2.1.2. Microscopy and Imaging

Images for neuronal reconstruction were taken as indicated in section 8.1.2.4

Images for PSP estimation were taken with a 60x oil immersion objective (1.4 NA), 63x water immersion objective (1.3 NA) or 100x oil immersion objective (1.4 NA). Images were 1024 x 1024 in size with resolution of 0.21µm/pixel, 0.1 µm/ pixel and 0.124µm/pixel and taken in z-stacks of 0.25 steps between images. Over- and under-saturated pixels were set independently in each channel and for each z-stack acquired during the acquisition sessions using NIS-Elements C program (Nikon software) or Zen2012 (Zweiss software) or Fluoview (Olympus Software)

6.2.1.3. Quantification of Inhibitory and Excitatory PSP.

For twelve fully recorded, labeled and reconstructed DA VTA neurons, a record was obtained of all Nb-labeled dendrites and soma for each section from the 3D neuron reconstruction procedure, facilitating the identification and quantification of Geph+ and Hom+ profiles colocalizing with dendrites and soma.

In order to estimate the number and density of inhibitory and excitatory synapses in single DA VTA neurons, an estimation of total Geph+ and Hom+ profiles from all sections containing Nb-labeled processes was performed. For this, z-stacks images (0.25 µm between images) taken from fragments of cell body and dendrites were acquired through the top 5 µm of sections using a laser-scanning confocal microscope. The z-stack image acquisition was carried out using two

different lasers: 554-nm excitation/568-nm emission for Nb (red) and 490-nm excitation/525-nm emission for Geph or Homer (green). It is important to emphasize that in each sampling area, before acquisition of z-stack images, background was adjusted for guaranteeing it did not acquire over- nor undersatured pixels.

All z-stacks images acquired in the confocal microscope were used to quantify inhibitory or excitatory PSP. Each possible PSP was assessed by viewing colocalization between Nb and Gephyrin or Nb and Homer, two postsynaptic elements, in three planes (xy, xz and yz) using FIJI software tool "Orthogonal view" (Schindelin et al., 2012). On the other hand, each identified PSP by immunostaining for Gephyrin or Homer and colocalizing with Nb-labeled process, was tagged in its position onto fully neuron reconstruction using Neurolucida software (Henny et al., 2014a). Finally, using the Neurolucida Explorer 11.02 software (MBF Bioscience, Williston, VT USA) it was possible to obtain from 3D neuron reconstruction the anatomical data such as: soma surface, dendritic length and surface area. These anatomical parameters added to the distribution of tagged $Geph^+$ profiles or Hom^+ profiles on the reconstruction allowed us to obtain data about density of inhibitory and excitatory PSP for total dendrites and cell body

6.1.2.4. Statistical Analysis

To assess whether data sets were normally distributed, we performed single sample Kolmogorov-Smirnov test or, if the n was too small, Shapiro-Wilk normality test using GraphPad Prism 7 in all data sets. In normally distributed datasets one-way or two-way ANOVA with Tukey's post hoc testing were performed using GraphPad Prism 7. Nonparametric tests were used in non-normally distributed data; Kruskal-Wallis with Dunn's post hoc testing and two-tailed

Mann-Whitney U test were performed using GraphPad Prism 7. Significance for all statistical tests was set at $p < 0.05$.

6.2.2 Results

6.2.2.1. Estimation and Distribution Analysis of Inhibitory and Excitatory Putative Postsynaptic Puncta (PSP).

Single three-dimensionally reconstructed VTA dopaminergic neurons labeled profiles were, additionally, labeled for the postsynaptic density protein markers gephyrin (inhibitory) or homer (excitatory) (Fig. 8). Each neuron was labeled for both proteins, but in alternate sections, as such, half of the sections were labeled with gephyrin whilst the remaining half was labeled with homer. The estimation of total PSP number was carried out with the optical fractionator probe from StereoInvestigator software. From 12 counted neurons we have an estimate average of approximately 1001 PSP and a density of 0.078 PSP/μm^2 onto dendrites (Table 3). From the first neurons we labeled and data from the substantia nigra compacta (Henny et al., 2012a) we had expected to find significantly more inhibitory PSPs, yet surprisingly we found similar numbers with 44.4 % of PSPs corresponding to inhibitory puncta and 55.6 % to excitatory puncta (Table 3).

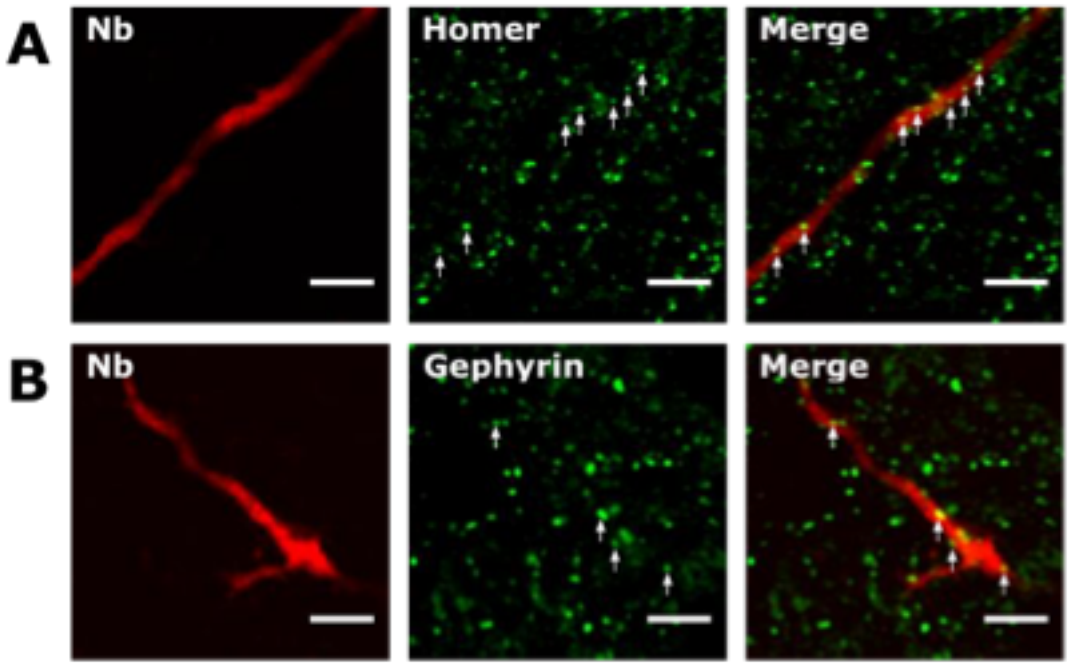

Figure 8: Detection of postsynaptic density proteins on neurobiotin labeled processes. Excitatory (A), and Inhibitory (B) postsynaptic density scaffolding proteins, homer and gephyrin respectively, were used to detect putative synaptic contacts onto VTA DA neurons labeled profiles. Scale bar, 18 µm.

Table 3: Estimates of postsynaptic puncta on the somatodendritic compartment of VTA DA single neurons

	Average	S. e. m.	range
All PSPs (n=11)			
Total number	1001	177	332 - 2457
Total density (PSPs/µm^2)	0.078	0.013	0.046 - 0.191
Geph$^+$ PSPs (n=10)			
Total PSPs number	452	75	216 - 878
% of PSPs Geph$^+$	44.4	4.5	29 - 66
Total density (Geph$^+$ PSPs/µm^2)	0.034	0.005	0.015 - 0.068
Hom$^+$ PSPs (n=12)			
Total PSPs number	597	107	116 - 1580
% of PSPs Hom$^+$	55.6	4.1	34 - 71
Total density (Hom$^+$ PSPs/µm^2)	0.046	0.008	0.021 - 0.122

We then proceeded to analyze whether there was a relationship between the location of the cell body in the VTA and the density of PSPs and found no correlations between the position of the neurons in any one of the axes and PSPs density (Fig 9A-F). Additionally, we evaluated if the different groups of neurons we had previously detected (dVTA and vVTA neurons) presented a differential density of PSPs, which was not the case (Fig. 9H). We also studied if there was a correlation between morphological size and complexity measures of VTA DA cells and the PSPs results, and found no correlations (Fig. 10).

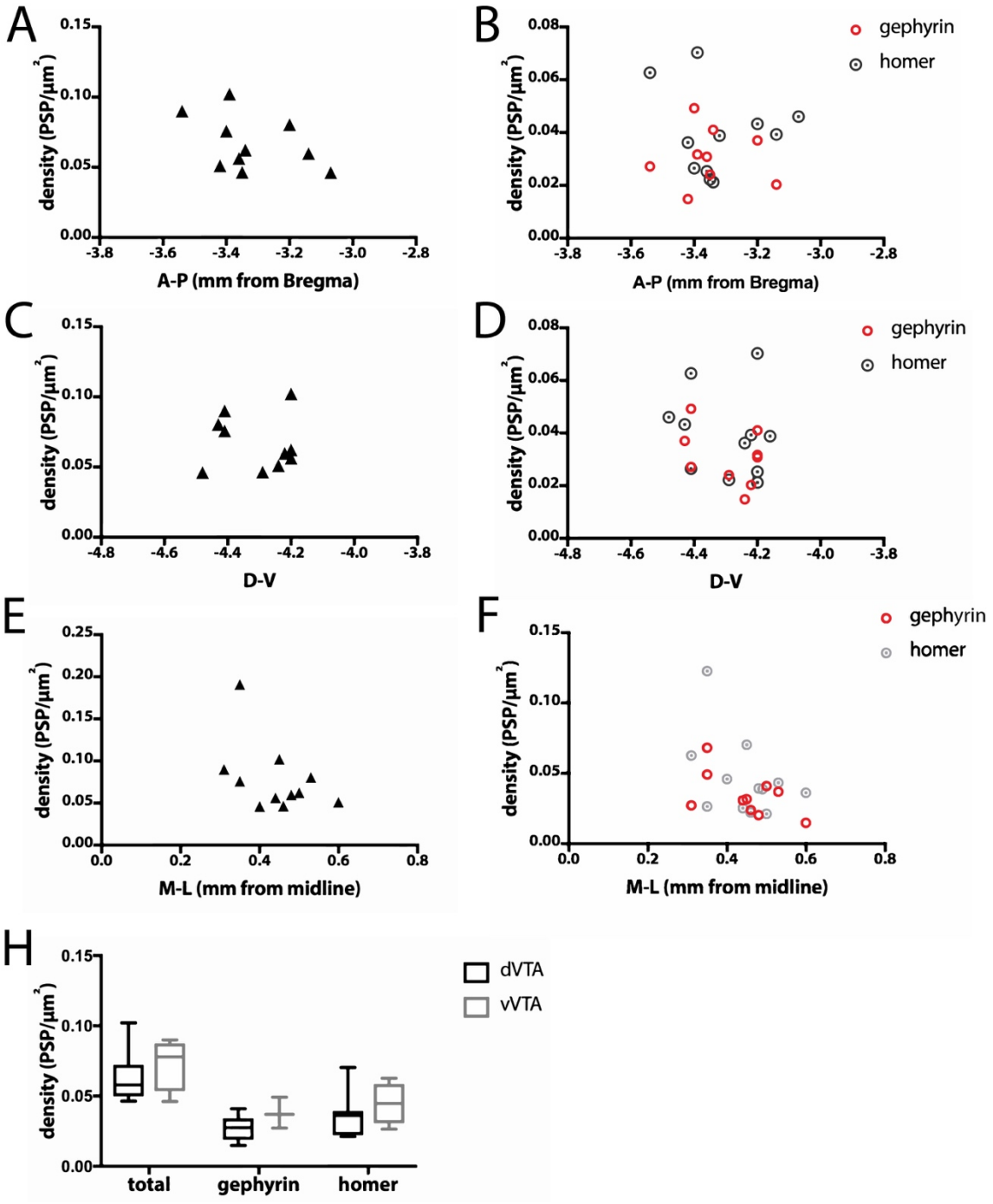

Figure 9: Correlations between location and PSP density of VTA DA neurons. (A, C, E) Relationship between the antero-posterior (A-P, A), dorso-ventral (D-V, C) or medio-lateral coordinates (M-L, E) of the neurons cell body and total PSP density. (A). (B, D, F) Gephyrin and homer PSP density in relationship with the antero-posterior (B), dorsoventral (D) or medio-lateral (F) position of the cell body. (H) Comparison of the previously defined, based on location, morphological groups, dVTA and vVTA neurons in relation with their PSP densities.

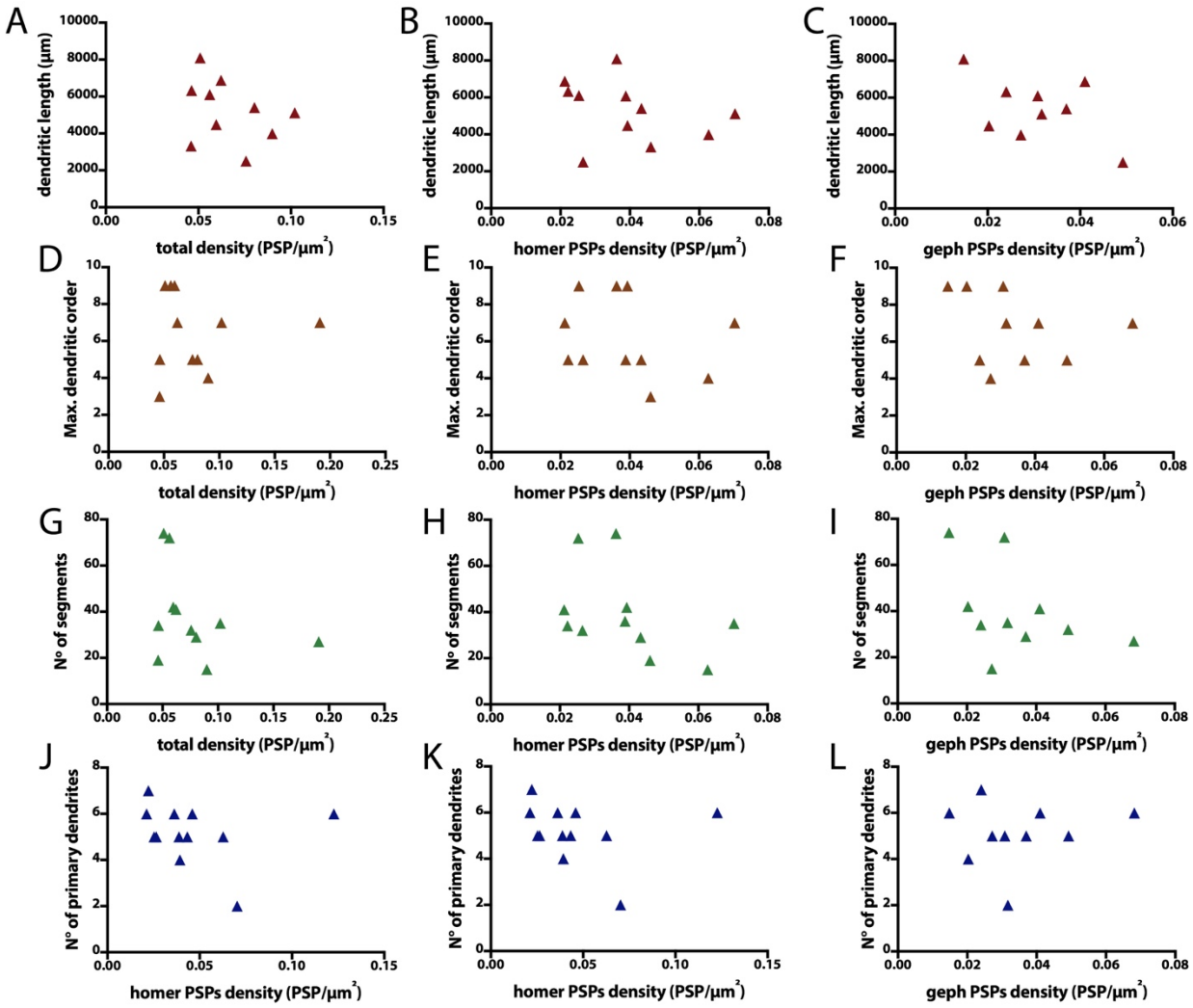

Figure 10: Correlations between size and complexity measures and PSPs estimates. (A, D, G, J) Relationship between total dendritic length (A), max. dendritic order (D), number of segments (G) and Number of primary dendrites (J) and total PSP density. (B, E, H, K) Relationship between dendritic length (B), Max. dendritic order (E), number of segments (H) and Number of primary dendrites (K) and homer PSP density. (C, F, I, L) Relationships between dendritic length (C), max. dendritic order (F), number of segments (I) and number of primary dendrites (L) and gephyrin PSP density.

A few studies have looked into the distribution of synapses onto VTA DA neurons dendritic tree. Smith and collaborators reported that distal dendrites had significantly more excitatory synapses. These results have several limitations though, because the sampling of the dendrites was not performed with a systematic and unbiased methodology and the definition of proximal vs distal dendrite is based on diameter and we know, from our studies, that there are very thin dendrites proximal to the cell body in DA neurons, all of this making those results difficult to interpret. Therefore, we performed a more detailed analysis of inputs distribution, to see if there was a preferential distribution either in dendritic order or in distance from the cell body (Fig. 11). In these finer analyses the density data was normalized to the total density of each neuron, so we may compare the distributions in each compartment independently of the differences in total density of PSPs. To examine the distribution in relation to the distance from the cell body we defined a proximal compartment as those dendrites within 20% of the distance from the cell body to the furthest dendritic tip and distal dendrites as those located in the remaining 80%. (20/80 criterium, Fig. 11D-F). This was done because we needed few compartments in order to have enough counted PSP in each of them and also to remain consistent with previous analyses made in our research group (Henny et al., 2012a). Firstly, we looked at PSPs densities in the cell bodies and found no differences between gephyrin and homer densities (Fig. 11A). Additionally, a significantly higher density of homer PSPs was found in the distal compartment (Fig 11A; Mann-Whitney $p = 0.0433$, two tailed), when analyzing all VTA neurons. When we analyzed dVTA and vVTA neurons, a trend for more homer PSP in distal dendrites could be observed for dVTA neurons only (Fig 11C, Mann-Whitney $p = 0.0728$, two tailed).

Moreover, we also analyzed whether there was a preferential distribution according to dendritic order (counted centrifugally from the cell body, as such lower order dendrites are closer to the cell body and higher order are more distal). The data had to be pooled, because there were too few counted PSPs in each order separately, so we defined a compartment consisting of first and second order dendrites and a higher order compartment composed by the third to the last dendritic order (ninth). We found a significant difference in the higher order dendrites, where a significantly higher density of homer puncta was detected (Fig. 11B; two-way ANOVA main effect of interaction $F_{(1,35)} = 4{,}87$, $p = 0.0339$, Tukey's *post hoc* test $p = 0.0393$). This result was lost when we evaluated the dVTA and vVTA neurons separately (Fig. 11D, F).

In summary, the density of PSPs we found was independent of the neuronal location in the brain (Fig. 9) or the neuron's morphological features (Fig. 10). Furthermore, by analyzing different cellular compartments we consistently found that either by compartmentalizing the cell according to dendritic order or by distance to the cell body there was significantly higher homer density in the distal (Fig. 11A) or higher order dendrites (Fig. 11B).

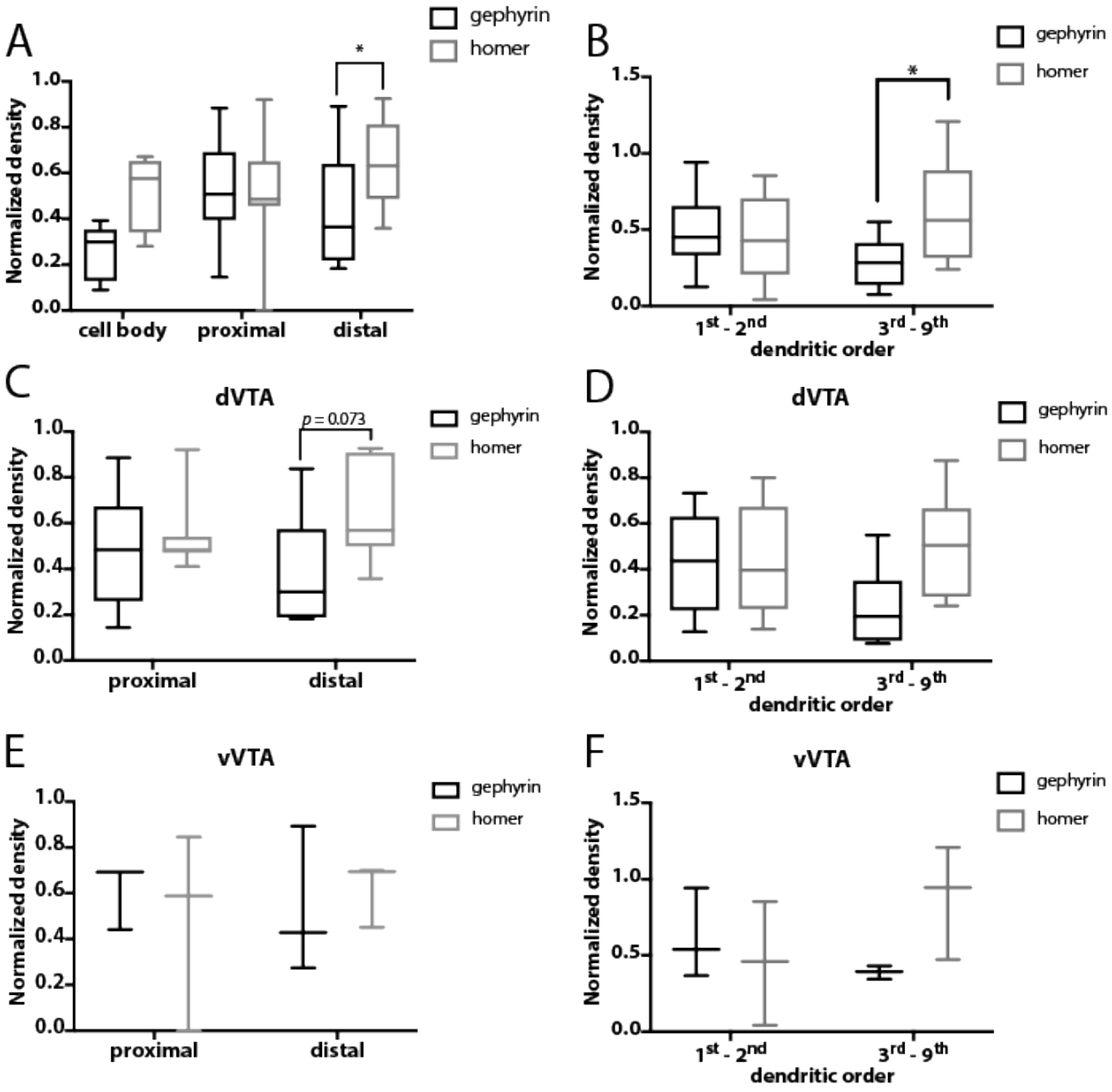

Figure 11: PSPs densities in different cellular compartments. (A, C, E) Gephyrin and Homer PSPs densities in proximal and distal compartments defined by their distance from the cell body in the total pool of neurons (A), only in dVTA neurons (C) and in vVTA neurons (E). (B, D, F) Gephyrin and Homer PSP densities in dendritic compartments defined by dendritic order in total sample of neurons (B), in dVTA neurons only (D) and in vVTA neurons (F). Graphs are shown with box and whiskers plots where whiskers are the min-max. interval, the hinges are the 25th and 75th percentile and the line inside the box is the median.

6.2.2.2 Description of the *in vivo* Spontaneous Activity Pattern and in Response to an Aversive Stimulus of VTA Dopaminergic Neurons in Anesthetized Mice

Extracellular baseline recordings and in response to 15 sec. aversive stimulation (a footpinch) were obtained for 21 VTA dopaminergic neurons. Examples of raw recordings, a DA neuron waveform and responses to the aversive stimulus can be appreciated in figure 12. After the recordings, neurons were labeled with neurobiotin and neurochemical phenotype was confirmed by tyrosine hydroxylase (TH) immunohistochemistry expression in labeled neurons. Location of cell bodies was determined upon examination of TH immunohistochemistry of the slice containing the soma and drawn on coronal sections of the midbrain taken from Fu et al., 2012 ((Fu et al., 2012a), Fig 13A-D).

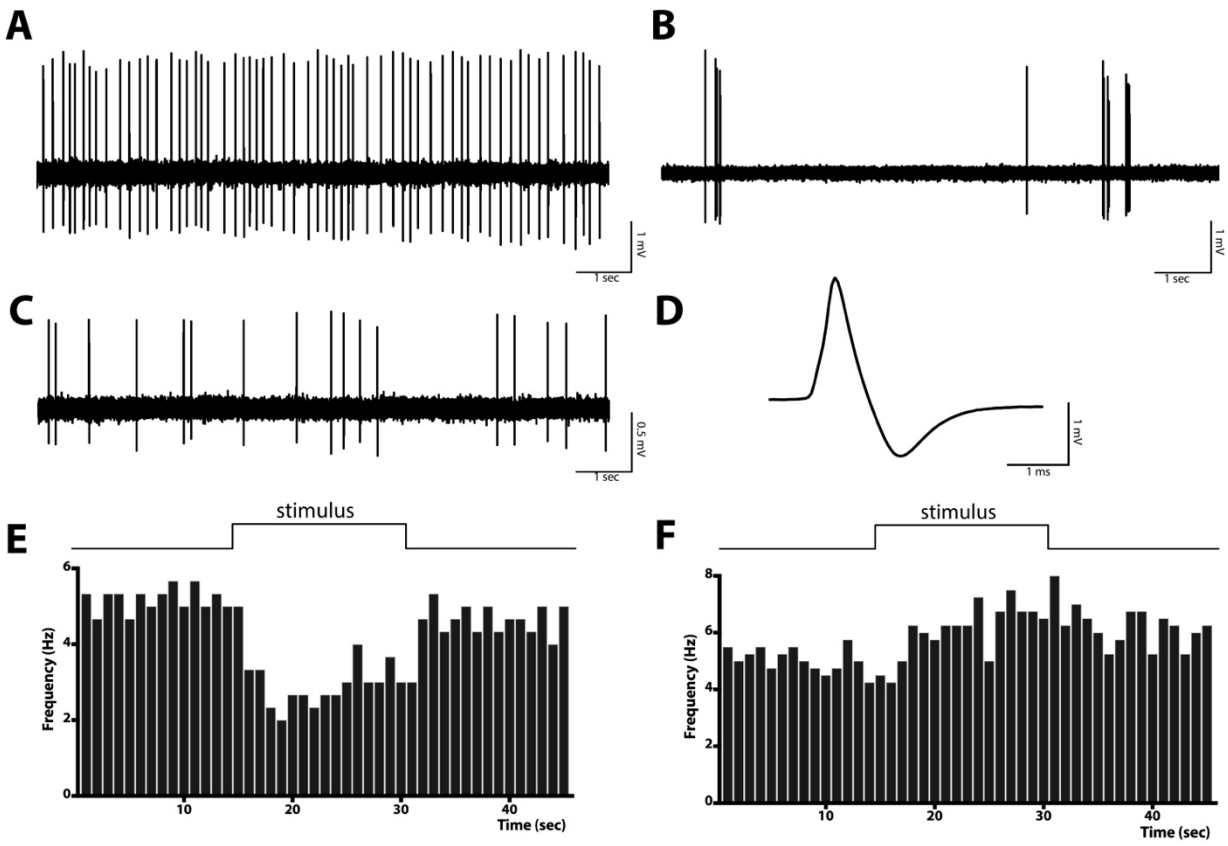

Figure 12: Spontaneous and driven activity recording of VTA DA neurons. (A-C) Spontenous firing of a neuron with no bursting and regular spiking (A), a neuron with a high percentage of spikes in burst (B) and a neuron with no bursting activity and an irregular spike train (C). (D) Waveform average of a DA neuron. (E-F) Peristimulus time histograms of an inhibited neuron (E) and an activated neuron (F).

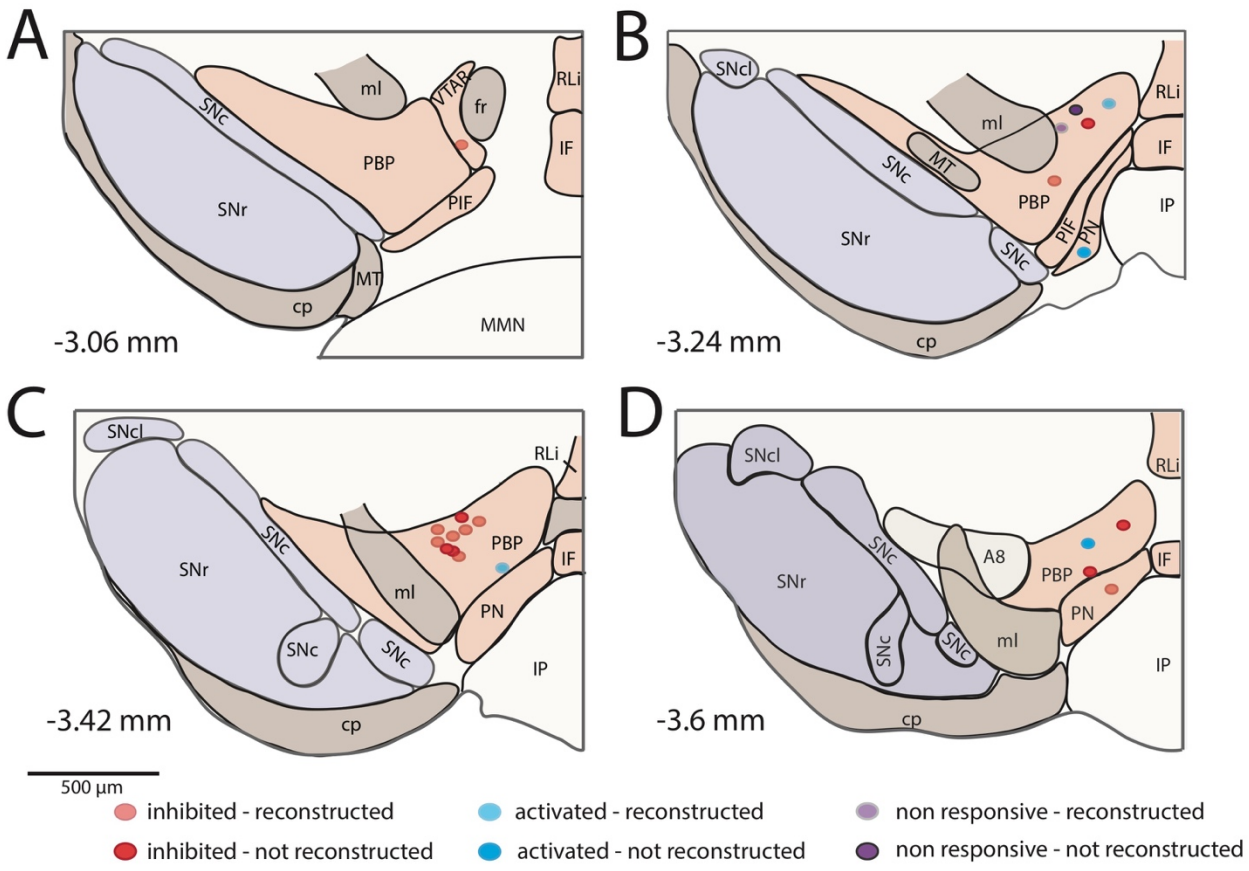

Figure 13: Location of electrophysiologically analyzed VTA DA neurons. Coronal views of the midbrain DA groups at bregma -3.06 mm (A), -3.24 mm (B), -3.42 mm (C) and -3.6 mm (D). red dots are inhibited neurons, blue dots are aversive stimulus activated neurons and purple is non-responsive. A8, retrorubral field; fr, fasciculus retroflexus; IF, interfascicular nucleus; ml, medial lemniscus; MT, medial terminal nucleus of the optic tract; PBP, parabrachial pigmented nucleus; PIF, parainterfascicular nucleus; PN paranigral nucleus; RLi, rostral linear nucleus; SNc, substantia nigra compacta; SNcl, substantia nigra compacta lateral; SNr substantia nigra reticulata; VTAR, rostral V TA

As shown in Figure 14, mean baseline frequencies range from almost 0 to 8.2Hz with a mean of 3.68Hz (Fig. 14A). The mean of the extracellular spike width, measured from the start of the spike to the through, was 1.66 ms with a range of 1.15 - 2.16 ms (Fig. 14B). Regularity of the spike train was analyzed, by calculating the coefficient of variation 2 (CV2), a measure that is less sensitive than the coefficient of variation (CV) to long term changes in frequency such as pauses. Because in our data we had neurons with those traits CV2 was preferred. CV2 values range from 0 to 2, where CV2 values close to 0 indicate regular firing and 2 is highly irregular. Our data showed a wide range of CV2 values from 0.11 to 1.52 with a mean of 0.76 (Fig. 14C). Bursting activity was calculated according to the Grace and Bunney criterion, namely that the first two spikes must show an interspike interval (ISI) below 80 ms and the last two spikes must show an ISI over 160 ms, with a minimum of 3 spikes. A wide range of bursting activity was found, with a mean of 22% of all spikes located in bursts (%SIB) and range of 0 to 67% SIB (Fig. 14D). Also, although most neurons decreased their firing rate in response to a nociceptive stimulus there were also neurons that were activated (Fig 14E)

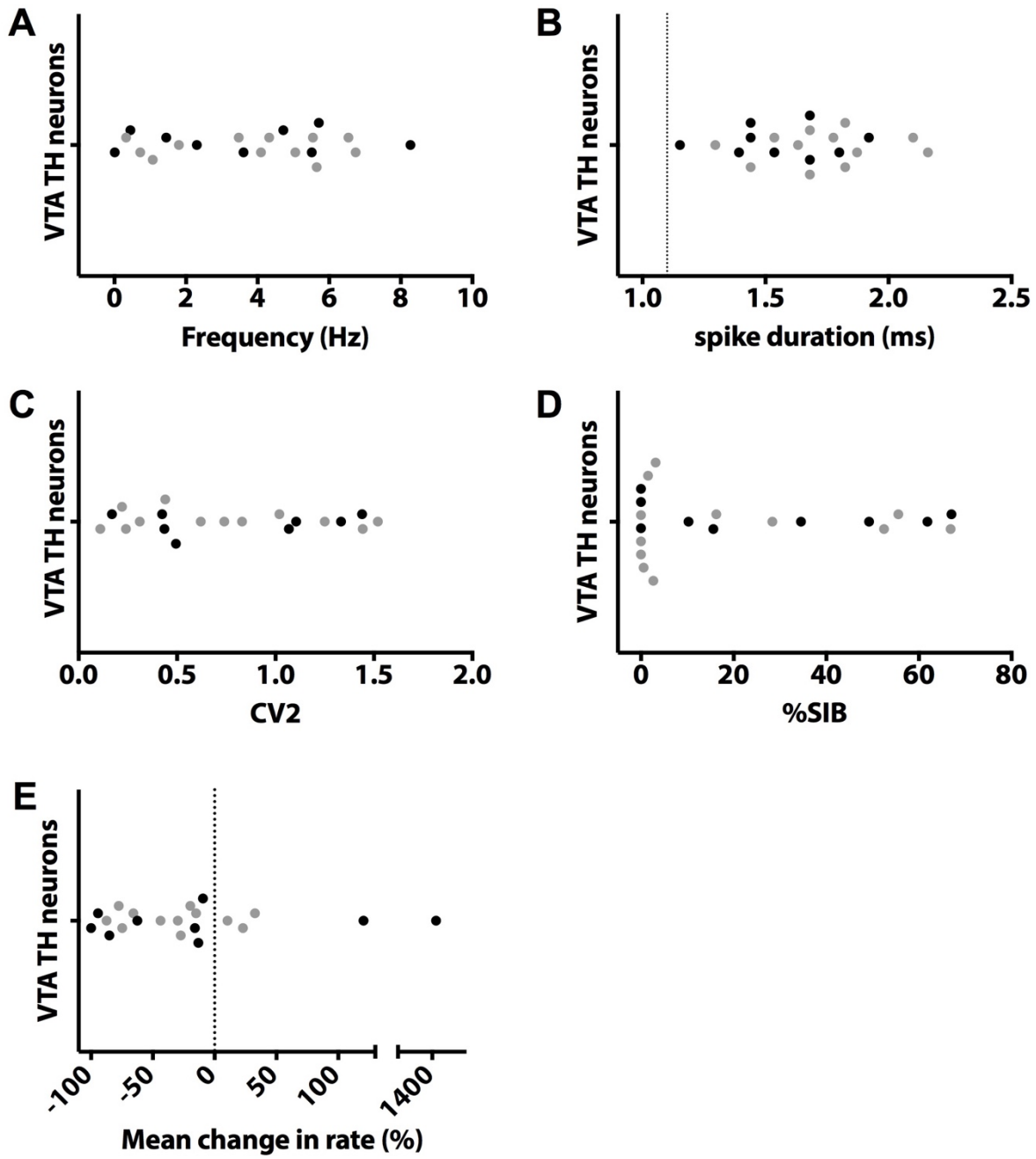

Figure 14: Characterization of recorded VTA DA neurons baseline activity and responses to nociceptive footpinch. (A-D) Baseline activity description included the analysis of frequency (A), spike duration (B), coefficient of variation (CV2, C) and % of spikes in burst (%SIB, D). (E) Aversive stimulus response is shown as the mean change in rate throughout the 15 second footpinch (percentage change = [(FR Post – FR Pre)/FR Pre] X 100; FR Pre = mean spontaneous firing rate immediately preceding the pinches, 15 s; FR Post = mean firing rate during the pinches, 15 s). Further reconstructed neurons are depicted in light grey circles.

In order to classify neurons as either activated, inhibited or non-responsive according to their response to the noxious footpinch, firing rate was plotted against time (1 sec. bins); a neuron was defined as being significantly responsive if at least two consecutive histogram bins, in the 15 sec stimulus period, lay outside 2 s.d. from the baseline mean rate obtained 15 s before the onset of the footpinch. Additionally, because we had some activated neurons that presented very fast and transient activation kinetics and thus were clearly activated but did not necessarily meet the above-mentioned criterion, we introduced an additional criterion for these few cases; the neuron was considered responsive if one histogram bin lay outside 3 s.d. from the baseline mean rate. Using these criteria, we found 3 groups of neurons: inhibited (15 neurons), activated (4 neurons) and non-responsive (NR, 2 neurons) (Fig. 15A) As appreciated in Figure 15 B-E there is an important degree of variability in the baseline data within each group. Mean frequency (Fig. 15B), %SIB (Fig. 15C), CV2 (Fig. 15D), and spike duration (Fig. 15E) were evaluated and no significant differences between groups were found.

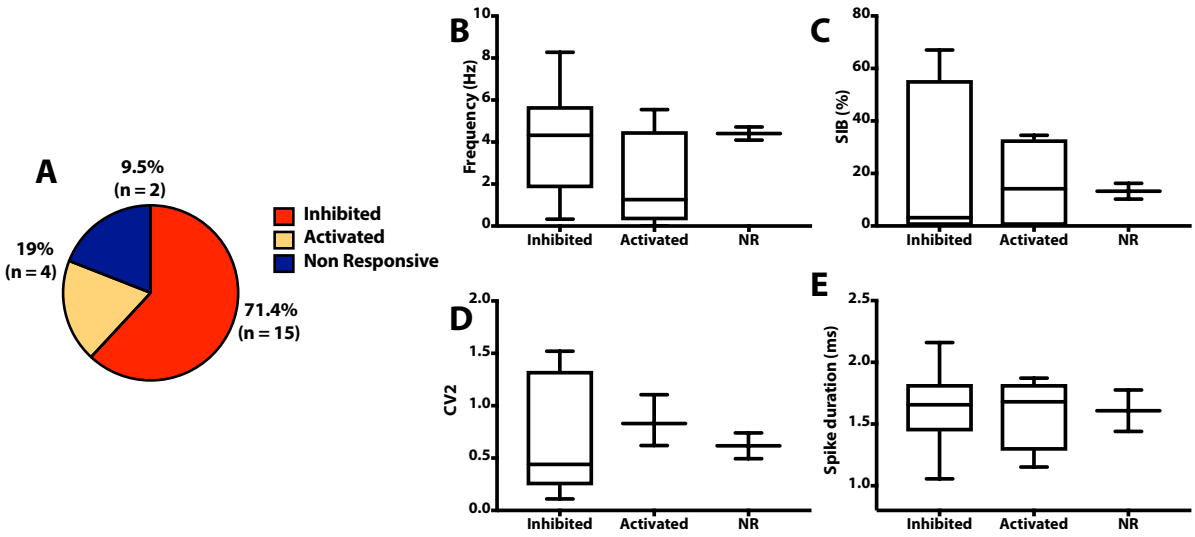

Figure 15: Baseline analysis of electrophysiological data according to their response to the aversive stimulus. Pie chart showing the distribution of the 3 groups found across the dataset (A). Plots of the different groups baseline frequency (B), %SIB (C), CV2 (D) and spike duration (E). Inhibited vs activated groups were tested with Mann-Whitney test with a $p < 0.05$. Graphs are shown with box and whiskers plots where whiskers are the min-max interval, the hinges are the 25th and 75th percentile and the line inside the box is the median

Because we found no differences between the groups and the variability inside groups was very high, we wanted to look at how the values of the different variables we were measuring were distributed within each group. To achieve this, instead of plotting each group as a discrete variable, we used a continuous variable and plotted the mean change in rate (%) following the footpinch against the frequency, CV2, %SIB or spike duration (Fig. 16). Just as in the column representations, a high variability of frequency and spike duration was found for all three groups. However, when CV2 and %SIB were analyzed we found that the inhibited neurons could be seen as distributed in 2 subgroups (Fig. 16B-C).

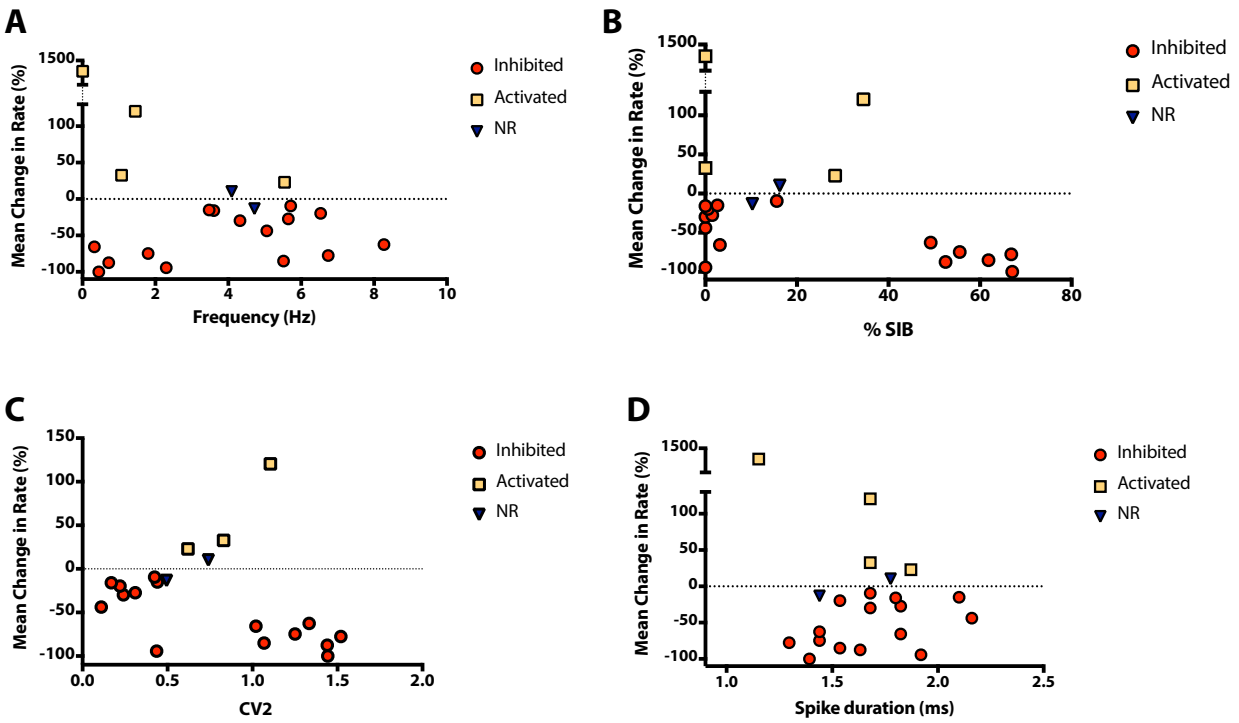

Figure 16: Baseline analysis of electrophysiological data according to their mean change in rate to the aversive stimulus. Baseline frequency (A), % SIB (B), CV2 (C) and spike duration (D) were plotted against the mean change in rate (percentage change = [(FR Post – FR Pre)/FR Pre] X 100; FR Pre = mean spontaneous firing rate immediately preceding the pinches, 15 s; FR Post = mean firing rate during the pinches, 15 s)

To test whether there were the same neurons that had different CV2 and %SIB, and thus, two different groups of inhibited neurons we first plotted the CV2 vs %SIB. As shown in figure 17 we found two clearly separated groups (Fig. 17A). According to this, we separated the inhibited neurons into two groups; Inhibited, regular and non-bursty (I-RNB) and inhibited, irregular and bursty (I-IB) neurons. Statistical differences were confirmed in their %SIB (Fig. 17B; Kruskal-Wallis, $p = 0.0002$ with Dunn's multiple comparisons I-RNB vs I-IB $p = 0.002$) and CV2 (Fig. 17C; Kruskal-Wallis, $p < 0.0001$ and Dunn's multiple comparisons I-RNB vs I-IB $p = 0.001$). In summary, I-RNB neurons are mainly regular and have zero to very few spikes in burst, whilst I-IB neurons are highly irregular and bursty.

A previous study described aversive stimulus activated VTA DANs as more irregular and bursty than inhibited neurons (Brischoux et al., 2009). As already mentioned, (Fig. 16D-E) we saw no differences between inhibited and activated neurons in those parameters. A possible explanation for this difference between our results and the above-mentioned study is that they had a much smaller sample of inhibited neurons (n=5), which might have led them to detect only those that have a more regular and non-bursting activity. Consequently we compared our two groups of inhibited neurons with the activated neurons (Fig. 17B-C), and on the contrary to what we expected from literature (Brischoux et al., 2009), we only found a trend for I-IB neurons to have more %SIB than activated neurons (Fig. 17B; Kruskal-Wallis, $p = 0.0002$ with Dunn's multiple comparisons I-IB vs activated $p = 0.053$), but no differences between activated and I-RNB neurons.

In summary we found a wide distribution of electrophysiological parameters in all groups analyzed. Moreover, the aversive stimulus inhibited neurons group could be further divided in two different groups based on differences on their spiking regularity and bursting activity; I-RNB

neurons are more regular and have very few bursts and I-IB which are significantly more bursting and irregular

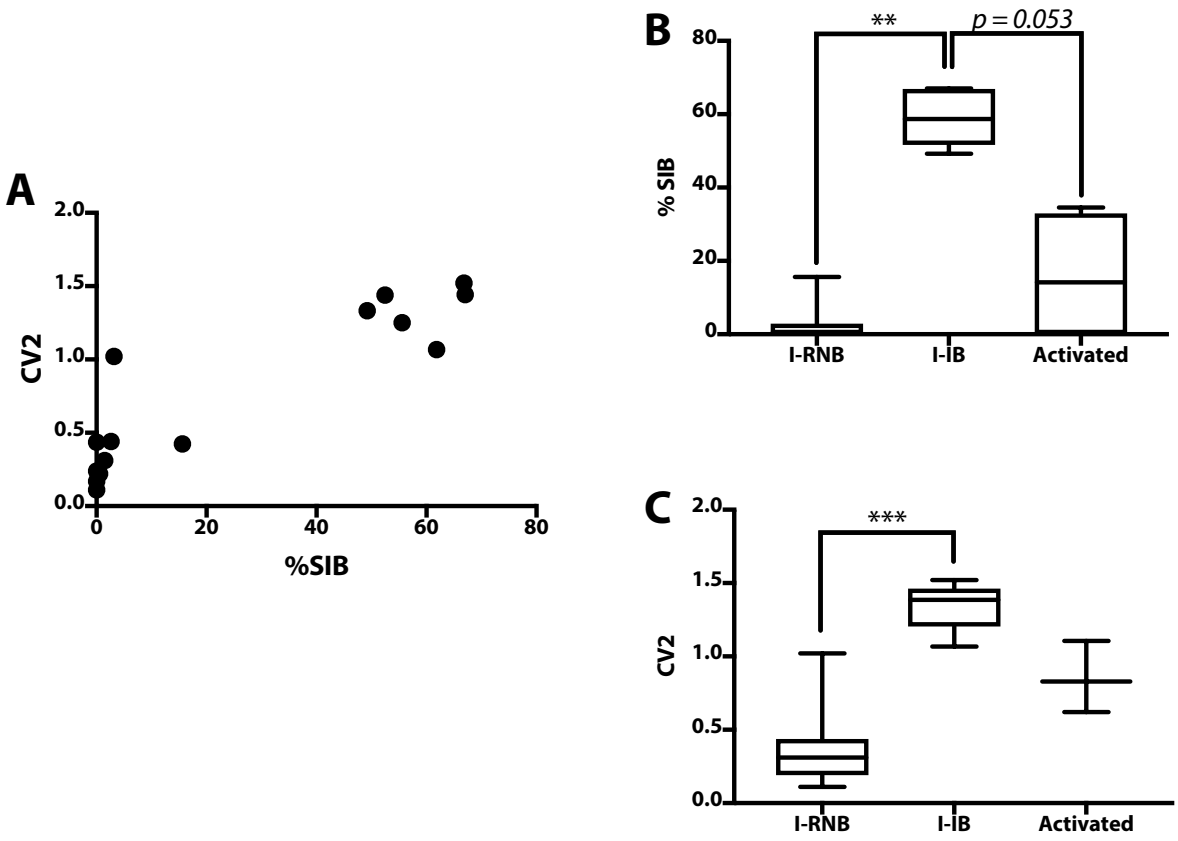

Figure 17: Aversive stimulus inhibited VTA dopaminergic neurons represent two different populations. (A) Inhibited neurons are separated in two groups according to their baseline CV2 and % SIB values. (B-C) I-RNB and I-IB neurons show statistical differences in their %SIB (B) and CV2 (C) (Kruskal-Wallis, $p < 0.05$)

6.2.2.3 Innervation Pattern Correlations with Spontaneous Activity and Aversive Stimulus Response.

Because it had been previously described that aversive stimulus activated VTA neurons are more ventrally located than inhibited neurons (Brischoux et al., 2009) we tested whether this was also the case in our data. Only inhibited and activated groups of neurons were analyzed, because the non-responsive group only had 2 neurons, not enough for statistical analyses. As shown in figure 18B we found no relationship between the dorso-ventral axis and response to the aversive stimulus (Fig. 18 B1-B2; unpaired t-test and Kruskal-Wallis $p > 0.05$). We also wanted to see if there was a segregation in the anteroposterior axis and the lateromedial and found that activated neurons were significantly more medially located than inhibited neurons (Figure 18 C1; unpaired t-test $p = 0.0025$) Furthermore, we also wanted to see if the inhibited subgroups, I-RNB and I-IB, segregated in space, still this was not the case (Fig. 18 A2, B2, C2, Kruskal-Wallis, $p > 0.05$). We also tested if a correlation could be found between the mean change in firing rate and the anatomical coordinates. As shown in figure 19, we found no correlations (Pearson's correlation, $p > 0.05$).

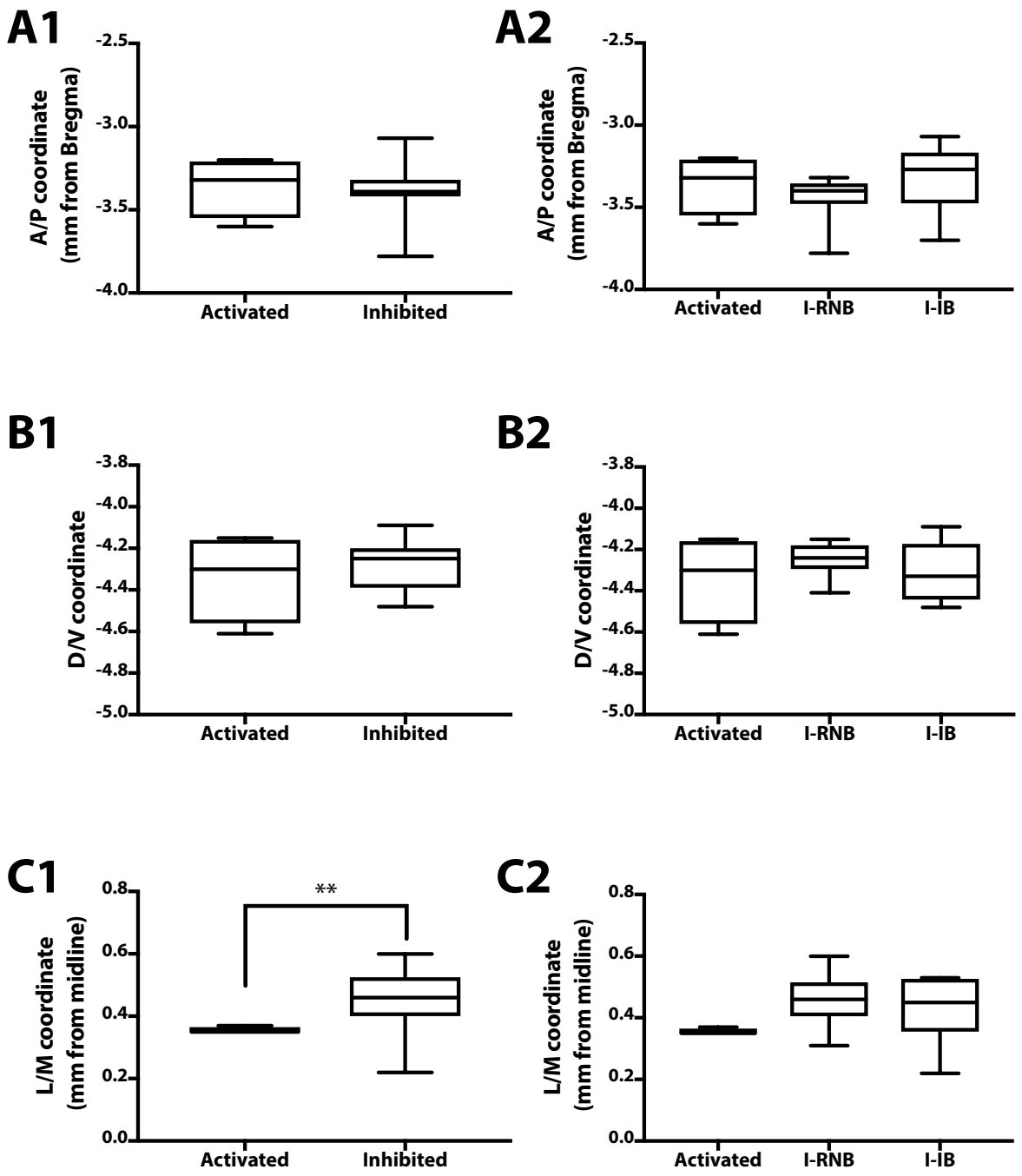

Figure 18: Aversive stimulus response groups distribution in VTA three-dimensional space. (A1, B1, C1) Activated and inhibited show no differential distribution in the antero-posterior (A/P, A1) and dorso-ventral (D/V, B1) axes but there was segregation between activated and inhibited neurons in latero-medial (L/M, C1) axis. (A2, B2, C2) Activated, I-RNB, I-IB and non-responsive neurons anatomical coordinates in A/P (A2), D/V (B2) and L/M (C2) axes were not significantly different.

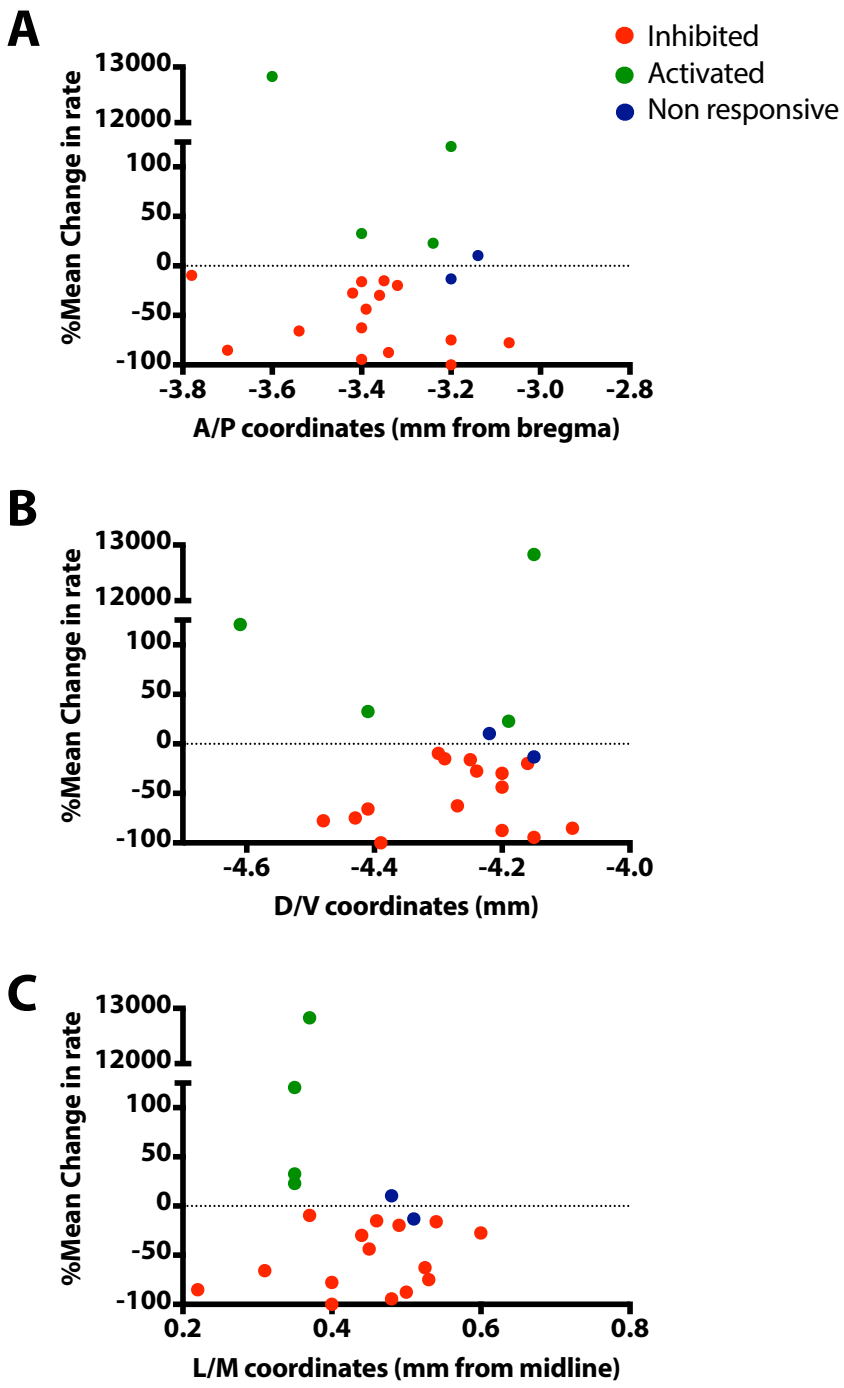

Figure 19: VTA DA neuron mean change in rate relationship with anatomical position. No correlation was found between position in the anteroposterior (A/P, A), dorsoventral (D/V, B) or lateromedial (L/M, C) axes and the % mean change in rate.

Of the twenty-two electrophysiologically analyzed neurons, twelve were three-dimensionally reconstructed and further analyzed; two were activated, nine inhibited and one non-responsive to the aversive stimulus. The inhibited group was composed by six I-RNB and three I-IB neurons, although we only counted both homer and gephyrin PSPs in five I-RNB and two I-IB neurons. With these reconstructed neurons, we proceeded with a more in-depth analysis of the different aversive stimulus response groups. First, we wanted to study whether the mean change in rate in response to the aversive stimulus of the different electrophysiological groups could be related to differences in morphological measurements of the reconstructed neurons. Complexity measures were analyzed and no relationship was found between the mean change in rate and number of primary dendrites (Fig. 20A, Spearman's correlation, $p > 0.05$), number of segments (Fig. 20B; Spearman's correlation, $p > 0.05$) or maximum dendritic order (Fig. 20C; Pearson's correlation, $p > 0.05$). Size measurements were also evaluated and no relationship was found between the mean change in rate and dendritic length (Fig. 20D; Pearson's correlation, $p > 0.05$), dendritic surface (Fig. 20E; Pearson's correlation, $p > 0.05$) and cell body surface (Fig. 20F; Pearson's correlation, $p > 0.05$) also showed no differences between different electrophysiological groups analyzed. In summary we found no correlation between aversive stimulus response group and complexity or size measurements of the neuronal dendritic tree.

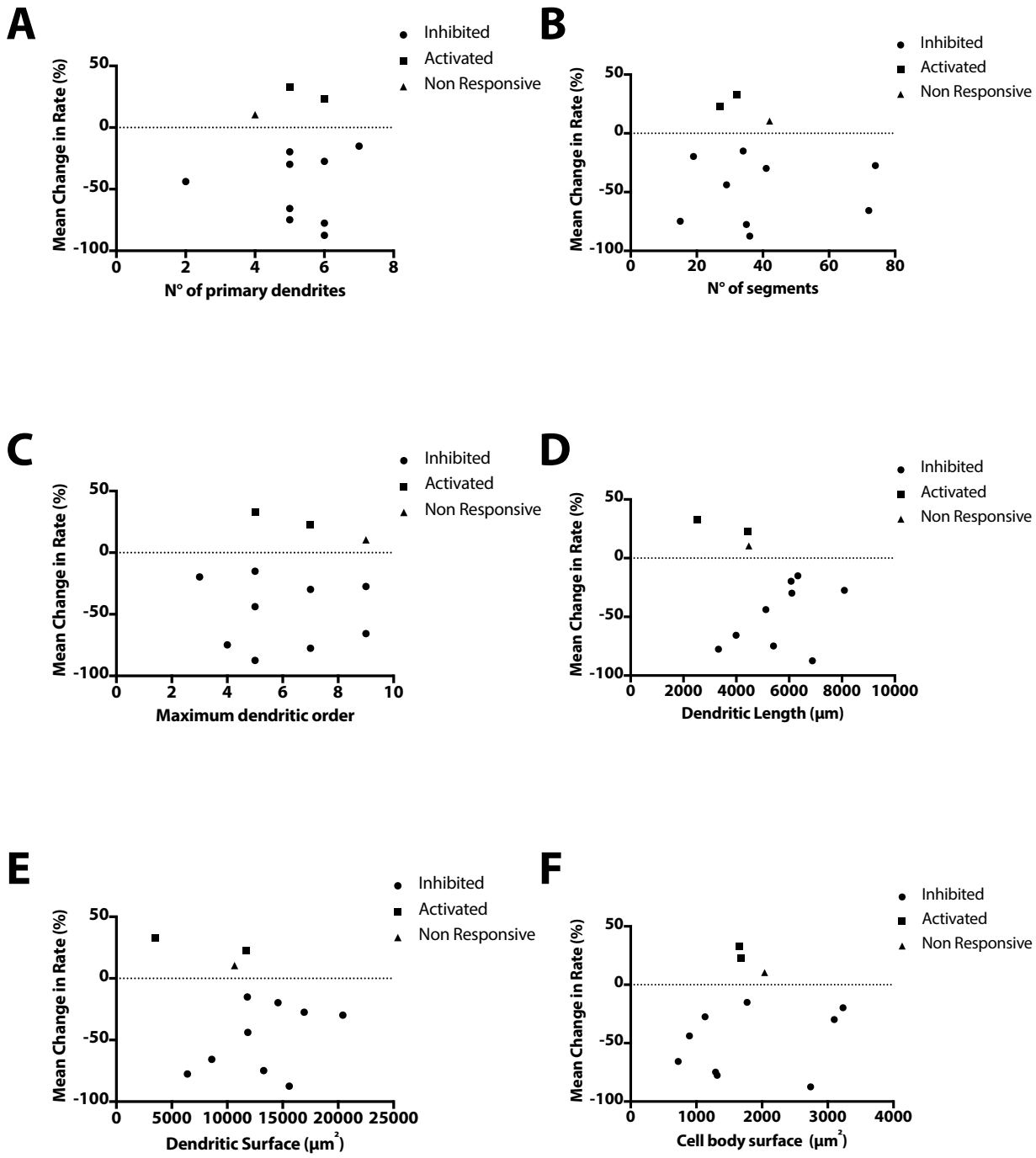

Figure 20: Aversive stimulus response groups relationships with complexity and size characteristics of reconstructed VTA DA neurons. Different aversive response electrophysiological groups mean change in rate was plotted against complexity (Number of primary dendrites [A], number of segments [B] and maximum dendritic order [C]) or size measurements (Dendritic length [D], dendritic surface [E] and cell body surface [F]) were compared and no significant relationships were found.

Following, we analyzed whether there where relationships between the inhibitory and excitatory PSP density and, on one hand the mean change in rate of response to the aversive stimulus and, on the other hand, spontaneous activity measurements such as frequency, %SIB, CV2 and spike duration. As shown in figure 21, we found that in inhibited neurons the greater the mean change in rate, the higher the inhibitory PSP density (Pearson correlation, $r^2 = 0.5718$, $p = 0.0492$) (Fig. 21A).

No relationships were found between excitatory overall density and mean change in rate (Fig. 21C). We studied possible relationships between either firing frequency (Fig. 21D-E), %SIB (Fig. 21F-G), CV2 (Fig. 21H-I), spike duration (Fig. 21J-K) and excitatory and inhibitory density finding no correlations.

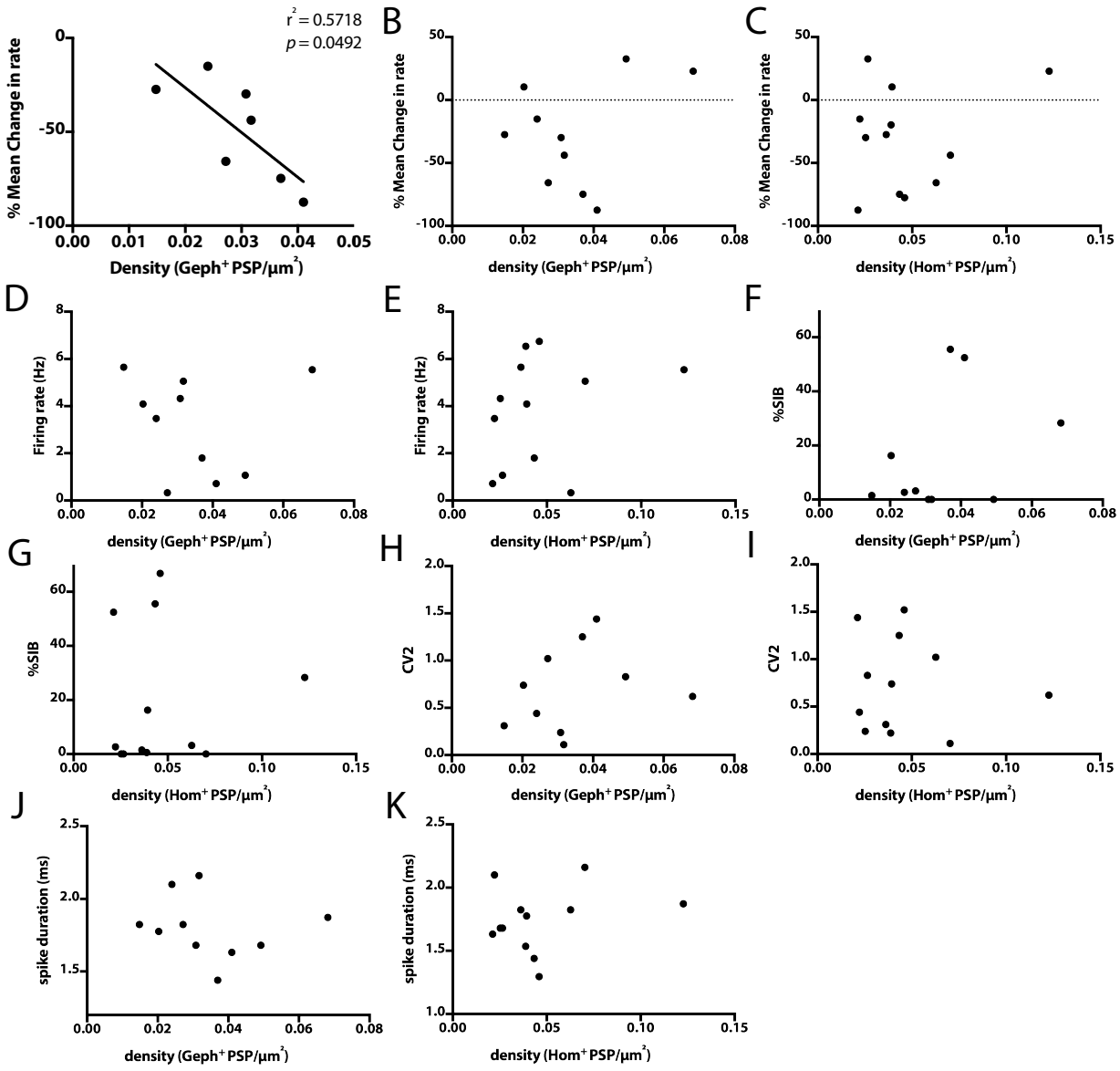

Figure 21: Spontaneous and driven electrophysiological activity correlations with inhibitory and excitatory PSP density. (A-C) Analysis of PSP density in relationship with aversive stimulus driven activity. (A) In non-activated neurons there is a correlation when analyzing the mean change in rate vs inhibitory PSP density. Inhibitory (B) and excitatory (C) PSP density in relationship with the mean change in rate in response to an aversive stimulus. (D-K) Spontaneous activity analysis related to PSP density. Analysis of firing rate (D-E), %SIB (F-G), CV2 (H-I) and spike duration (J-K) vs inhibitory (D,F,H,J)) and excitatory (E, G, I, K) PSP density.

Because from our reconstructions we have found that VTA DA neurons dendritic tree can be rather large and the location of inputs influences its capacity to affect the production of the action potential, we studied in detail the distribution of inputs. Moreover, there are no reports where the synaptic input to a single cell is correlated with the cell's activity in VTA DA neurons. Firstly, we analyzed glutamatergic and GABAergic inputs density in cell bodies of the different aversive stimulus response groups (Fig. 22) and found a correlation between the amount of GABAergic PSPs and the mean change in rate of aversive stimulus inhibited neurons (Fig. 22 C; Pearson's correlation $r^2 = 0.999$, $p = 0.0095$), thus the higher the relative density of gephyrin positive puncta in the cell body the greater the inhibition by the aversive stimulus. There were only two inhibited neurons where we counted homer PSP in the cell body so we could not perform this more detailed analysis.

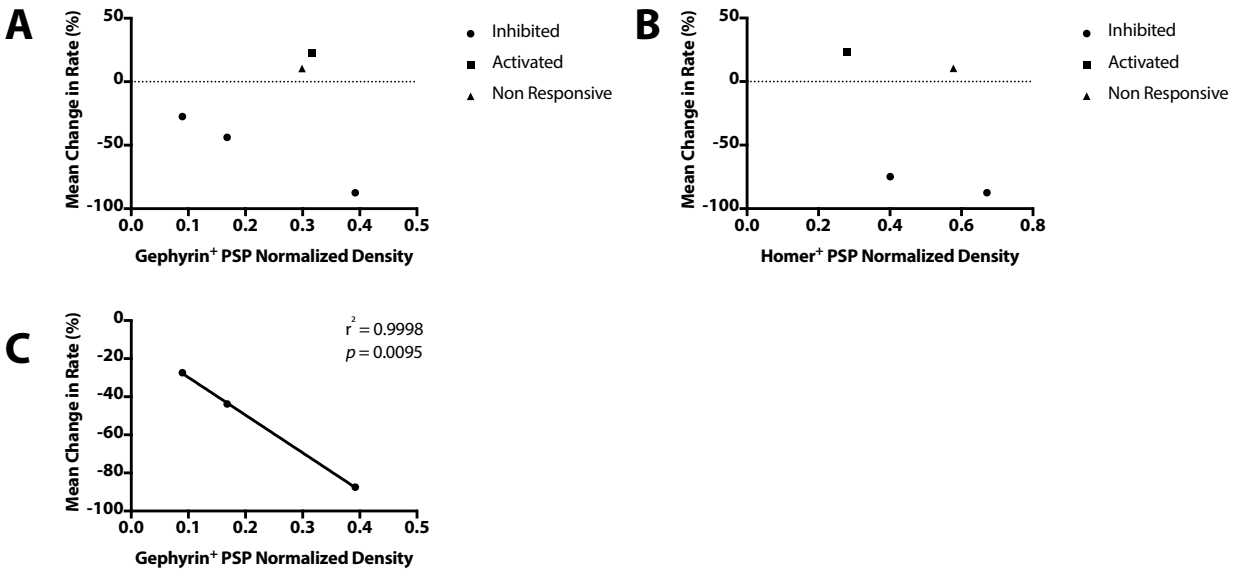

Figure 22: Electrophysiological groups cell body glutamatergic and GABAergic PSP density. (A, B) Relationship between gephyrin and homer PSP densities and response to the aversive stimulus in cell bodies of the different aversive stimulus response groups. (C) Relationship between aversive stimulus response and density of gephyrin PSP only in inhibited neurons.

Following, we analyzed the distribution of inputs by using the 20/80 criterium. We looked at relationships between the response to the aversive stimulus and the amount of GABAergic or glutamatergic innervation the neurons received in the proximal and distal compartments (Fig. 23A-D). We found no correlations between the mean change in rate in response to the aversive stimulus and the density of inhibitory (Fig. 23A, C; Pearson's correlation $p > 0.05$) or excitatory (Figs. 23B, D; Pearson's correlation $p > 0.05$) innervation in the proximal and distal cellular compartments.

.

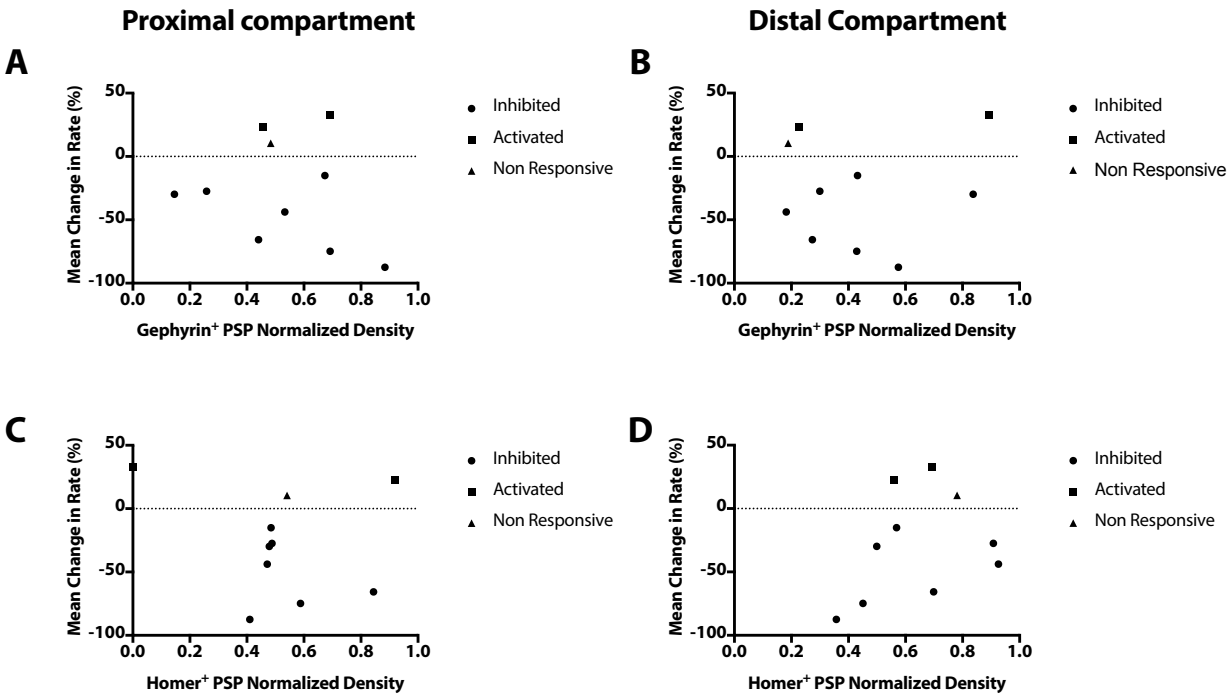

Figure 23: Electrophysiological groups PSP distribution in proximal-distal cellular compartments. Mean change in rate to the aversive stimulus of VTA DA neurons is plotted against gephyrin (A, B) and homer (C, D) PSP densities in proximal (A, C) and distal (B, D) compartment of all the electrophysiological groups found.

Finally, we also studied the distribution of inputs by their location in the different dendritic orders, which we grouped in lower order (1st and 2nd) and higher order dendrites (3rd - 9th; Fig. 24). No significant correlations were found between the mean change in rate in response to the aversive stimulus and density of GABAergic or glutamatergic PSPs in lower order dendrites (Fig. 24 A1, B1; Pearson's correlation $p > 0.05$) or higher order dendrites (Fig. 24 A2, B2; Pearson's correlation $p > 0.05$). In summary, we found that aversive stimulus inhibited neurons show a correlation between their degree of inhibition and the total density of GABAergic innervation they receive (Fig. 21A). Additionally, we see a similar correlation when looking only at the cell bodies of inhibited neurons, thus a higher degree of inhibition is associated with a higher density of gephyrin positive PSP (Fig. 22C).

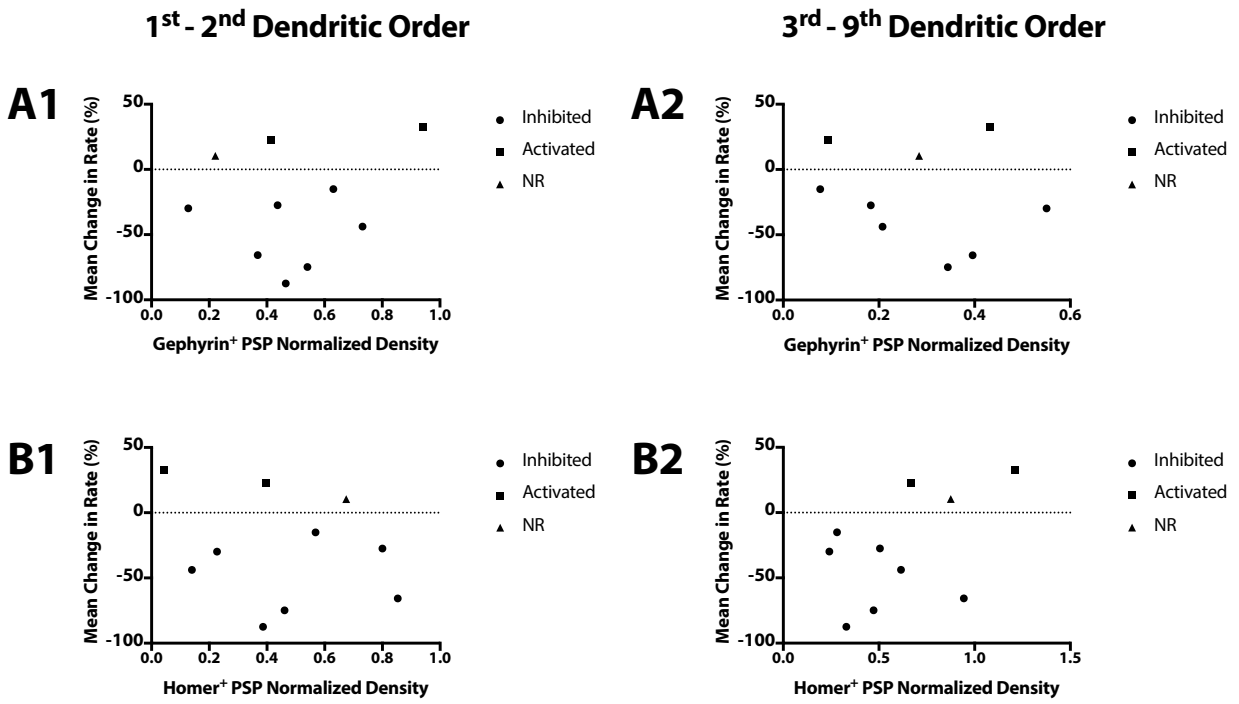

Figure 24: Electrophysiological groups PSP distribution in cellular compartments defined by dendritic order. (A1-A2) Gephyrin PSP densities in the lower and higher order dendritic compartments of the aversive stimulus response groups. (B1-B2) Homer PSP densities in the different compartments of inhibited, activated and non-responsive VTA DA neurons

7. Discussion

7.1. Technical Considerations.

The greatest technical challenge of this study was obtaining electrophysiologically recorded VTA DA neurons, with a strong enough labeling for three-dimensional reconstruction of the entire dendritic tree. Although our laboratory had ample experience with juxtacellular labeling of SNc DA neurons, moving to the VTA proved harder than what we initially thought. For this reason, when recording and labeling VTA neurons we mostly targeted the anatomical location we had had success (-3.1 mm from bregma and 0.4 mediolaterally). Consequently, as shown in figure 1 almost all our neurons are medial to the medial lemniscus, in the parabrachial pigmented (PBP) nucleus. Nevertheless, if we consider that the PBP is the largest VTA nucleus encompassing more than 50% of its total volume (PBP volume is 0.25 mm^3 and total VTA volume is 0.45 mm^3) having most of our neurons in the PBP can be considered representative of the VTA. Moreover, although, due to the above mentioned difficulties in obtaining well labeled VTA DA neurons we would look, when recording, for previously described DA-like electrophysiological activity (slow and irregular spontaneous firing rate and ideally inhibited by the aversive stimulus), we nevertheless found variability in our electrophysiological data that is in line with has been previously described for VTA DA neuronal population (Marinelli and McCutcheon, 2014) and also found aversive stimulus activated neurons (Figure 14, 15 and 16)

Additionally, there are some electrophysiologically atypical populations that have been described; putative VTA DA neurons that in basal conditions (non-stimulated) are silent (Floresco et al., 2003) and also VTA DA neurons that can sustain higher firing frequencies (≤ 20 Hz) and

have smaller amplitude action potentials (Lammel et al., 2008). Although we have some very slow firing neurons, that might be considered as silent (see figure 14A) , it is unlikely we have samples of these alternative populations because we cannot detect with a recording electrode a completely silent neuron and also the smaller amplitude of the neurons described by Lammel and colleagues make it hard to select those neurons for a juxta/intracellular recording with sharp electrodes where we stablish a minimum potential of the extracellular spike as a proxy of proximity to the neuron. With a small amplitude action potential, we might never reach a sufficiently big extracellular spike to select that neuron for labeling. Nevertheless, in our lab a study that characterized VTA neurons by recording spiking activity without applying any criteria, recorded 38 neurons, 10 of which were DA and did not find not a single fast spiking DA neuron as those described by Lammel (Gonzalez-Cabrera et al., manuscript in preparation; (Lammel et al., 2008)).

In summary, we have an electrophysiologically diverse and anatomically spread sampling of VTA DA neurons. Moreover we would like to highlight the fact that we did a very thorough localization effort of the cell bodies and also that the dopaminergic phenotype of our neurons was confirmed by TH immunochemistry a procedure not always performed when studying midbrain dopaminergic neurons (for example, see (Floresco et al., 2003; Stopper et al., 2014; Valenti et al., 2012)

In this work we used two PSD markers as putative synapse makers; gephyrin a component of the inhibitory PSD and homer an excitatory PSD scaffold protein. The gold standard for detecting synapses is EM coupled to immunohistochemistry to securely ascertain the neurochemical phenotype of the synaptic terminal, as was done in Henny and collaborators report (Henny et al., 2014a; 2012a). However, EM is extremely labor intensive and time consuming

which leads to a lower number of replicas and also, in the case of stereological studies, to a low amount of sampled tissue. Henny and colleagues that did stereology on EM and sampled only 1% of the total tissue, because of the above mentioned issue (Henny et al., 2012a). With this study we wanted to increase the number of independent replicas (number of neurons) and the amount of tissue and thus, the number profiles that we could stereologically count, with the aim of improving the statistic power of our comparisons. To do so we designed a study based on immunofluorescence instead of EM, the former being significantly less labor intensive allowing us to process more neurons (12 neurons compared to only 6 in Henny et al., 2012) and to count a much larger percentage of the tissue (~25% of tissue for each postsynaptic density marker). On the other hand, a downside to immunofluorescence is that identification of synapses is a bit less straightforward than in EM where synapses are structurally seen in the images. Yet, EM studies usually rely on Gray's synapse types (type I are excitatory and type II inhibitory) to classify whether a synapse is excitatory or inhibitory (Sizemore et al., 2016) an assumption that has been questioned in the literature (Klemann and Roubos, 2011). The ideal is to use EM to identify synapses coupled to immunohistochemistry to detect the neurochemical phenotype of the presynaptic terminal associated to the synapse, as was done by Henny and collaborators (Henny et al., 2012a). In the case of immunofluorescence, just presynaptic terminal labeling is not so informative because synapses are not structurally seen, and a terminal can be very close to a dendritic process and not necessarily stablish a synaptic connection. This latter issue is what led us to use PSD markers instead of labeling presynaptic terminals. Gephyrin was chosen because is a main scaffolding protein of the inhibitory PSD that interacts with $GABA_A$ receptors a1, a2, a3, a5, ß2 and ß3 subunits and also with several other components of the PSD such as tubulin, Neuroligin2, collybistin and GRIP-1 (Pizzarelli et al., 2019). More importantly for the objective

of this thesis are the studies showing that is present in most inhibitory PSD of several CNS synapses (Essrich et al., 1998; Geiman et al., 2002; Sassoè-Pognetto et al., 2000; 1995) making in it a suitable GABAergic PSD marker (Belmer et al., 2017; Bragina and Conti, 2018; Henny and Jones, 2008; 2006). Homer proteins, on the other hand, were used because they are excitatory PSD scaffold proteins that bind to dynamin3, drebrin and shank, among other proteins (Gray et al., 2003; Shiraishi-Yamaguchi et al., 2009; Tu et al., 1999; Xiao et al., 1998). Importantly, several studies have shown that homer is present at different excitatory PSD of the CNS (Brandstätter et al., 2004; Gutierrez-Mecinas et al., 2016; Shiraishi et al., 2004; Tao-Cheng et al., 2014).

Finally, as already explained, we used immunofluorescent methods with the goal of increasing the pool of analyzed neurons and amount of tissue used, which was accomplished. We recorded, labeled, reconstructed 12 VTA DA neurons, counting PSPs in approximately 50% of the tissue (~25% for each PSP marker). Nevertheless, some morphological and also electrophysiological aversive stimulus response groups had very low numbers of neurons and consequently we believe that the paucity of results regarding the correlations of innervation pattern and electrophysiological activity are associated with this phenomenon. Additionally, because we changed to a stricter criterion regarding the response to the aversive stimulus, we only had two activated neurons that were reconstructed and further analyzed. Consequently, in some cases, we could not perform statistical analyses comparing inhibited and activated neurons and thus, we performed correlation analyses to see if there were relationships with the magnitude of the response (Figs. 20-24)

7.2. Anatomical Description of Single VTA Dopaminergic Neurons Dendritic Tree Organization.

Concerning the morphological characteristics of our reconstructed neurons we found a wide range in the parameters that have been analyzed. For instance, these are similar to what we have seen in mouse SNc DA neurons with a reported range of dendritic length of 1,618 – 6,339 μm and 2-8 primary dendrites vs our range of 2,508 – 8,094 μm^2 of dendritic length and 2-7 primary dendrites (Table 1, Montero et al., manuscript in preparation). Regarding the primary dendrites it is interesting to note that historically the literature reports 3-5 (Kita et al., 1986) or 3-6 (Grace and Onn, 1989; J. Jang et al., 2014) at most. However, in our group we consistently find a wider range (2-7, Table 1), which is probably explained by the fact that we perform our analyses in tissue instead of cultures (J. Jang et al., 2014; Kita et al., 1986), and also we do high resolution reconstructions using 60x objective, instead of using 20x or 40x objectives used by others. Interestingly while reconstructing we noticed it was fairly common, for both SNc and VTA neurons, that second or even first order dendrites had small diameters (> 2 μm). This hinders the interpretation of previous works where dendrites are classified as proximal or distal based solely on their diameter (Smith et al., 1996).

Moreover, if we compare our morphological measurements with data taken from published three dimensional reconstructions from CA1 pyramidal neurons (neuromorpho.org, (Lee et al., 2014)), VTA DA neurons, regarding size measurements are not so different from hippocampal neurons (average VTA dendritic length 5,096 μm vs CA1 average length 5,236 μm and VTA average surface 14,192 μm^2 vs hippocampus neurons 19,585 μm^2). However, when comparing complexity data VTA neurons are less complex than CA1 mouse neurons (VTA average number of branches is 45.1 vs 113.8 in CA1 and our DA neurons have on average 7.3 maximum dendritic

order vs 20.2 in hippocampal neurons). Overall, VTA neurons have big and relatively simple dendritic trees

Regarding the orientation of dendritic trees, our results are consistent with what has been previously described in coronal views of VTA neurons as a mediolateral orientation (Fu et al., 2012a; Halliday and Törk, 1986; Phillipson, 1979a)(Fig. 3). We further add the three-dimensional view where we saw no clear orientation of the dendritic tree when analyzed from an anteroposterior or dorsoventral view (Fig 3).

We also studied the DA neurons dendritic fields and how much they overlap between cells, meaning that we looked not only at how long or how much surface dendrites have but also at how these dendrites are distributed in the three-dimensional space. In the VTA only a single study has ever looked at the neurons dendritic fields, and even though the author only studied neurons from a two-dimensional view on incompletely drawn trees, without quantifying their size, the author anyway could appreciate there was a high degree of overlapping (Phillipson, 1979a). In this work, by using the three-dimensional reconstructions we can better appreciate how big both DA of VTA and SNc neurons actually are in relation to their nuclei with neurons stretching on average ~50% of the total mediolateral extension, also they stretch ~40% of the dorsoventral extension and ~30% of the anteroposterior extension of VTA or SNc.

The morphology we describe of VTA neurons is consistent with the "isodendritic neurons" described by Ramon-Moliner and Nauta in 1966, with relatively straight dendrites, relatively few ramifications, extensive and highly overlapping dendritic fields (Ramón-Moliner and Nauta, 1966). These dendritic properties, specially their extension and overlapping, we believe, may partly explain why only highly intersecting topologies have been described for the distribution of inputs into the VTA. If the dendritic tree is so big and overlapping with others, it does not matter

if the axons arrive at a specific location in the VTA, still the probability of contacting several neurons with their cell bodies in different parts of the nucleus is high. Nevertheless, we must add that a previous report injected an anterograde tracer at 14 already known input areas of the VTA and analyzed, although they did not quantify, the terminals distribution in the VTA (Geisler and Zahm, 2005a). They found that almost every input area had a similar pattern of terminals distribution that spread throughout the entire mediolateral and dorsoventral VTA (Geisler and Zahm, 2005a), also explaining why no highly specific inputs have been found. In summary the reported lack of very specific input topography in VTA DA neurons is probably the result of this big and spread dendritic trees that may receive inputs from terminals that are actually far away from the cell body and also from a lack of specific distribution of the terminals themselves as previously reported (Geisler and Zahm, 2005a). This is in contrast with what can be found in the SN where two very different receptive regions, substantia nigra compacta (SNc) and substantia nigra reticulata (SNr), receive different inputs specially regarding GABAergic inputs, where SNr receives significantly more GABA terminals than SNc (Bolam and Smith, 1990b) and thus, SNc DA neurons with dendrites that extend into the SNr receive more GABAergic innervation (Henny et al., 2012a)

By performing this very thorough and detailed description of VTA DA neurons dendritic tree, with size, complexity, orientation and overlapping of dendritic trees data we are improving our basic knowledge of the VTA DA system and thus, stablishing sorely needed fundamentals that help explain some phenomena that have been already described, such as highly overlapping input topology.

7.3. Estimation and Distribution Analysis of Inhibitory and Excitatory PSP.

The estimated number of putative synaptic contacts was on average 1001 with 44.4% inhibitory PSPs and 55.6% excitatory PSPs (Table 3). Overall, from previous results we did not expect to find such a high proportion of excitatory PSPs. In an earlier publication, Henny and collaborators had reported that VGluT2 synapses in rat SNc dopaminergic neurons consisted 26 - 38% of total synapses (Henny et al., 2012a). However, our results are consistent with other published works on VTA neurons, where a report on the distribution of glutamate enriched terminals in contact with dopaminergic processes of the SNc and VTA in squirrel monkey shows a clear difference in the amount of glutamatergic innervation both groups receive, with SNc receiving more GABA terminals and VTA more glutamatergic innervation (Smith et al., 1996). Also, it has been well established that VTA neurons present more burst firing that SNc neurons (Clark and Chiodo, 1988; Grenhoff et al., 1988) and burst firing is strongly related to glutamate mediated excitation (Mercuri et al., 1992; Morikawa et al., 2003; Overton and Clark, 1992), thus it is not surprising that VTA neurons display more excitatory inputs than SNc DA neurons.

Moreover, Henny and collaborators had previously reported approximately 8,000 synapses on average on SNc DA neurons in the rat (Henny et al., 2012a) which makes our 1,001 seem low. On one hand there are several differences that can account for the difference in numbers; reports from CA1 hippocampal pyramidal neurons describe 30,637 excitatory synapses in the rat, whilst in mouse 9,500 have been reported. (Bloss et al., 2016; Megías et al., 2001) indicating that mouse neurons are receiving less synapses. Additionally, a work that counted varicosities immunopositive for excitatory and inhibitory vesicular transporters as a method of counting putative synapses in orofacial brainstem motor nuclei of the mouse also shows low number of synapses in mouse neurons (Faunes et al., 2016). Although they do not report data of synapses per cell those numbers

can be calculated from the study; 74.2 synapses per cell in the nucleus ambiguus, 130.8 in the hypoglossal, 822.3 in the trigeminal and 1561.18 in the facial nucleus (Faunes et al., 2016). These numbers are in the same range as our average of 1001 putative synaptic puncta, which if we add the above-mentioned difference for CA1 pyramidal neurons they all point to the fact that mouse neurons, in comparison with rat neurons, receive and process a significant lower number of synaptic inputs. Yet it should be also considered that in the SNc study they used EM which has considerably higher resolution than confocal microscopy allowing them to resolve small synapses that were sometimes very close together (P.H. personal communication) and also allows for counting of every kind of synapse (inhibitory, excitatory, serotoninergic, cholinergic, etc.) not only excitatory and inhibitory as we did (Henny et al., 2012a), indicating that we might be underestimating the real number of synapses.

7.3.1 Correlations Between PSPs Estimation and Anatomical and Morphological Data.

Although no clear specific associations have been made between cell body location in VTA DA neurons and specific inputs or projection targets, several studies have reported a degree of topography in some cases (Geisler and Zahm, 2005a; Ikemoto, 2007; Menegas et al., 2015). Moreover some input/output relationships have started to arise, i.e. the LHb inputs that synapses onto medial VTA neurons which project to the mPFC and also and LH inputs on medial VTA neurons that project to NAc ventral medial shell (de Jong et al., 2019; Lammel et al., 2012). Hence, we tested if there was a correlation between anatomical location and PSP density and found no significant correlations either for total PSP or Homer or Gephyrin PSPs (Fig. 9A-F). We also tested if there was some relation between morphological size or complexity measurements and PSP densities finding no correlations (Fig. 10). Thus, it was not the case that larger neurons had higher

density of excitatory PSPs or smaller neurons higher density of inhibitory PSPs. On the other hand, it might well be that, although our neurons might be involved in different circuits, with some of them participating in reward process and maybe others signaling salience, that does not necessarily mean they will have different synaptic density or different proportion of excitatory or inhibitory innervation.

7.3.2. Distribution of PSP onto the Somatodendritic Domain.

When we looked at the distribution of the inputs onto the somatodendritic tree we found some differences and trends. Firstly, we found no significant differences between excitatory and inhibitory PSP in the cell bodies of VTA DA neurons. This is dissimilar to a recent EM study that reports that VTA cell bodies in the rat have approximately 63% of symmetric synapses indicating they have more inhibitory inputs (Sizemore et al., 2016). The cited study and ours have several differences that might explain this; they worked on rats, with EM and report an estimate of symmetric synapses (which not always means they are inhibitory, see (Klemann and Roubos, 2011)), whilst we worked on mice with immunofluorescence and specific labeling of the neurochemical nature of the PSD. Next, we analyzed the proximal and distal compartments of the cell, and found no differences between excitatory and inhibitory PSP density in the proximal compartment, but interestingly in the distal dendrites there was a significantly higher density of homer (Fig. 11A) which was maintained as trend in dVTA neurons group (Fig. 11C). Similarly, we found that higher order dendrites, and thus more distal dendrites, have significantly higher density of homer PSPs (Fig. 11B). These results are consistent between each other because higher order dendrites are farther away from the cell body than lower order dendrites and both are in agreement with a previous report where they looked at glutamate terminals in the squirrel monkey

and found a much higher proportion of excitatory terminals on distal VTA dendrites (Smith et al., 1996). Moreover, it is interesting to note that in the coupled oscillator model of Wilson and Callaway (Wilson and Callaway, 2000), thinner dendrites have faster calcium oscillations due to their smaller diameter, which the authors propose that in certain conditions might drive bursting activity. We find, also, in distal dendrites a more pronounced glutamatergic innervation which is similarly associated with bursting activity.

7.4 Description of the *in vivo* Spontaneous Activity Pattern and in Response to an Aversive Stimulus of VTA Dopaminergic Neurons.

Regarding the spontaneous firing activity and baseline parameters calculated, the data are well within range for what has been reported for midbrain dopamine neurons (Grace and Bunney, 1984a; Marinelli and McCutcheon, 2014). Frequency average was 3.69 Hz (range 0.007 - 8.2 Hz; Fig. 15A), which is similar to the 4.5 Hz average described by Grace and Bunney (Grace and Bunney, 1984a). We also analyzed extracellular spike duration, from start to through, mainly because it has been shown to be particularly long for mesencephalic dopaminergic neurons, and it has been proposed as an electrophysiological criterion to identify DA neurons (Ungless et al., 2004) but also see (Margolis et al., 2006). Accordingly, all our neurons met the criteria of start to through, spike duration ≥ 1,1ms (Ungless et al., 2004) (Fig. 14B). Concerning firing regularity, we changed from the classical CV measure because, in some recordings, especially in slow firing neurons with long pauses, the CV values were too high and clearly not representative of the spiking behavior, e.g. one neuron had a relatively regular spiking activity but also a very long pause making the CV value quite high which indicated the neuron was irregular. The CV2 value of this same neuron was, on the other hand, markedly lower and in our appreciation more representative

of its spiking activity. The issue is that the CV is highly sensitive to long term changes in firing rate, such as pauses, leading us to search for a more suitable variability measure. The CV2 is less sensitive to these long-term changes, because it only compares adjacent ISI intervals, as such, CV2 value is high for spike trains with a high interval-to-interval variability, but much lower for spike trains with frequency variations occurring on a longer time scale (Holt et al., 1996).

When analyzing the response to the aversive stimulus we changed to a more stringent criteria, thus diminishing the probability of classifying a neuron as responsive (inhibited or activated) to the stimulus when it wasn't actually responding and also remaining consistent with previous works (Henny et al., 2012a). The consequence of this change was that one previously activated neuron is now considered unresponsive to the stimulus, so we now have 15 inhibited neurons, 4 activated neurons and 2 non-responsive. Inhibited and activated neurons (non-responsive were not analyzed due to small sample size) were not significantly different in any of the electrophysiological parameters analyzed; there were no differences in frequency, spike duration, CV2 nor percentage of spikes in burst (Fig. 15B-E). This is at odds with a previous report in the rat where, identified VTA DA neurons activated by an aversive stimulus were found to be more irregular and bursty than inhibited neurons (Brischoux et al., 2009), yet in this work the number of inhibited neurons is lower than ours (n = 5 vs n = 15 in our work) and seemed a fairly homogeneous population whilst we had a very high variability in our electrophysiological measurements (Fig. 15B-E). Moreover, because we had such a high variability within the inhibited neurons, we analyzed them more closely and found that we actually had two groups; inhibited regular, non-bursty (I-RNB) and inhibited irregular-bursty (I-IB, Figs. 16 and 17) neurons. We then compared these two groups of inhibited neurons with aversive stimulus activated neurons, and although we did not find differences between I-RNB (which are more similar to the group of

inhibited neurons previously reported in (Brischoux et al., 2009) and activated neurons, we found a trend of I-IB neurons having a higher percentage of spikes in burst than activated neurons. Though we found a different result as previously reported, differences in the methodologies must be taken into account such as model species (rat vs mouse), anesthetic used (urethane and ketamine/xylazine vs urethane) delivery of the aversive stimulus (footshocks vs footpinch), duration of the stimulus (4 vs 15 seconds), and criterion used to determine the type of response to the aversive stimulus, albeit similar, (Brischoux's and our work consider 1.96 standard deviations from the baseline as a significant change), the time frame used in Brischoux and collaborators report is only 500 ms after onset of the stimulus while we analyze the complete 15 seconds of duration of the footpinch.

Furthermore, it has also been reported, in rats and mice, that aversive stimulus activated neurons are more ventrally located than inhibited neurons (Brischoux et al., 2009; Eddine et al., 2015), a phenomena we did not find within our data (Figs. 18 and 19). We found a significant difference in the mediolateral location of the cell bodies with activated neurons more medially located (Fig 18 C1 and 19 C). However, there are several differences to consider, firstly, we used a different and much longer aversive stimulus, a 15 sec. footpinch vs the other two works that did 3 sec. footshock or a 3 sec. tailpinch. Moreover, in these reports stimulus response is evaluated in the 0.5 or 5 seconds following stimulus onset, whilst we analyzed throughout the 15 seconds of footpinch duration. Consequently, when analyzing our four activated neurons, only two are rapidly and transiently activated and interestingly both are ventrally located in the VTA as had been previously described for these neurons (Brischoux et al., 2009). On the other hand, the other two neurons show slower activation kinetics and interestingly are more dorsal and located in the PBP. One might speculate that, because these activated neurons have different activation kinetics and

are located more dorsally on the VTA, they constitute a different population of neurons that are not signaling salience as has been suggested for aversive-stimulus activated neurons (Brischoux et al., 2009), but something different like a antinociceptive DA activity for example. Actually, several studies have reported increases in DA concentration in target areas after aversive stimulation (Abercrombie et al., 1989; Badrinarayan et al., 2012; Budygin et al., 2012) and more importantly, dopamine release in ventral striatum has been associated with pain modulation (Leknes and Tracey, 2008; Wood et al., 2007). However, a greater number of activated neurons and more experiments are necessary to evaluate this hypothesis.

Additionally, we were interested in analyzing if there were any relationships between the morphologies of the neurons and their response to the aversive stimulus. However, this was not the case, as we found no relationships between morphological size and complexity measures and aversive stimulus response (Fig. 20).

Finally, we set out to describe the innervation pattern in the different electrophysiological groups. We looked at excitatory and inhibitory PSP densities and their possible correlation with spontaneous firing measurements (frequency, CV2, %SIB and spike duration) or with the response to the aversive stimulus (Fig. 21). We found a correlation, in aversive stimulus inhibited neurons, between % mean change in rate and the density of inhibitory PSPs (Fig. 21A), the higher the gephyrin PSP density the greater de inhibition by the footpinch. This result is similar to Henny and colleagues finding, where the see a correlation in the degree of inhibition by the aversive stimulus and the length of the dendrites into the SNr (Henny et al., 2012a), Figure 5f in their paper), which in their case is directly associated with the amount of GABAergic inhibition the neuron received. As already discussed, the VTA lacks the organization of SN, with a SNc where the DA cell bodies lie and a SNr that receives a prominent GABAergic innervation. Consequently, in the VTA we do

not have dendrites that extend into a different receptive domain equivalent to SNr, but nevertheless we see a correlation of the amount of GABAergic innervation and the degree of inhibition by the aversive stimulus. Moreover, we wanted to see if there was a finer pattern and looked at dendritic and somatic distribution of excitatory and inhibitory inputs and at different compartments of the dendritic tree (Figs. 22, 23 and 24). We found a correlation between the magnitude of inhibition by the aversive stimulus and the density of inhibitory PSPs in the cell bodies (Fig. 22C), similar to what we saw for the whole neuron (Fig. 21A). Thus, inhibitory responses of VTA DA neurons, which decreases the release of DA in target areas and are associated with learning of avoidance behaviors, are related to the density of GABAergic inputs they receive.

Nevertheless, we must not forget that the firing behavior is determined not only by the distribution of inputs onto the somatodendritic tree, but also by several other variables such as the expression of ionic channels (de Vrind et al., 2016; Shepard and Bunney, 1988) and neurotransmitter receptors (Marrion, 1997), D2 receptor activation (Hahn et al., 2006; Pucak and Grace, 1994), the size of the axon initial segment (Meza et al., 2018a), the activity of the input nuclei (Floresco et al., 2003) and also the activity other neurotransmitters systems within the VTA, such as acetylcholine (Pidoplichko et al., 1997), serotonin (Cameron et al., 1997) and noradrenaline (Mejias-Aponte, 2016), among others.

In summary, we are the first to perform high resolution, three-dimensional reconstructions of VTA DA neurons entire somatodendritic domain and perform detailed anatomical and geometrical analysis of their dendritic tree. We also, count and describe the distribution of inhibitory and excitatory putative synaptic contacts onto the somatodendritic domain. Finally, we stablish a direct correlation between synaptic inputs and *in vivo* firing by describing that the density of inhibitory contacts is related to the degree of inhibition by an aversive stimulus. In consequence,

degree of inhibition of VTA DA neurons, that in turns decreases DA release in target areas and participates in signaling and learning of avoidance behaviors in response to aversive stimuli (Bromberg-Martin et al., 2010; Schultz, 2007), is related to the density of inhibitory contacts and GABAergic inputs.

8. Conclusions

Morphologically, we see a topographical organization of VTA DA neurons with dorsally located neurons presenting larger and more complex dendritic trees than ventrally located neurons.

Irrespective of their location, VTA DA neurons have big, relatively simple and spread dendritic trees with a preferentially medio-dorsal and ventro-lateral orientation of their dendrites.

The spreading of the dendrites determines very extensive dendritic trees with the consequence that there is a significant overlap between different neurons. This phenomenon, in turn, partially explains why only highly overlapping input topologies have been described.

From immunohistochemical PSD stainings and stereological estimation methods we determine that VTA DA neurons receive on average 1001 glutamatergic (55.6%) and GABAergic (44.4%) inputs. The inputs are evenly distributed in the proximal compartment but in the distal dendrites and higher order dendrites we see there are significantly more glutamatergic than GABAergic inputs.

Electrophysiologically we found neurons inhibited, activated and non-responsive to the aversive footpinch. Inhibited neurons were composed by two different groups according to their baseline firing: inhibited, regular, non-bursty neurons (I-RNB) and inhibited, irregular, bursty neurons (I-IB).

Inhibited VTA DA neurons, independently whether they were I-RNB or I-IB, showed a correlation between their degree of inhibition by the aversive stimulus and the amount of inhibitory innervation they received; neurons with larger inhibitions received more GABAergic inputs.

9. Bibliography

Abercrombie, E.D., Keefe, K.A., DiFrischia, D.S., Zigmond, M.J., 1989. Differential effect of stress on in vivo dopamine release in striatum, nucleus accumbens, and medial frontal cortex. J. Neurochem. 52, 1655–1658. doi:10.1111/j.1471-4159.1989.tb09224.x

Anstrom, K.K., Miczek, K.A., Budygin, E.A., 2009. Increased phasic dopamine signaling in the mesolimbic pathway during social defeat in rats. Neuroscience 161, 3–12. doi:10.1016/j.neuroscience.2009.03.023

Aransay, A., RodrÃ guez-LÃ pez, C., GarcÃ a-Amado, M.A., ClascÃ, F., Prensa, L.A., 2015. Long-range projection neurons of the mouse ventral tegmental area: a single-cell axon tracing analysis. Front Neuroanat 9. doi:10.3389/fnana.2015.00059

Ascoli, G.A., 2006. Mobilizing the base of neuroscience data: the case of neuronal morphologies. Nat. Rev. Neurosci. 7, 318–324.

Badrinarayan, A., Wescott, S.A., Vander Weele, C.M., Saunders, B.T., Couturier, B.E., Maren, S., Aragona, B.J., 2012. Aversive stimuli differentially modulate real-time dopamine transmission dynamics within the nucleus accumbens core and shell. Journal of Neuroscience 32, 15779–15790. doi:10.1523/JNEUROSCI.3557-12.2012

Bae, J.A., Mu, S., Kim, J.S., Turner, N.L., Tartavull, I., Kemnitz, N., Jordan, C.S., Norton, A.D., Silversmith, W.M., Prentki, R., Sorek, M., David, C., Jones, D.L., Bland, D., Sterling, A.L.R., Park, J., Briggman, K.L., Seung, H.S., 2018. Digital Museum of Retinal Ganglion Cells with Dense Anatomy and Physiology. Cell 173, 1293–1306.e19. doi:10.1016/j.cell.2018.04.040

Bayer, V.E., Pickel, V.M., 1991. GABA-labeled terminals form proportionally more synapses with dopaminergic neurons containing low densities of tyrosine hydroxylase-immunoreactivity in rat ventral tegmental area. Brain Research 559, 44–55. doi:10.1016/0006-8993(91)90285-4

Beier, K.T., Steinberg, E.E., DeLoach, K.E., Xie, S., Miyamichi, K., Schwarz, L., Gao, X.J., Kremer, E.J., Malenka, R.C., Luo, L., 2015. Circuit Architecture of VTA Dopamine Neurons Revealed by Systematic Input-Output Mapping. Cell 162, 622–634. doi:10.1016/j.cell.2015.07.015

Belmer, A., Klenowski, P.M., Patkar, O.L., Bartlett, S.E., 2017. Mapping the connectivity of serotonin transporter immunoreactive axons to excitatory and inhibitory neurochemical synapses in the mouse limbic brain. Brain Struct Funct 222, 1297–1314. doi:10.1007/s00429-016-1278-x

Berke, J.D., Hyman, S.E., 2000. Addiction, dopamine, and the molecular mechanisms of memory. Neuron.

Bioulac, B., Benazzouz, A., Burbaud, P., Gross, C., 1997. Chronic administration of DL-allyl-glycine into the neostriatum, disorganises the firing modes of the nigral dopaminergic neurons in the rat. Neurosci. Lett. 226, 21–24.

Bloss, E.B., Cembrowski, M.S., Karsh, B., Colonell, J., Fetter, R.D., Spruston, N., 2016. Structured Dendritic Inhibition Supports Branch-Selective Integration in CA1 Pyramidal Cells. Neuron 89, 1016–1030. doi:10.1016/j.neuron.2016.01.029

Bocklisch, C., Pascoli, V., Wong, J.C.Y., House, D.R.C., Yvon, C., de Roo, M., Tan, K.R., Lüscher, C., 2013. Cocaine disinhibits dopamine neurons by potentiation of GABA transmission in the ventral tegmental area. Science 341, 1521–1525. doi:10.1126/science.1237059

Bodea, G.O., Spille, J.-H., Abe, P., Andersson, A.S., Acker-Palmer, A., Stumm, R., Kubitscheck, U., Blaess, S., 2014. Reelin and CXCL12 regulate distinct migratory behaviors during the development of the dopaminergic system. Development 141, 661–673. doi:10.1242/dev.099937

Bolam, J.P., Pissadaki, E.K., 2012. Living on the edge with too many mouths to feed: why dopamine neurons die. Mov. Disord. 27, 1478–1483. doi:10.1002/mds.25135

Bolam, J.P., Smith, Y., 1990. The GABA and substance P input to dopaminergic neurones in the substantia nigra of the rat. Brain Research 529, 57–78. doi:10.1016/0006-8993(90)90811-o

Bragina, L., Conti, F., 2018. Expression of Neurofilament Subunits at Neocortical Glutamatergic and GABAergic Synapses. Front Neuroanat 12, 74. doi:10.3389/fnana.2018.00074

Brandstätter, J.H., Dick, O., Boeckers, T.M., 2004. The postsynaptic scaffold proteins ProSAP1/Shank2 and Homer1 are associated with glutamate receptor complexes at rat retinal synapses. J. Comp. Neurol. 475, 551–563. doi:10.1002/cne.20194

Breton, J.M., Charbit, A.R., Snyder, B.J., Fong, P.T.K., Dias, E.V., Himmels, P., Lock, H., Margolis, E.B., 2019. Relative contributions and mapping of ventral tegmental area dopamine and GABA neurons by projection target in the rat. J. Comp. Neurol. 527, 916–941. doi:10.1002/cne.24572

Brichta, L., Greengard, P., 2014. Molecular determinants of selective dopaminergic vulnerability in Parkinson's disease: an update. Front Neuroanat 8, 152. doi:10.3389/fnana.2014.00152

Brignani, S., Pasterkamp, R.J., 2017. Neuronal Subset-Specific Migration and Axonal Wiring Mechanisms in the Developing Midbrain Dopamine System. Front Neuroanat 11, 55. doi:10.3389/fnana.2017.00055

Brischoux, F., Chakraborty, S., Brierley, D.I., Ungless, M.A., 2009. Phasic excitation of dopamine neurons in ventral VTA by noxious stimuli. Proc. Natl. Acad. Sci. U.S.A. 106, 4894–4899. doi:10.1073/pnas.0811507106

Bromberg-Martin, E.S., Matsumoto, M., Hikosaka, O., 2010. Dopamine in motivational control: rewarding, aversive, and alerting. Neuron 68, 815–834. doi:10.1016/j.neuron.2010.11.022

Budygin, E.A., Park, J., Bass, C.E., Grinevich, V.P., Bonin, K.D., Wightman, R.M., 2012. Aversive stimulus differentially triggers subsecond dopamine release in reward regions. Neuroscience 201, 331–337. doi:10.1016/j.neuroscience.2011.10.056

Cameron, D.L., Wessendorf, M.W., Williams, J.T., 1997. A subset of ventral tegmental area neurons is inhibited by dopamine, 5-hydroxytryptamine and opioids. Neuroscience 77, 155–166. doi:10.1016/S0306-4522(96)00444-7

Carr, D.B., Sesack, S.R., 2000. Projections from the rat prefrontal cortex to the ventral tegmental area: target specificity in the synaptic associations with mesoaccumbens and mesocortical neurons. Journal of Neuroscience 20, 3864–3873.

Carr, G.V., Maltese, F., Sibley, D.R., Weinberger, D.R., Papaleo, F., 2017. The Dopamine D5 Receptor Is Involved in Working Memory. Front Pharmacol 8, 666. doi:10.3389/fphar.2017.00666

Chaudhury, D., Walsh, J.J., Friedman, A.K., Juarez, B., Ku, S.M., Koo, J.W., Ferguson, D., Tsai, H.-C., Pomeranz, L., Christoffel, D.J., Nectow, A.R., Ekstrand, M., Domingos, A., Mazei-Robison, M.S., Mouzon, E., Lobo, M.K., Neve, R.L., Friedman, J.M., Russo, S.J., Deisseroth, K., Nestler, E.J., Han, M.-H., 2013. Rapid regulation of depression-related behaviours by control of midbrain dopamine neurons. Nature 493, 532–536. doi:10.1038/nature11713

Chergui, K., Charléty, P.J., Akaoka, H., Saunier, C.F., Brunet, J.L., Buda, M., Svensson, T.H., Chouvet, G., 1993. Tonic activation of NMDA receptors causes spontaneous burst discharge of rat midbrain dopamine neurons in vivo. Eur. J. Neurosci. 5, 137–144.

Chudasama, Y., Robbins, T.W., 2004. Dopaminergic modulation of visual attention and working memory in the rodent prefrontal cortex. Neuropsychopharmacology 29, 1628–1636. doi:10.1038/sj.npp.1300490

Clark, D., Chiodo, L.A., 1988. Electrophysiological and pharmacological characterization of identified nigrostriatal and mesoaccumbens dopamine neurons in the rat. Synapse 2, 474–485. doi:10.1002/syn.890020503

Coban, A., Filipov, N.M., 2007. Dopaminergic toxicity associated with oral exposure to the herbicide atrazine in juvenile male C57BL/6 mice. J. Neurochem. 100, 1177–1187. doi:10.1111/j.1471-4159.2006.04294.x

Comoli, E., Coizet, V., Boyes, J., Bolam, J.P., Canteras, N.S., Quirk, R.H., Overton, P.G., Redgrave, P., 2003. A direct projection from superior colliculus to substantia nigra for detecting salient visual events. Nat. Neurosci. 6, 974–980. doi:10.1038/nn1113

Costa, R.M., Lin, S.-C., Sotnikova, T.D., Cyr, M., Gainetdinov, R.R., Caron, M.G., Nicolelis, M.A.L., 2006. Rapid alterations in corticostriatal ensemble coordination during acute dopamine-dependent motor dysfunction. Neuron 52, 359–369. doi:10.1016/j.neuron.2006.07.030

da Silva, J.A., Tecuapetla, F., Paixão, V., Costa, R.M., 2018. Dopamine neuron activity before action initiation gates and invigorates future movements. Nature 554, 244–248. doi:10.1038/nature25457

Dahan, L., Astier, B., Vautrelle, N., Urbain, N., Kocsis, B., Chouvet, G., 2007. Prominent burst firing of dopaminergic neurons in the ventral tegmental area during paradoxical sleep. Neuropsychopharmacology 32, 1232–1241. doi:10.1038/sj.npp.1301251

de Jong, J.W., Afjei, S.A., Pollak Dorocic, I., Peck, J.R., Liu, C., Kim, C.K., Tian, L., Deisseroth, K., Lammel, S., 2019. A Neural Circuit Mechanism for Encoding Aversive Stimuli in the Mesolimbic Dopamine System. Neuron 101, 133–151.e7. doi:10.1016/j.neuron.2018.11.005

de Vrind, V., Scuvée-Moreau, J., Drion, G., Hmaied, C., Philippart, F., Engel, D., Seutin, V., 2016. Interactions between calcium channels and SK channels in midbrain dopamine neurons and their impact on pacemaker regularity: Contrasting roles of N- and L-type channels. Eur. J. Pharmacol. 788, 274–279. doi:10.1016/j.ejphar.2016.06.046

Dodson, P.D., Dreyer, J.K., Jennings, K.A., Syed, E.C.J., Wade-Martins, R., Cragg, S.J., Bolam, J.P., Magill, P.J., 2016. Representation of spontaneous movement by dopaminergic neurons is cell-type selective and disrupted in parkinsonism. Proc. Natl. Acad. Sci. U.S.A. 113, E2180–8. doi:10.1073/pnas.1515941113

Dommett, E., Coizet, V., Blaha, C.D., Martindale, J., Lefebvre, V., Walton, N., Mayhew, J.E.W., Overton, P.G., Redgrave, P., 2005. How visual stimuli activate dopaminergic neurons at short latency. Science 307, 1476–1479. doi:10.1126/science.1107026

Drion, G., Bonjean, M., Waroux, O., Scuvée-Moreau, J., Liégeois, J.-F., Sejnowski, T.J., Sepulchre, R., Seutin, V., 2010. M-type channels selectively control bursting in rat dopaminergic neurons. Eur. J. Neurosci. 31, 827–835. doi:10.1111/j.1460-9568.2010.07107.x

Eddine, R., Valverde, S., Tolu, S., Dautan, D., Hay, A., Morel, C., Cui, Y., Lambolez, B., Venance, L., Marti, F., Faure, P., 2015. A concurrent excitation and inhibition of dopaminergic subpopulations in response to nicotine. Sci Rep 5, srep08184. doi:10.1038/srep08184

Erhardt, S., Mathé, J.M., Chergui, K., Engberg, G., Svensson, T.H., 2002a. GABA(B) receptor-mediated modulation of the firing pattern of ventral tegmental area dopamine neurons in vivo. Naunyn Schmiedebergs Arch. Pharmacol. 365, 173–180. doi:10.1007/s00210-001-0519-5

Erhardt, S., Schwieler, L., Engberg, G., 2002b. Excitatory and inhibitory responses of dopamine neurons in the ventral tegmental area to nicotine. Synapse 43, 227–237. doi:10.1002/syn.10044

Essrich, C., Lorez, M., Benson, J.A., Fritschy, J.M., Lüscher, B., 1998. Postsynaptic clustering of major GABAA receptor subtypes requires the gamma 2 subunit and gephyrin. Nat. Neurosci. 1, 563–571. doi:10.1038/2798

Fahn, S., 2008. The history of dopamine and levodopa in the treatment of Parkinson's disease. Mov. Disord. 23 Suppl 3, S497–508. doi:10.1002/mds.22028

Fallon, J.H., 1981. Collateralization of monoamine neurons: mesotelencephalic dopamine projections to caudate, septum, and frontal cortex. J. Neurosci. 1, 1361–1368.

Farajian, R., Raven, M.A., Cusato, K., Reese, B.E., 2004. Cellular positioning and dendritic field size of cholinergic amacrine cells are impervious to early ablation of neighboring cells in the mouse retina. Vis. Neurosci. 21, 13–22. doi:10.1017/S0952523804041021

Faunes, M., Oñate-Ponce, A., Fernández-Collemann, S., Henny, P., 2016. Excitatory and inhibitory innervation of the mouse orofacial motor nuclei: A stereological study. J. Comp. Neurol. 524, 738–758. doi:10.1002/cne.23862

Ferreira, J.G.P., Del-Fava, F., Hasue, R.H., Shammah-Lagnado, S.J., 2008. Organization of ventral tegmental area projections to the ventral tegmental area-nigral complex in the rat. NSC 153, 196–213. doi:10.1016/j.neuroscience.2008.02.003

Fiorillo, C.D., 2013. Two dimensions of value: dopamine neurons represent reward but not aversiveness. Science 341, 546–549. doi:10.1126/science.1238699

Flores, C., 2011. Role of netrin-1 in the organization and function of the mesocorticolimbic dopamine system. J Psychiatry Neurosci 36, 296–310. doi:10.1503/jpn.100171

Floresco, S.B., West, A.R., Ash, B., Moore, H., Grace, A.A., 2003. Afferent modulation of dopamine neuron firing differentially regulates tonic and phasic dopamine transmission. Nat. Neurosci. 6, 968–973. doi:10.1038/nn1103

François, C., Yelnik, J., Percheron, G., 1987. Golgi-Study of the Primate Substantia-Nigra .2. Spatial-Organization of Dendritic Arborizations in Relation to the Cytoarchitectonic Boundaries and to the Striatonigral Bundle. J. Comp. Neurol. 265, 473–493. doi:10.1002/cne.902650403

Fu, Y., Yuan, Y., Halliday, G., Rusznák, Z., Watson, C., Paxinos, G., 2012. A cytoarchitectonic and chemoarchitectonic analysis of the dopamine cell groups in the substantia nigra, ventral tegmental area, and retrorubral field in the mouse. Brain Struct Funct 217, 591–612. doi:10.1007/s00429-011-0349-2

Gantz, S.C., Ford, C.P., Morikawa, H., Williams, J.T., 2018. The Evolving Understanding of Dopamine Neurons in the Substantia Nigra and Ventral Tegmental Area. Annu. Rev. Physiol. 80, 219–241. doi:10.1146/annurev-physiol-021317-121615

Geiman, E.J., Zheng, W., Fritschy, J.-M., Alvarez, F.J., 2002. Glycine and GABA(A) receptor subunits on Renshaw cells: relationship with presynaptic neurotransmitters and postsynaptic gephyrin clusters. J. Comp. Neurol. 444, 275–289. doi:10.1002/cne.10148

Geisler, S., Derst, C., Veh, R.W., Zahm, D.S., 2007. Glutamatergic afferents of the ventral tegmental area in the rat. Journal of Neuroscience 27, 5730–5743. doi:10.1523/JNEUROSCI.0012-07.2007

Geisler, S., Zahm, D.S., 2005. Afferents of the ventral tegmental area in the rat-anatomical substratum for integrative functions. J. Comp. Neurol. 490, 270–294. doi:10.1002/cne.20668

Gerfen, C.R., BAIMBRIDGE, K.G., MILLER, J.J., 1985. The Neostriatal Mosaic - Compartmental Distribution of Calcium-Binding Protein and Parvalbumin in the Basal Ganglia of the Rat and Monkey. Proc. Natl. Acad. Sci. U.S.A. 82, 8780–8784. doi:10.1073/pnas.82.24.8780

Gertler, T.S., Chan, C.S., Surmeier, D.J., 2008. Dichotomous anatomical properties of adult striatal medium spiny neurons. Journal of Neuroscience 28, 10814–10824. doi:10.1523/JNEUROSCI.2660-08.2008

Gonon, F.G., 1988. Nonlinear relationship between impulse flow and dopamine released by rat midbrain dopaminergic neurons as studied by in vivo electrochemistry. NSC 24, 19–28.

Grace, A.A., Bunney, B.S., 1985. Opposing effects of striatonigral feedback pathways on midbrain dopamine cell activity. Brain Research 333, 271–284.

Grace, A.A., Bunney, B.S., 1984a. The control of firing pattern in nigral dopamine neurons: single spike firing. J. Neurosci. 4, 2866–2876.

Grace, A.A., Bunney, B.S., 1984b. The control of firing pattern in nigral dopamine neurons: burst firing. J. Neurosci. 4, 2877–2890.

Grace, A.A., Bunney, B.S., 1983. Intracellular and Extracellular Electrophysiology of Nigral Dopaminergic-Neurons .2. Action-Potential Generating Mechanisms and Morphological Correlates. NSC 10, 317–. doi:10.1016/0306-4522(83)90136-7

Grace, A.A., Onn, S.-P., 1989. Morphology and electrophysiological properties of immunocytochemically identified rat dopamine neurons recorded in vitro. J. Neurosci. 9, 3463–3481.

Gray, N.W., Fourgeaud, L., Huang, B., Chen, J., Cao, H., Oswald, B.J., Hémar, A., McNiven, M.A., 2003. Dynamin 3 is a component of the postsynapse, where it interacts with mGluR5 and Homer. Current Biology 13, 510–515. doi:10.1016/s0960-9822(03)00136-2

Grenhoff, J., Ugedo, L., Svensson, T.H., 1988. Firing patterns of midbrain dopamine neurons: differences between A9 and A10 cells. Acta Physiol. Scand. 134, 127–132. doi:10.1111/j.1748-1716.1988.tb08468.x

Gulyás, A.I., Megías, M., Emri, Z., Freund, T.F., 1999. Total number and ratio of excitatory and inhibitory synapses converging onto single interneurons of different types in the CA1 area of the rat hippocampus. J. Neurosci. 19, 10082–10097.

Gutierrez-Mecinas, M., Kuehn, E.D., Abraira, V.E., Polgár, E., Watanabe, M., Todd, A.J., 2016. Immunostaining for Homer reveals the majority of excitatory synapses in laminae I-III of the mouse spinal dorsal horn. Neuroscience 329, 171–181. doi:10.1016/j.neuroscience.2016.05.009

Haber, S.N., Fudge, J.L., McFarland, N.R., 2000. Striatonigrostriatal pathways in primates form an ascending spiral from the shell to the dorsolateral striatum. J. Neurosci. 20, 2369–2382.

Hahn, J., Kullmann, P.H.M., Horn, J.P., Levitan, E.S., 2006. D2 autoreceptors chronically enhance dopamine neuron pacemaker activity. Journal of Neuroscience 26, 5240–5247. doi:10.1523/JNEUROSCI.4976-05.2006

Hajós, M., Greenfield, S.A., 1994. Synaptic connections between pars compacta and pars reticulata neurones: electrophysiological evidence for functional modules within the substantia nigra. Brain Research 660, 216–224.

Halliday, G.M., Törk, I., 1986. Comparative anatomy of the ventromedial mesencephalic tegmentum in the rat, cat, monkey and human. J. Comp. Neurol. 252, 423–445. doi:10.1002/cne.902520402

Häusser, M., Spruston, N., Stuart, G.J., 2000. Diversity and dynamics of dendritic signaling. Science 290, 739–744. doi:10.1126/science.290.5492.739

Häusser, M., Stuart, G., Racca, C., Sakmann, B., 1995. Axonal initiation and active dendritic propagation of action potentials in substantia nigra neurons. Neuron 15, 637–647.

Heien, M.L.A.V., Wightman, R.M., 2006. Phasic dopamine signaling during behavior, reward, and disease states. CNS Neurol Disord Drug Targets 5, 99–108.

Henny, P., Brown, M.T.C., Micklem, B.R., Magill, P.J., Bolam, J.P., 2014. Stereological and ultrastructural quantification of the afferent synaptome of individual neurons. Brain Struct Funct 219, 631–640. doi:10.1007/s00429-013-0523-9

Henny, P., Brown, M.T.C., Northrop, A., Faunes, M., Ungless, M.A., Magill, P.J., Bolam, J.P., 2012. Structural correlates of heterogeneous in vivo activity of midbrain dopaminergic neurons. Nat. Neurosci. 15, 613–619. doi:10.1038/nn.3048

Henny, P., Jones, B.E., 2008. Projections from basal forebrain to prefrontal cortex comprise cholinergic, GABAergic and glutamatergic inputs to pyramidal cells or interneurons. Eur. J. Neurosci. 27, 654–670. doi:10.1111/j.1460-9568.2008.06029.x

Henny, P., Jones, B.E., 2006. Innervation of orexin/hypocretin neurons by GABAergic, glutamatergic or cholinergic basal forebrain terminals evidenced by immunostaining for presynaptic vesicular transporter and postsynaptic scaffolding proteins. J. Comp. Neurol. 499, 645–661. doi:10.1002/cne.21131

Holt, G.R., Softky, W.R., Koch, C., Douglas, R.J., 1996. Comparison of discharge variability in vitro and in vivo in cat visual cortex neurons. J. Neurophysiol. 75, 1806–1814.

Howe, M.W., Dombeck, D.A., 2016. Rapid signalling in distinct dopaminergic axons during locomotion and reward. Nature 535, 505–510. doi:10.1038/nature18942

Hyland, B.I., Reynolds, J.N.J., Hay, J., Perk, C.G., Miller, R., 2002. Firing modes of midbrain dopamine cells in the freely moving rat. NSC 114, 475–492.

Ikemoto, S., 2007. Dopamine reward circuitry: two projection systems from the ventral midbrain to the nucleus accumbens-olfactory tubercle complex. Brain Res Rev 56, 27–78. doi:10.1016/j.brainresrev.2007.05.004

Jan, Y.-N., Jan, L.Y., 2010. Branching out: mechanisms of dendritic arborization. Nat. Rev. Neurosci. 11, 316–328. doi:10.1038/nrn2836

Jang, J., Um, K.B., Jang, M., Kim, S.H., Cho, H., Chung, S., Kim, H.J., Park, M.K., 2014. Balance between the proximal dendritic compartment and the soma determines spontaneous firing rate in midbrain dopamine neurons. The Journal of Physiology 592, 2829–2844. doi:10.1113/jphysiol.2014.275032

Jang, M., Jang, J.Y., Kim, S.H., Uhm, K.B., Kang, Y.K., Kim, H.J., Chung, S., Park, M.K., 2011. Functional organization of dendritic Ca2+ signals in midbrain dopamine neurons. Cell Calcium 50, 370–380. doi:10.1016/j.ceca.2011.06.007

Jhou, T.C., Geisler, S., Marinelli, M., Degarmo, B.A., Zahm, D.S., 2009. The mesopontine rostromedial tegmental nucleus: A structure targeted by the lateral habenula that projects to the ventral tegmental area of Tsai and substantia nigra compacta. J. Comp. Neurol. 513, 566–596. doi:10.1002/cne.21891

Johnson, S.W., Wu, Y.-N., 2004. Multiple mechanisms underlie burst firing in rat midbrain dopamine neurons in vitro. Brain Research 1019, 293–296. doi:10.1016/j.brainres.2004.06.022

Jones, B.E., 1995. Reticular formation: cytoarchitecture, transmitters and projections, in: Paxinos, G. (Ed.), The Rat Nervous System. Academic Sydney, pp. 155–171.

Juraska, J.M., Wilson, C.J., Groves, P.M., 1977. The substantia nigra of the rat: a Golgi study. J. Comp. Neurol. 172, 585–600. doi:10.1002/cne.901720403

Kalivas, P.W., Churchill, L., Klitenick, M.A., 1993. GABA and enkephalin projection from the nucleus accumbens and ventral pallidum to the ventral tegmental area. NSC 57, 1047–1060.

Katz, Y., Menon, V., Nicholson, D.A., Geinisman, Y., Kath, W.L., Spruston, N., 2009. Synapse distribution suggests a two-stage model of dendritic integration in CA1 pyramidal neurons. Neuron 63, 171–177. doi:10.1016/j.neuron.2009.06.023

KAWANO, H., OHYAMA, K., KAWAMURA, K., NAGATSU, I., 1995. Migration of Dopaminergic-Neurons in the Embryonic Mesencephalon of Mice. Brain Res. Dev. Brain Res. 86, 101–113. doi:10.1016/0165-3806(95)00018-9

Khaliq, Z.M., Bean, B.P., 2010. Pacemaking in dopaminergic ventral tegmental area neurons: depolarizing drive from background and voltage-dependent sodium conductances. Journal of Neuroscience 30, 7401–7413. doi:10.1523/JNEUROSCI.0143-10.2010

Kim, J.-I., Ganesan, S., Luo, S.X., Wu, Y.-W., Park, E., Huang, E.J., Chen, L., Ding, J.B., 2015. Aldehyde dehydrogenase 1a1 mediates a GABA synthesis pathway in midbrain dopaminergic neurons. Science 350, 102–106. doi:10.1126/science.aac4690

Kita, T., Kita, H., Kitai, S.T., 1986. Electrical membrane properties of rat substantia nigra compacta neurons in an in vitro slice preparation. Brain Research 372, 21–30.

Kitai, S.T., Shepard, P.D., Callaway, J.C., Scroggs, R., 1999. Afferent modulation of dopamine neuron firing patterns. Curr. Opin. Neurobiol. 9, 690–697.

Klausberger, T., Somogyi, P., 2008. Neuronal diversity and temporal dynamics: the unity of hippocampal circuit operations. Science 321, 53–57. doi:10.1126/science.1149381

Klemann, C.J.H.M., Roubos, E.W., 2011. The gray area between synapse structure and function-Gray's synapse types I and II revisited. Synapse 65, 1222–1230. doi:10.1002/syn.20962

Kline, S., Felten, D.L., 1985. Ventral Tegmental Area of the Rabbit Brain - a Developmental Golgi-Study. Brain Res. Bull. 14, 485–492. doi:10.1016/0361-9230(85)90027-9

Kole, M.H.P., Stuart, G.J., 2012. Signal processing in the axon initial segment. Neuron 73, 235–247. doi:10.1016/j.neuron.2012.01.007

Lalive, A.L., Munoz, M.B., Bellone, C., Slesinger, P.A., Lüscher, C., Tan, K.R., 2014. Firing modes of dopamine neurons drive bidirectional GIRK channel plasticity. Journal of Neuroscience 34, 5107–5114. doi:10.1523/JNEUROSCI.5203-13.2014

Lammel, S., Hetzel, A., Häckel, O., Jones, I., Liss, B., Roeper, J., 2008. Unique properties of mesoprefrontal neurons within a dual mesocorticolimbic dopamine system. Neuron 57, 760–773. doi:10.1016/j.neuron.2008.01.022

Lammel, S., Lim, B.K., Ran, C., Huang, K.W., Betley, M.J., Tye, K.M., Deisseroth, K., Malenka, R.C., 2012. Input-specific control of reward and aversion in the ventral tegmental area. Nature 491, 212–217. doi:10.1038/nature11527

Lavoie, B., Parent, A., 1994. Pedunculopontine Nucleus in the Squirrel-Monkey - Cholinergic and Glutamatergic Projections to the Substantia-Nigra. J. Comp. Neurol. 344, 232–241. doi:10.1002/cne.903440205

Lee, S.-H., Marchionni, I., Bezaire, M., Varga, C., Danielson, N., Lovett-Barron, M., Losonczy, A., Soltesz, I., 2014. Parvalbumin-positive basket cells differentiate among hippocampal pyramidal cells. Neuron 82, 1129–1144. doi:10.1016/j.neuron.2014.03.034

Lefebvre, J.L., Sanes, J.R., Kay, J.N., 2015. Development of dendritic form and function. Annu. Rev. Cell Dev. Biol. 31, 741–777. doi:10.1146/annurev-cellbio-100913-013020

Leknes, S., Tracey, I., 2008. A common neurobiology for pain and pleasure. Nat. Rev. Neurosci. 9, 314–320. doi:10.1038/nrn2333

Loughlin, S.E., Fallon, J.H., 1984. Substantia nigra and ventral tegmental area projections to cortex: topography and collateralization. NSC 11, 425–435. doi:10.1016/0306-4522(84)90034-4

López-Jury, L., Meza, R.C., Brown, M.T.C., Henny, P., Canavier, C.C., 2018. Morphological and Biophysical Determinants of the Intracellular and Extracellular Waveforms in Nigral Dopaminergic Neurons: A Computational Study. Journal of Neuroscience 38, 8295–8310. doi:10.1523/JNEUROSCI.0651-18.2018

Lynd-Balta, E., Haber, S.N., 1994. The Organization of Midbrain Projections to the Ventral Striatum in the Primate. NSC 59, 609–623. doi:10.1016/0306-4522(94)90181-3

Maeda, H., Mogenson, G.J., 1982. Effects of peripheral stimulation on the activity of neurons in the ventral tegmental area, substantia nigra and midbrain reticular formation of rats. Brain Res. Bull. 8, 7–14.

MALMIERCA, M.S., SEIP, K.L., OSEN, K.K., 1995. Morphological Classification and Identification of Neurons in the Inferior Colliculus - a Multivariate-Analysis. Anat. Embryol. 191, 343–350. doi:10.1007/bf00534687

Margolis, E.B., Lock, H., Hjelmstad, G.O., Fields, H.L., 2006. The ventral tegmental area revisited: is there an electrophysiological marker for dopaminergic neurons? The Journal of Physiology 577, 907–924. doi:10.1113/jphysiol.2006.117069

Marinelli, M., Cooper, D.C., Baker, L.K., White, F.J., 2003. Impulse activity of midbrain dopamine neurons modulates drug-seeking behavior. Psychopharmacology (Berl.) 168, 84–98. doi:10.1007/s00213-003-1491-1

Marinelli, M., McCutcheon, J.E., 2014. Heterogeneity of dopamine neuron activity across traits and states. Neuroscience 282C, 176–197. doi:10.1016/j.neuroscience.2014.07.034

Marrion, N.V., 1997. Control of M-current. Annu. Rev. Physiol. 59, 483–504. doi:10.1146/annurev.physiol.59.1.483

Matsumoto, M., Hikosaka, O., 2009. Two types of dopamine neuron distinctly convey positive and negative motivational signals. Nature 459, 837–841. doi:10.1038/nature08028

Maurin, Y., Banrezes, B., Menetrey, A., Mailly, P., Deniau, J.M., 1999. Three-dimensional distribution of nigrostriatal neurons in the rat: relation to the topography of striatonigral projections. NSC 91, 891–909. doi:10.1016/s0306-4522(98)00681-2

McCormack, A.L., Atienza, J.G., Langston, J.W., Di Monte, D.A., 2006. Decreased susceptibility to oxidative stress underlies the resistance of specific dopaminergic cell populations to paraquat-induced degeneration. NSC 141, 929–937. doi:10.1016/j.neuroscience.2006.03.069

Megías, M., Emri, Z., Freund, T.F., Gulyás, A.I., 2001. Total number and distribution of inhibitory and excitatory synapses on hippocampal CA1 pyramidal cells. NSC 102, 527–540.

Mejias-Aponte, C.A., 2016. Specificity and impact of adrenergic projections to the midbrain dopamine system. Brain Research 1641, 258–273. doi:10.1016/j.brainres.2016.01.036

Mena-Segovia, J., Winn, P., Bolam, J.P., 2008. Cholinergic modulation of midbrain dopaminergic systems. Brain Res Rev 58, 265–271. doi:10.1016/j.brainresrev.2008.02.003

Menegas, W., Bergan, J.F., Ogawa, S.K., Isogai, Y., 2015. Dopamine neurons projecting to the posterior striatum form an anatomically distinct subclass. Elife. doi:10.7554/eLife.10032.001

Mercuri, N.B., Stratta, F., Calabresi, P., Bernardi, G., 1992. A voltage-clamp analysis of NMDA-induced responses on dopaminergic neurons of the rat subtantia nigra zona compacta and ventral tegmental area. Brain Research.

Meza, R.C., López-Jury, L., Canavier, C.C., Henny, P., 2018. Role of the Axon Initial Segment in the Control of Spontaneous Frequency of Nigral Dopaminergic Neurons In Vivo. Journal of Neuroscience 38, 733–744. doi:10.1523/JNEUROSCI.1432-17.2017

MITANI, A., ITO, K., MITANI, Y., MCCARLEY, R.W., 1988. Morphological and Electrophysiological Identification of Gigantocellular Tegmental Field Neurons with Descending Projections in the Cat .1. Pons. J. Comp. Neurol. 268, 527–545. doi:10.1002/cne.902680405

Mongia, S., Yamaguchi, T., Liu, B., Zhang, S., Wang, H., Morales, M., 2019. The Ventral Tegmental Area has calbindin neurons with the capability to co-release glutamate and dopamine into the nucleus accumbens. Eur. J. Neurosci. doi:10.1111/ejn.14493

Morales, M., Margolis, E.B., 2017. Ventral tegmental area: cellular heterogeneity, connectivity and behaviour. Nat. Rev. Neurosci. 18, 73–85. doi:10.1038/nrn.2016.165

Morikawa, H., Khodakhah, K., Williams, J.T., 2003. Two intracellular pathways mediate metabotropic glutamate receptor-induced Ca2+ mobilization in dopamine neurons. Journal of Neuroscience 23, 149–157.

Moriya, S., Yamashita, A., Kawashima, S., Nishi, R., Yamanaka, A., Kuwaki, T., 2018. Acute Aversive Stimuli Rapidly Increase the Activity of Ventral Tegmental Area Dopamine Neurons in Awake Mice. Neuroscience 386, 16–23. doi:10.1016/j.neuroscience.2018.06.027

Moubarak, E., Engel, D., Dufour, M.A., Tapia, M., Tell, F., Goaillard, J.-M., 2019. Robustness to Axon Initial Segment Variation Is Explained by Somatodendritic Excitability in Rat Substantia Nigra Dopaminergic Neurons. Journal of Neuroscience 39, 5044–5063. doi:10.1523/JNEUROSCI.2781-18.2019

Mulinari, S., 2012. Monoamine theories of depression: historical impact on biomedical research. Journal of the History of the Neurosciences 21, 366–392. doi:10.1080/0964704X.2011.623917

Nair-Roberts, R.G., Chatelain-Badie, S.D., Benson, E., White-Cooper, H., Bolam, J.P., Ungless, M.A., 2008. Stereological estimates of dopaminergic, GABAergic and glutamatergic neurons in the ventral tegmental area, substantia nigra and retrorubral field in the rat. NSC 152, 1024–1031. doi:10.1016/j.neuroscience.2008.01.046

Nieoullon, A., 2002. Dopamine and the regulation of cognition and attention. Prog. Neurobiol. 67, 53–83.

Omelchenko, N., Sesack, S.R., 2009. Ultrastructural analysis of local collaterals of rat ventral tegmental area neurons: GABA phenotype and synapses onto dopamine and GABA cells. Synapse 63, 895–906. doi:10.1002/syn.20668

Omelchenko, N., Sesack, S.R., 2007. Glutamate synaptic inputs to ventral tegmental area neurons in the rat derive primarily from subcortical sources. NSC 146, 1259–1274. doi:10.1016/j.neuroscience.2007.02.016

Overton, P., Clark, D., 1992. Iontophoretically administered drugs acting at the N-methyl-D-aspartate receptor modulate burst firing in A9 dopamine neurons in the rat. Synapse 10, 131–140. doi:10.1002/syn.890100208

Owesson-White, C.A., Roitman, M.F., Sombers, L.A., Belle, A.M., Keithley, R.B., Peele, J.L., Carelli, R.M., Wightman, R.M., 2012. Sources contributing to the average extracellular concentration of dopamine in the nucleus accumbens. J. Neurochem. 121, 252–262. doi:10.1111/j.1471-4159.2012.07677.x

Paladini, C.A., Tepper, J.M., 1999. GABA(A) and GABA(B) antagonists differentially affect the firing pattern of substantia nigra dopaminergic neurons in vivo. Synapse 32, 165–176. doi:10.1002/(SICI)1098-2396(19990601)32:3<165::AID-SYN3>3.0.CO;2-N

Palmer, L.M., Stuart, G.J., 2006. Site of action potential initiation in layer 5 pyramidal neurons. Journal of Neuroscience 26, 1854–1863. doi:10.1523/JNEUROSCI.4812-05.2006

Paxinos, G., Franklin, K.B.J., 2007. The Mouse Brain in Stereotaxic Coordinates. Academic Press.

Pekcec, A., Schülert, N., Stierstorfer, B., Deiana, S., Dorner Ciossek, C., Rosenbrock, H., 2018. Targeting the dopamine D1 receptor or its downstream signalling by inhibiting phosphodiesterase-1 improves cognitive performance. British Journal of Pharmacology 175, 3021–3033. doi:10.1111/bph.14350

Phillipson, O.T., 1979a. A Golgi study of the ventral tegmental area of Tsai and interfascicular nucleus in the rat. J. Comp. Neurol. 187, 99–115.

Phillipson, O.T., 1979b. The cytoarchitecture of the interfascicular nucleus and ventral tegmental area of Tsai in the rat. J. Comp. Neurol. 187, 85–98.

Pidoplichko, V.I., DeBiasi, M., Williams, J.T., Dani, J.A., 1997. Nicotine activates and desensitizes midbrain dopamine neurons. Nature 390, 401–404. doi:10.1038/37120

Pinault, D., 1996. A novel single-cell staining procedure performed in vivo under electrophysiological control: morpho-functional features of juxtacellularly labeled thalamic cells and …. J. Neurosci. Methods 65, 113–136. doi:10.1016/0165-0270(95)00144-1

Pizzarelli, R., Griguoli, M., Zacchi, P., Petrini, E.M., Barberis, A., Cattaneo, A., Cherubini, E., 2019. Tuning GABAergic Inhibition: Gephyrin Molecular Organization and Functions. Neuroscience. doi:10.1016/j.neuroscience.2019.07.036

Prasad, K., Richfield, E.K., 2008. Sporadic midbrain dopamine neuron abnormalities in laboratory mice. Neurobiol. Dis. 32, 262–272. doi:10.1016/j.nbd.2008.07.007

Pucak, M.L., Grace, A.A., 1994. Evidence that systemically administered dopamine antagonists activate dopamine neuron firing primarily by blockade of somatodendritic autoreceptors. J. Pharmacol. Exp. Ther. 271, 1181–1192.

Ramón-Moliner, E., Nauta, W.J., 1966. The isodendritic core of the brain stem. J. Comp. Neurol. 126, 311–335. doi:10.1002/cne.901260301

Roeper, J., 2013. Dissecting the diversity of midbrain dopamine neurons. Trends Neurosci. 36, 336–342. doi:10.1016/j.tins.2013.03.003

Root, D.H., Mejias-Aponte, C.A., Zhang, S., Wang, H.-L., Hoffman, A.F., Lupica, C.R., Morales, M., 2014. Single rodent mesohabenular axons release glutamate and GABA. Nature Publishing Group 17, 1543–1551. doi:10.1038/nn.3823

Sanchez-Catalan, M.J., Kaufling, J., Georges, F., Veinante, P., Barrot, M., 2014. The antero-posterior heterogeneity of the ventral tegmental area. Neuroscience 282, 198–216. doi:10.1016/j.neuroscience.2014.09.025

Sassoè-Pognetto, M., Kirsch, J., Grünert, U., Greferath, U., Fritschy, J.M., Möhler, H., Betz, H., Wässle, H., 1995. Colocalization of gephyrin and GABAA-receptor subunits in the rat retina. J. Comp. Neurol. 357, 1–14. doi:10.1002/cne.903570102

Sassoè-Pognetto, M., Panzanelli, P., Sieghart, W., Fritschy, J.M., 2000. Colocalization of multiple GABA(A) receptor subtypes with gephyrin at postsynaptic sites. J. Comp. Neurol. 420, 481–498.

Schindelin, J., Arganda-Carreras, I., Frise, E., Kaynig, V., Longair, M., Pietzsch, T., Preibisch, S., Rueden, C., Saalfeld, S., Schmid, B., Tinevez, J.-Y., White, D.J., Hartenstein, V., Eliceiri, K., Tomancak, P., Cardona, A., 2012. Fiji: an open-source platform for biological-image analysis. Nat. Methods 9, 676–682. doi:10.1038/nmeth.2019

Schmidt-Hieber, C., Jonas, P., Bischofberger, J., 2008. Action potential initiation and propagation in hippocampal mossy fibre axons. The Journal of Physiology 586, 1849–1857. doi:10.1113/jphysiol.2007.150151

Schultz, W., 2007. Behavioral dopamine signals. Trends Neurosci. 30, 203–210. doi:10.1016/j.tins.2007.03.007

Schultz, W., Dayan, P., Montague, P.R., 1997. A neural substrate of prediction and reward. Science 275, 1593–1599.

Sesack, S.R., Grace, A.A., 2010. Cortico-Basal Ganglia reward network: microcircuitry. Neuropsychopharmacology 35, 27–47. doi:10.1038/npp.2009.93

Seutin, V., Verbanck, P., Massotte, L., Dresse, A., 1990. Evidence for the presence of N-methyl-D-aspartate receptors in the ventral tegmental area of the rat: an electrophysiological in vitro study. Brain Research 514, 147–150.

Shepard, P.D., Bunney, B.S., 1988. Effects of apamin on the discharge properties of putative dopamine-containing neurons in vitro. Brain Research 463, 380–384.

Shiraishi, Y., Mizutani, A., Yuasa, S., Mikoshiba, K., Furuichi, T., 2004. Differential expression of Homer family proteins in the developing mouse brain. J. Comp. Neurol. 473, 582–599. doi:10.1002/cne.20116

Shiraishi-Yamaguchi, Y., Sato, Y., Sakai, R., Mizutani, A., Knöpfel, T., Mori, N., Mikoshiba, K., Furuichi, T., 2009. Interaction of Cupidin/Homer2 with two actin cytoskeletal regulators, Cdc42 small GTPase and Drebrin, in dendritic spines. BMC Neurosci 10, 25. doi:10.1186/1471-2202-10-25

Sizemore, R.J., Zhang, R., Lin, N., Goddard, L., Wastney, T., Parr-Brownlie, L.C., Reynolds, J.N.J., Oorschot, D.E., 2016. Marked differences in the number and type of synapses innervating the somata and primary dendrites of midbrain dopaminergic neurons, striatal cholinergic interneurons, and striatal spiny projection neurons in the rat. J. Comp. Neurol. 524, 1062–1080. doi:10.1002/cne.23891

Smith, Y., Bevan, M.D., Shink, E., Bolam, J.P., 1998. Microcircuitry of the direct and indirect pathways of the basal ganglia. NSC 86, 353–387. doi:10.1016/s0306-4522(98)00004-9

Smith, Y., Charara, A., Parent, A., 1996. Synaptic innervation of midbrain dopaminergic neurons by glutamate-enriched terminals in the squirrel monkey. J. Comp. Neurol. 364, 231–253. doi:10.1002/(SICI)1096-9861(19960108)364:2<231::AID-CNE4>3.0.CO;2-6

Smith, Y., Hazrati, L.N., Parent, A., 1990. Efferent projections of the subthalamic nucleus in the squirrel monkey as studied by the PHA-L anterograde tracing method. J. Comp. Neurol. 294, 306–323. doi:10.1002/cne.902940213

Spruston, N., 2008. Pyramidal neurons: dendritic structure and synaptic integration. Nat. Rev. Neurosci. 9, 206–221. doi:10.1038/nrn2286

Stopper, C.M., Tse, M.T.L., Montes, D.R., Wiedman, C.R., Floresco, S.B., 2014. Overriding phasic dopamine signals redirects action selection during risk/reward decision making. Neuron 84, 177–189. doi:10.1016/j.neuron.2014.08.033

Swanson, L.W., 1982. The projections of the ventral tegmental area and adjacent regions: a combined fluorescent retrograde tracer and immunofluorescence study in the rat. Brain Res. Bull. 9, 321–353.

Tahvildari, B., Alonso, A., 2005. Morphological and electrophysiological properties of lateral entorhinal cortex layers II and III principal neurons. J. Comp. Neurol. 491, 123–140. doi:10.1002/cne.20706

Tan, K.R., Yvon, C., Turiault, M., Mirzabekov, J.J., Doehner, J., Labouèbe, G., Deisseroth, K., Tye, K.M., Lüscher, C., 2012. GABA neurons of the VTA drive conditioned place aversion. Neuron 73, 1173–1183. doi:10.1016/j.neuron.2012.02.015

Tao-Cheng, J.H., Thein, S., Yang, Y., Reese, T.S., Gallant, P.E., 2014. Homer is concentrated at the postsynaptic density and does not redistribute after acute synaptic stimulation. Neuroscience 266, 80–90. doi:10.1016/j.neuroscience.2014.01.066

Tepper, J.M., Sawyer, S.F., Groves, P.M., 1987. Electrophysiologically identified nigral dopaminergic neurons intracellularly labeled with HRP: light-microscopic analysis. The Journal of neuroscience.

Tritsch, N.X., Ding, J.B., Sabatini, B.L., 2012. Dopaminergic neurons inhibit striatal output through non-canonical release of GABA. Nature 490, 262–266. doi:10.1038/nature11466

Tritsch, N.X., Oh, W.-J., Gu, C., Sabatini, B.L., 2014. Midbrain dopamine neurons sustain inhibitory transmission using plasma membrane uptake of GABA, not synthesis. Elife 3, e01936. doi:10.7554/eLife.01936

Tritsch, N.X., Sabatini, B.L., 2012. Dopaminergic modulation of synaptic transmission in cortex and striatum. Neuron 76, 33–50. doi:10.1016/j.neuron.2012.09.023

Trutti, A.C., Mulder, M.J., Hommel, B., Forstmann, B.U., 2019. Functional neuroanatomical review of the ventral tegmental area. NeuroImage 191, 258–268. doi:10.1016/j.neuroimage.2019.01.062

Tsai, H.-C., Zhang, F., Adamantidis, A., Stuber, G.D., Bonci, A., de Lecea, L., Deisseroth, K., 2009. Phasic firing in dopaminergic neurons is sufficient for behavioral conditioning. Science 324, 1080–1084. doi:10.1126/science.1168878

Tu, J.C., Xiao, B., Naisbitt, S., Yuan, J.P., Petralia, R.S., Brakeman, P., Doan, A., Aakalu, V.K., Lanahan, A.A., Sheng, M., Worley, P.F., 1999. Coupling of mGluR/Homer and PSD-95 complexes by the Shank family of postsynaptic density proteins. Neuron 23, 583–592.

Ungless, M.A., Magill, P.J., Bolam, J.P., 2004. Uniform inhibition of dopamine neurons in the ventral tegmental area by aversive stimuli. Science 303, 2040–2042. doi:10.1126/science.1093360

Usuda, I., Tanaka, K., Chiba, T., 1998. Efferent projections of the nucleus accumbens in the rat with special reference to subdivision of the nucleus: biotinylated dextran amine study. Brain Research 797, 73–93. doi:10.1016/s0006-8993(98)00359-x

Valenti, O., Gill, K.M., Grace, A.A., 2012. Different stressors produce excitation or inhibition of mesolimbic dopamine neuron activity: response alteration by stress pre-exposure. Eur. J. Neurosci. 35, 1312–1321. doi:10.1111/j.1460-9568.2012.08038.x

Vetter, P., Roth, A., Häusser, M., 2001. Propagation of action potentials in dendrites depends on dendritic morphology. J. Neurophysiol. 85, 926–937. doi:10.1152/jn.2001.85.2.926

Vrieler, N., Loyola, S., Yarden-Rabinowitz, Y., Hoogendorp, J., Medvedev, N., Hoogland, T.M., De Zeeuw, C.I., De Schutter, E., Yarom, Y., Negrello, M., Torben-Nielsen, B., Uusisaari, M.Y., 2019. Variability and directionality of inferior olive neuron dendrites revealed by detailed 3D characterization of an extensive morphological library. Brain Struct Funct 224, 1677–1695. doi:10.1007/s00429-019-01859-z

Waroux, O., Massotte, L., Alleva, L., Graulich, A., Thomas, E., Liégeois, J.-F., Scuvée-Moreau, J., Seutin, V., 2005. SK channels control the firing pattern of midbrain dopaminergic neurons in vivo. Eur. J. Neurosci. 22, 3111–3121. doi:10.1111/j.1460-9568.2005.04484.x

Watabe-Uchida, M., Eshel, N., Uchida, N., 2017. Neural Circuitry of Reward Prediction Error. Annu. Rev. Neurosci. 40, 373–394. doi:10.1146/annurev-neuro-072116-031109

Watabe-Uchida, M., Zhu, L., Ogawa, S.K., Vamanrao, A., Uchida, N., 2012a. Whole-brain mapping of direct inputs to midbrain dopamine neurons. Neuron 74, 858–873. doi:10.1016/j.neuron.2012.03.017

Watabe-Uchida, M., Zhu, L., Ogawa, S.K., Vamanrao, A., Uchida, N., 2012b. Whole-brain mapping of direct inputs to midbrain dopamine neurons. Neuron 74, 858–873. doi:10.1016/j.neuron.2012.03.017

Willuhn, I., Burgeno, L.M., Everitt, B.J., Phillips, P.E.M., 2012. Hierarchical recruitment of phasic dopamine signaling in the striatum during the progression of cocaine use. Proc. Natl. Acad. Sci. U.S.A. 109, 20703–20708. doi:10.1073/pnas.1213460109

Wilson, C.J., Callaway, J.C., 2000. Coupled oscillator model of the dopaminergic neuron of the substantia nigra. J. Neurophysiol. 83, 3084–3100.

Wise, R.A., 2009. Roles for nigrostriatal--not just mesocorticolimbic--dopamine in reward and addiction. Trends Neurosci. 32, 517–524. doi:10.1016/j.tins.2009.06.004

Wise, R.A., 2004. Dopamine, learning and motivation. Nat. Rev. Neurosci. 5, 483–494. doi:10.1038/nrn1406

Wood, P.B., Schweinhardt, P., Jaeger, E., Dagher, A., Hakyemez, H., Rabiner, E.A., Bushnell, M.C., Chizh, B.A., 2007. Fibromyalgia patients show an abnormal dopamine response to pain. Eur. J. Neurosci. 25, 3576–3582. doi:10.1111/j.1460-9568.2007.05623.x

Xiao, B., Tu, J.C., Petralia, R.S., Yuan, J.P., Doan, A., Breder, C.D., Ruggiero, A., Lanahan, A.A., Wenthold, R.J., Worley, P.F., 1998. Homer regulates the association of group 1 metabotropic glutamate receptors with multivalent complexes of homer-related, synaptic proteins. Neuron 21, 707–716.

Yamaguchi, T., Wang, H.-L., Li, X., Ng, T.H., Morales, M., 2011. Mesocorticolimbic glutamatergic pathway. Journal of Neuroscience 31, 8476–8490. doi:10.1523/JNEUROSCI.1598-11.2011

Yelnik, J., François, C., Percheron, G., Heyner, S., 1987. Golgi study of the primate substantia nigra. I. Quantitative morphology and typology of nigral neurons. J. Comp. Neurol. 265, 455–472. doi:10.1002/cne.902650402

Yetnikoff, L., Lavezzi, H.N., Reichard, R.A., Zahm, D.S., 2014. An update on the connections of the ventral mesencephalic dopaminergic complex. Neuroscience 282, 23–48. doi:10.1016/j.neuroscience.2014.04.010

Young, A.M.J., 2004. Increased extracellular dopamine in nucleus accumbens in response to unconditioned and conditioned aversive stimuli: studies using 1 min microdialysis in rats. J. Neurosci. Methods 138, 57–63. doi:10.1016/j.jneumeth.2004.03.003

Zhang, S., Qi, J., Li, X., Wang, H.-L., Britt, J.P., Hoffman, A.F., Bonci, A., Lupica, C.R., Morales, M., 2015. Dopaminergic and glutamatergic microdomains in a subset of rodent mesoaccumbens axons. Nature Publishing Group 18, 386–392. doi:10.1038/nn.3945